Theoretical Tools and Software for Modeling, Simulation and Control Design of Rocket Test Facilities
- Report -

Hanz Richter
NRC Research Associate

July 30, 2004

Contents

List of Figures

Chapter 1

Introduction

The following report describes the research activity performed by the Associate during the period starting January 14th, 2002 until August 16th, 2004 at the NASA John C. Stennis Space Center (SSC) in Mississippi. The Associate wishes to thank his advisor, Dr. Fernando Figueroa; Dr. Enrique Barbieri, a summer visiting faculty from Tulane University; Dr. Bill St.Cyr, Dr. Bob Field and Mr. Jared Sass, NASA engineers; and Ms. Jamie Granger, a summer undergraduate student from Tulane University for their valuable cooperation in the project.

1.1 Objectives, Scope and Methodology

A rocket test stand and associated subsystems are complex devices whose operation requires that certain preparatory calculations be carried out before a test. In addition, real-time control calculations must be performed during the test, and further calculations are carried out after a test is completed. The latter may be required in order to evaluate if a particular test conformed to specifications. These calculations are used to set valve positions, pressure setpoints, control gains and other operating parameters so that a desired system behavior is obtained and the test can be successfully carried out. Currently, calculations are made in an ad-hoc fashion and involve trial-and-error procedures that may involve activating the system with the sole purpose of finding the correct parameter settings. The goals of this project are to develop mathematical models, control methodologies and associated simulation environments to provide a systematic and comprehensive prediction and real-time control capability. The models and controller designs are expected to be useful in two respects:

1. As a design tool, a model is the only way to determine the effects of design choices without building a prototype, which is, in the context of rocket test stands, impracticable.

2. As a prediction and tuning tool, a good model allows to set system parameters off-line, so that the expected system response conforms to specifications. This includes the setting of physical parameters, such as valve positions, and the configuration and tuning of any feedback controllers in the loop.

This work fits into a framework of current efforts in developing a set of tools that simplify prediction tasks routinely done at the test stands. The tools are user-friendly software that incorporates knowledge about particular systems and uses it to carry out predictions of system

operation under diverse conditions. Building such knowledge is the most important part of the work and involves mathematical modeling, data collection, model validation and analysis of model properties. Work on a graphical user interface (GUI) for the E-1 hydrogen mixer is also considered a project goal.

The following specific activities have been carried out as part of the research project:

1. Literature review and consultation with NASA engineers.
2. Construction of mathematical models.
3. Data collection and organization.
4. Use and development of simulation programs.
5. Model validation with experimental data.
6. Dynamic model analysis and controller synthesis.
7. Closed-loop control simulations and feasibility studies.
8. Work in control-theoretical problems inspired by practical problems.
9. Preparation of technical articles and presentations.
10. Programming of specialized simulation environments.

The work methodology roughly follows the sequence of activities presented above. Some iterations are often required for model and control law refinement.

1.2 Summary of Accomplishments

The tenure period has been very productive, as evidenced by the number of technical papers resulting from the research project. The following list of achievements summarizes the main points:

- Construction and experimental validation of a model for the E-1 Hydrogen Mixer.
- Dynamic analysis: equilibrium, controllability, linearizability.
- Simulation tools in Matlab/Simulink.
- Controller designs: Small-signal and feedback linearization, Sliding Mode.
- Theoretical work on constrained Sliding Mode Control (new contribution to the field).
- Design and programming of Matlab-based Graphical User Interface.
- Preliminary studies in Run Tank dynamics.

Seven conference presentations [3, 21, 22, 25, 26, 27] -and corresponding proceedings articles- have resulted from the project, along with one accepted journal article [23] and one in the submission process. In addition, the work in the Graphical User Interface has resulted in a NASA Software Disclosure, to be reported in the NASA Tech Briefs [24].

Chapter 2

The E-1 Hydrogen Mixer

The hydrogen mixer subsystem of the E-1 test facility is used to condition the flow of liquid hydrogen (LH2) before it is fed into a test article. Specifically, the temperature of the liquid at the exit of the mixer must be controlled, along with the pressure inside the mixer and the total output flow rate. This is accomplished in the mixer by injection of a stream of gaseous hydrogen (GH2). The rate at which GH2 is injected determines both the transient and steady-state temperature behavior of the conditioned propellant. The system is depicted in Fig. 2.1 below.

2.1 Assumptions - Preliminary Model

A preliminary model is derived based on the following assumptions:

- Thermodynamic properties of LH2 and GH2 at the mixer inputs are constant.
- The mass flow rates of LH2, GH2 and output mixture are independent control variables that can be manipulated at will.
- The mixer operates adiabatically (i.e., is thermally insulated from the surroundings) and isobarically (the pressure drop in the mixer is negligible).
- Thermodynamic properties of the exit stream (i.e., temperature) equal those inside the mixing chamber. Also, GH2 condenses completely inside the mixer, rejecting heat to the LH2 and thus increasing its temperature. There is no two-phase flow at the exit.
- The output flow is incompressible.

2.1.1 Governing equations

The two primary equations used to model the process in the mixer are the conservation of mass and the conservation of energy (first law of thermodynamics for a control volume). Both equations are used in their more general forms, to account for transient effects. The conservation of mass equation is

$$\dot{m}_{cv} = \sum \dot{m}_i - \sum \dot{m}_e \tag{2.1}$$

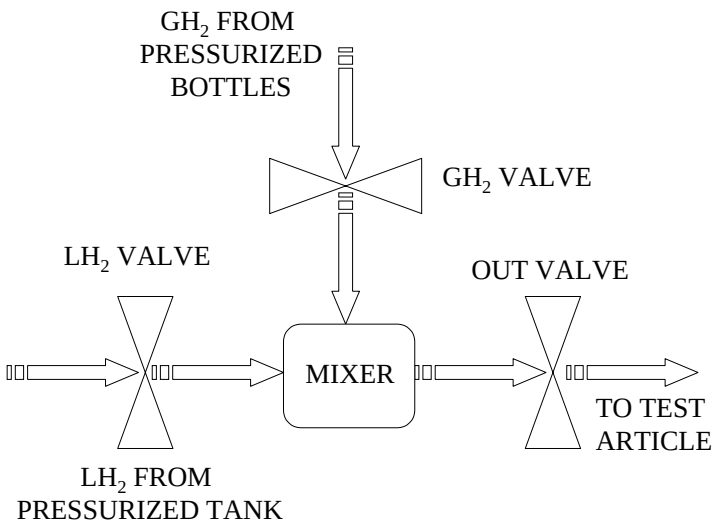

Figure 2.1: Mixer Subsystem

where m_{cv} is the mass inside the mixer (control volume) and $\dot{m}_i$ and $\dot{m}_e$ are the input and exit mass flows, respectively. In this case, there are two input and one exit mass flows. Under transient conditions, the time derivative of m_{cv} is nonzero. Denoting the LH2 input mass flow as $\dot{m}_l$, the GH2 mass flow as $\dot{m}_g$, and the exit mass flow as $\dot{m}_e$, the mass balance equation becomes

$$\dot{m}_{cv} = \dot{m}_l + \dot{m}_g - \dot{m}_e \tag{2.2}$$

The first law of thermodynamics for a control volume is stated as:

$$\frac{dU_{cv}}{dt} = \sum \dot{m}_i(h_i + \frac{V_i^2}{2} + gZ_i) - \sum \dot{m}_e(h_e + \frac{V_e^2}{2} + gZ_e) + \dot{Q}_{cv} - \dot{W}_{cv} \tag{2.3}$$

Here U_{cv} is the (internal) energy of the mass inside the mixer, h_i and h_e are the specific enthalpies of the input and exit flows, and V_i, V_e, Z_i and Z_e denote their velocities and elevations. Since the mixer does not introduce important velocity changes, the kinetic energy terms will be neglected, and so will be the changes potential energy due to elevation. The rate of heat transferred through mixer walls, $\dot{Q}_{cv}$, and the mechanical work done inside the mixer are considered zero. The derivative of the internal energy of the mixer can be expanded as:

$$\frac{dU_{cv}}{dt} = \frac{d(m_{cv}u_{cv})}{dt} = \dot{m}_{cv}u_{cv} + \dot{u}_{cv}m_{cv}$$

where u_{cv} is the specific internal energy of the mixer. Following the assumption of constant input properties, the energy equation becomes

$$\dot{m}_{cv}u_{cv} + \dot{u}_{cv}m_{cv} = \dot{m}_l h_l + \dot{m}_g h_g - \dot{m}_e h_e \tag{2.4}$$

where h_l and h_g are the constant input enthalpies and h_e is the exit enthalpy, which will vary under transient conditions. If the three mass flows are specified, Eqs. (2.2) and (2.4)

form a system of ordinary differential equations on the variables m_{cv} and u_{cv}. However, the exit enthalpy h_e is unknown, and therefore a solution cannot be obtained. An additional assumption is therefore necessary to completely determine the system. It will be assumed that the thermodynamic properties inside and at the exit of the mixer are the same. Specifically, the exit internal energy u_e is equal to the mixer internal internal energy u_{cv}. Using the definition of enthalpy and differentiating:

$$dh_e = du_e + dp_e v_e + p_e dv_e$$

Using the constant pressure and incompressibilty assumptions gives

$$\dot{h}_e = \dot{u}_e = \dot{u}_{cv}$$

therefore

$$h_e = u_{cv} + C \tag{2.5}$$

where C is a constant determined from the initial conditions. Now, Eqs. (2.2), (2.4),and (2.5) can be solved for any set of initial conditions. Note that the initial values of m_{cv} and u_{cv} are not easily measurable in the real process, but that can be indirectly calculated from the input and output properties.

2.1.2 The mixer as a control system

The mixer equations must be put in a form adequate for control system analysis and design. One of such forms is the state-space representation, which has a convenient mathematical form. Let the independent control inputs be defined as:

$$\begin{aligned} \psi_1 &= \dot{m}_l \\ \psi_2 &= \dot{m}_g \\ \psi_3 &= \dot{m}_e \end{aligned}$$

Let the two states be denoted as:

$$\begin{aligned} x_1 &= u_{cv} \\ x_2 &= m_{cv} \end{aligned}$$

Using the governing equations and the above definitions, the mixer control system can be represented as:

$$\dot{x}_1 = \frac{1}{x_2} h_l \psi_1 + h_g \psi_2 - C\psi_3 - x_1(\psi_1 + \psi_2) \tag{2.6}$$

$$\dot{x}_2 = \psi_1 + \psi_2 - \psi_3 \tag{2.7}$$

In vector form, the mathematical model falls in the category of a 2-state, 3-input bi-linear model of the form

$$\begin{aligned} \dot{x}_1 &= f^T(x_1, x_2)\psi \\ \dot{x}_2 &= g(\psi) \end{aligned}$$

where $\psi = [\psi_1 \;\; \psi_2 \;\; \psi_3]^T$ is the vector of control flows and the functions f and g are given by

$$f(x_1, x_2) = \begin{bmatrix} \frac{h_l - x_1}{x_2} \\ \\ \frac{h_g - x_1}{x_2} \\ \\ -\frac{C}{x_2} \end{bmatrix} \tag{2.8}$$

$$g(\psi_1, \psi_2, \psi_3) = \psi_1 + \psi_2 - \psi_3 \tag{2.9}$$

Preliminary observations indicate that the methods of feedback linearization [6], backstepping control [13, 29] or differential flatness [18] could be candidates for controller designs.

2.1.3 Control valve models

The following expression models the volumetric flow of liquid through a valve:

$$Q = C\frac{C_v\sqrt{P_{in} - P_{out}}}{\sqrt{S_w}}$$

where C is a constant dependent on choice of units, C_v is the valve flow coefficient, S_w is the specific gravity of the liquid relative to water, and P_{in} and P_{out} are the inlet and exit pressures, respectively. The specific gravity is taken constant, at a reference temperature. For compressible fluid, the following formulas are considered:

$$Q = \begin{cases} CC_v\sqrt{\frac{P_{in}^2 - P_{out}^2}{^\circ R S_a}} & \text{,when } P_{in} < 2P_{out} \\ \\ C'\frac{C_v P_{in}}{\sqrt{^\circ R S_a}} & \text{,when } P_{in} \geq 2P_{out} \end{cases}$$

Here, $^\circ R$ is the fluid temperature in degrees Rankine, S_a is the specific gravity of the gas relative to the air, taken constant at 14.7 psia and $60^\circ F$ and C, C' are constants depending on the choice of units. Note that the flow given by these expressions is in Standard Cubic Feet per Second (SCFS), that is at 14.7 psia and $520^\circ R$. A modification must be introduced to adjust for actual flow conditions using the ideal gas law. The actual flow Q_a is computed as

$$Q_a = \frac{14.7}{P}\frac{T}{520}Q$$

whereas the mass flow is obtained by multiplying Q_a by the density of the fluid matching P and T. The P, T, ρ combination may be taken at valve inlet or outlet, the result being theoretically the same. For the case of hydrogen, the formulas for mass flow become:

For LH2 flow:

$$W = 1.76 \times 10^{-2} C_v\sqrt{(P_{in} - P_{out})\rho} \tag{2.10}$$

For GH2 flow:

$$W = \begin{cases} 2.857 \times 10^{-2} C_v \sqrt{P_{in}^2 - P_{out}^2} \frac{\sqrt{T}\rho}{P} & \text{,when } P_{in} < 2P_{out} \\ \\ 2.423 \times 10^{-2} C_v P_{in} \frac{\sqrt{T}\rho}{P} & \text{,when } P_{in} \geq 2P_{out} \end{cases} \tag{2.11}$$

In the above formulas, the mass flow is given in lb/s, the pressures in psi, the densities in lb/ft^3, and the temperature in $^\circ R$. The value used for the specific gravity of hydrogen is $Sa = 0.0699$ (relative to air at 1 atm and $70^\circ F$) and the density of water in Eq. (2.10) has be taken as 62.4 lbm/ft^3.

2.1.4 Example

The following numerical example compares the values given by the above formulas with the ones in [2], where the formula for LH2 was used for GH2. Let $P_{in} = 13500$ psia, $P_{out} = 6000$ psia, $T_{in} = 90^\circ F$, $T_{out} = 135^\circ F$, $\rho_{in} = 2.9\ lbm/ft^3$ and $\rho_{out} = 1.53\ lbm/ft^2$. Let the flow coefficient for a fully open valve be 230 and let the valve be 4.35 percent open. This gives $C_v = 10$. Since $P_{in} \geq 2P_{out}$, the second of Eq. (2.11) is used, yielding a mass flow of 16.54 lbm/s when inlet conditions are used, and of 20.36 lbm/s when oulet conditions are used. If the formula for liquid is used, the mass flow is 26 lbm/s. It should be noted that there are more sophisticated gas flow formulas which employ empirical correlations from the manufacturer. At this point, however, the above formulas will be considered to provide sufficient information for control analysis and design purposes.

2.2 Revised mixer model

A more realistic model can be derived by relaxing the constant liquid density and mixer pressure assumptions. This will require, however, the inclusion of a functional thermodynamic relation, which increases the complexity of the model. The mixer pressure as a function of density and temperature will appear either as a table look-up, or explicitly as a correlation formula. Modeling assumptions are the same as in the preliminary model, except that the density at the output and mixer pressure are allowed to vary. Also, the control flows are related to fluid properties and valve characteristics through valve models. The control variables now become the valve C_v coefficients, which in turn can be ultimately related to stem position and voltage. The latter is expected to be the controlled variable in an actual system. Considering that the output flow is entirely in the liquid phase and using the above valve models, the mass conservation equation becomes:

$$\dot{\rho}_{cv} = \frac{1}{V}\left[C_1 C_{vl}\sqrt{(P_l - P)\rho_l} + C_2 C_{vg}\frac{f(P_g, P)}{P_g}\sqrt{T_g}\rho_g - C_3 C_{ve}\sqrt{(P - P_s)\rho_{cv}}\right] \tag{2.12}$$

where V is the constant mixer volume, C_1, C_2 and C_3 are constants, C_{vl}, C_{vg} and C_{ve} are the valve flow coefficients for the LH2, GH2 and exit flow control valves, P_l, P_g are the pressures of the LH2 and GH2 upstream of the input control valves, and P is the mixer pressure, assumed to be varying in time but uniform throughout the mixer. The function $f(P_g, P)$ is chosen

according to Eq. (2.11). Note that it has been assumed that the exit density equals the density of the mixer. The energy conservation equation becomes:

$$\dot{u}_{cv} = \frac{1}{V\rho_{cv}}\left[C_1 C_{vl}\sqrt{(P_l - P)\rho_l}h_l + C_2 C_{vg}\frac{f(P_g, P)}{P_g}\sqrt{T_g}\rho_g h_g - C_3 C_{ve}\sqrt{(P - P_s)\rho_{cv}}h_{cv} - \dot{m}_{cv}u_{cv}\right] \tag{2.13}$$

Again, the exit enthalpy and density are considered equal to those within the control volume. The enthalpy at the exit can be related to other variables:

$$h_{cv} = h_e = u_e + \frac{P}{\rho_e} = u_{cv} + \frac{P}{\rho_{cv}}$$

Also, the mixer pressure is a function of the density and internal energy:

$$P = P(u_{cv}, \rho_{cv})$$

This function can be implemented as a table look-up or as an empirical correlation. For simulation purposes, the time variation of P_l, P_g, P_s, h_l, h_g and T are supposed to be known. As the model is expanded to include the run tank dynamics, some of these variables will be put in terms of quantities that are measurable in the real system. For analysis purposes, the mixer model is a system of two ordinary differential equations with three independent inputs (the valve flow coefficients). The equations become:

$$\begin{aligned}
\dot{\rho}_{cv} &= \frac{1}{V}\left[C_1 C_{vl}\sqrt{(P_l - P(u_{cv},\rho_{cv}))\rho_l} + C_2 C_{vg}\frac{f(P_g, P(u_{cv},\rho_{cv}))}{P_g}\sqrt{T_g}\rho_g - C_3 C_{ve}\sqrt{(P(u_{cv},\rho_{cv}) - P_s)\rho_{cv}}\right] \\
\dot{u}_{cv} &= \frac{1}{V\rho_{cv}}\left[C_1 C_{vl}\sqrt{(P_l - P(u_{cv},\rho_{cv}))\rho_l}(h_l - u_{cv}) + C_2 C_{vg}\frac{f(P_g, P(u_{cv},\rho_{cv}))}{P_g}\sqrt{T_g}\rho_g(h_g - u_{cv})\right. \\
&- \left. 0.185 C_3 C_{ve}\sqrt{\frac{P(u_{cv},\rho_{cv}) - P_s}{\rho_{cv}}}P(u_{cv},\rho_{cv})\right]
\end{aligned} \tag{2.14}$$

2.3 Mixer Model: Static Properties

For controller design purposes, it is of interest to gain insight on the mathematical properties of the model. Model structure can be often exploited to design better controllers. In particular, the number and nature of the equilibrium points should be investigated, as well as dynamic properties such as linearizability, stability of internal dynamics, etc.

2.3.1 Characterization of the Equilibrium Point

The equilibrium points are defined as the constant values of the state which result in zero derivatives for constant control inputs. In this case, the control inputs are the C_v coefficients. The equilibrium point indicates the steady values of the density and internal energy of the mixer when the control valves are set at fixed positions, for a given set of input flow characteristics. For given values of the input fluid properties and C_v coefficients, setting $\dot{\rho}_{cv} = 0$ establishes that $\dot{m}_e = \dot{m}_g + \dot{m}_l$ and results in an expression relating the equilibrium density $\bar{\rho}_{cv}$ to the equilibrium mixer pressure $\bar{P}$:

$$\bar{\rho}_{cv} = \rho(\bar{P}) \tag{2.15}$$

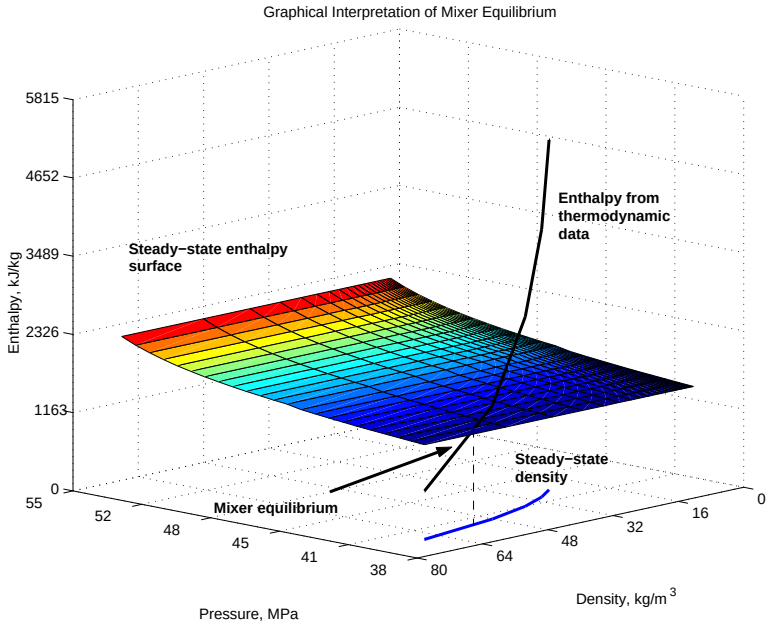

Figure 2.2: Mixer equilibrium

Setting $\dot{u}_{cv} = 0$ gives the equilibrium exit enthalpy $h_e = h_{cv}$ in terms of the input enthalpies and the mass flows:

$$\bar{h}_{cv} = \frac{\dot{m}_l h_l + \dot{m}_g h_g}{\dot{m}_l + \dot{m}_g} = \bar{h}(P) \tag{2.16}$$

The above enthalpy must match the thermodynamic property data at $\bar{P}$ and $\bar{\rho}_{cv}$ of Eq. 2.15, that is

$$\bar{h}_{cv} = h_{th}(\bar{\rho}_{cv}, \bar{P})$$

Substituting Eqs. 2.15 and 2.16 into the above equation results in a single expression which gives the equilibrium pressure:

$$\bar{h}(P) = h_{th}(\rho(\bar{P}), \bar{P}) \tag{2.17}$$

A graphical interpretation of the equilibrium solution is shown in Fig. 2.2. The curve $\rho\bar{P}$ vs. $\bar{P}$ has been drawn on the base plane. This plane curve is mapped to a space curve by the thermodynamic property function h_{th}. The equilibrium exit enthalpy $\bar{h}(P)$ is a function of pressure only and the corresponding surface has also been graphed. The point where the space curve pierces the surface is the equilibrium point of the system. It is seen to happen approximately at $P = 5800$ psia and $\rho_{cv} = 3.5 lbm/ft^3$. The monotonicity of the curve and surface suggests that there exists only one equilibrium point in the general case.

2.3.2 Iterative solution for the equilibrium point

An iteration scheme can be used to find the exact value of the equilibrium, perhaps using a graph to first find an approximate solution, as above. One possible iteration method is given below:

1. Start with an initial pressure guess, P_0.
2. Calculate the mixer equilibrium density ρ_{cv} from Eq. (2.15).
3. With P_0 and ρ_{cv} calculate the enthalphy h_{th} using thermodynamic data.
4. With P_0 calculate the steady-state enthalpy h_{cv} from Eq. (2.16).
5. Calculate the error $e = h_{cv} - h_{th}$.
6. Correct the pressure guess using $P \leftarrow P + ke$, where k is a convergence factor.
7. Repeat steps 2 through 6 until the error is within a prescribed tolerance.

The above steps have been coded in Matlab and it has been determined that, for the expected values of mixer operation, $k = 0.1$ is a good convergence factor. The following is a sample run using the pressure guess value from the graphical method:

```
>> solv_mxr_eq

ans =

Convergence achieved in 23 iterations


P =

  5.8745e+003


e =

  9.6981e-004


rho_cv =

    3.2538


h_th =

  609.8934
```

2.3.3 Methods of evaluating $P(\rho, u)$

The NIST thermodynamic data for Hydrogen can be accessed using a the MIPROPS program. For Matlab simulation purposes, it would be desirable to have the pressure information as a

table, since the table look-up blocks included in Simulink greatly simplify the simulation setup. However, MIPROPS provides density, internal energy, -and other thermodynamic data- for regularly spaced temperature points and a specific pressure. Conversion of such data into a rectangular array with pressure entries for given density and internal energy is not a trivial task. If pressure and temperature ranges are set, and density and energy data are extracted using MIPROPS, it is seen that the set of all density-energy pairs has a non-rectangular boundary upon plotting. Moreover, the density-energy points are irregularly spaced. Extending such boundary to a rectangular one and regularizing the grid of points to conform a rectangular array is cumbersome and introduces error due to interpolation. Instead of attempting to obtain a pressure table, it is more convenient to write a function that determines the pressure based on available data. Three methods are considered and explained as follows.

2.3.4 Method 1

This method considers that the internal energy is a function of temperature only. In reality, the energy-temperature curve varies with pressure. The given internal energy is mapped into temperature using the curve for some pressure within the expected range of operation. Once the temperature has been obtained, a pair of bracketing temperatures are found in the density-energy table, and interpolation is used to find the pressure.

2.3.5 Method 2

This method finds bracketing energies among all entries of the density-energy table. From the bracketing energies found, only those whose corresponding densities bracket the given density are kept. Those energy brackets are interpolated for density using the given energy, and the bracket that yields the interpolated density that is closest to the given density is selected. The pressure corresponding to the bracket is returned by the function.

2.3.6 Method 3

This method uses Method 1 to find the pressure once the temperature is known. The temperature, however, is not found exclusively from the energy, but from the full density-energy data. The above methods have been programmed in the Matlab function files **getpress.m**, **gettemp.m** and **getpt.m** listed at the appendix.

2.3.7 Comparison of Methods

The Simulink diagrams of the mixer model using Methods 1,2 and 3 are shown in Figs. 2.3, 2.4,and 2.5.

A comparison of the methods is shown in Fig. 2.6. It is seen that methods 2 and 3 provide results that are closer together relative to method 1. It is also seen that the basic model of Section 2.1.1 introduces significant error in energy. However, upon translation of the energy into temperature, the error is reduced. It must also be pointed that method 2 has the largest execution time, while method 1 and the basic model have the smallest. Method 3 provides a good compromise between speed of execution and accuracy. Fig. 2.7 shows how the model in conjunction with method 3 can be used to simulate a change in valve position. Initially,

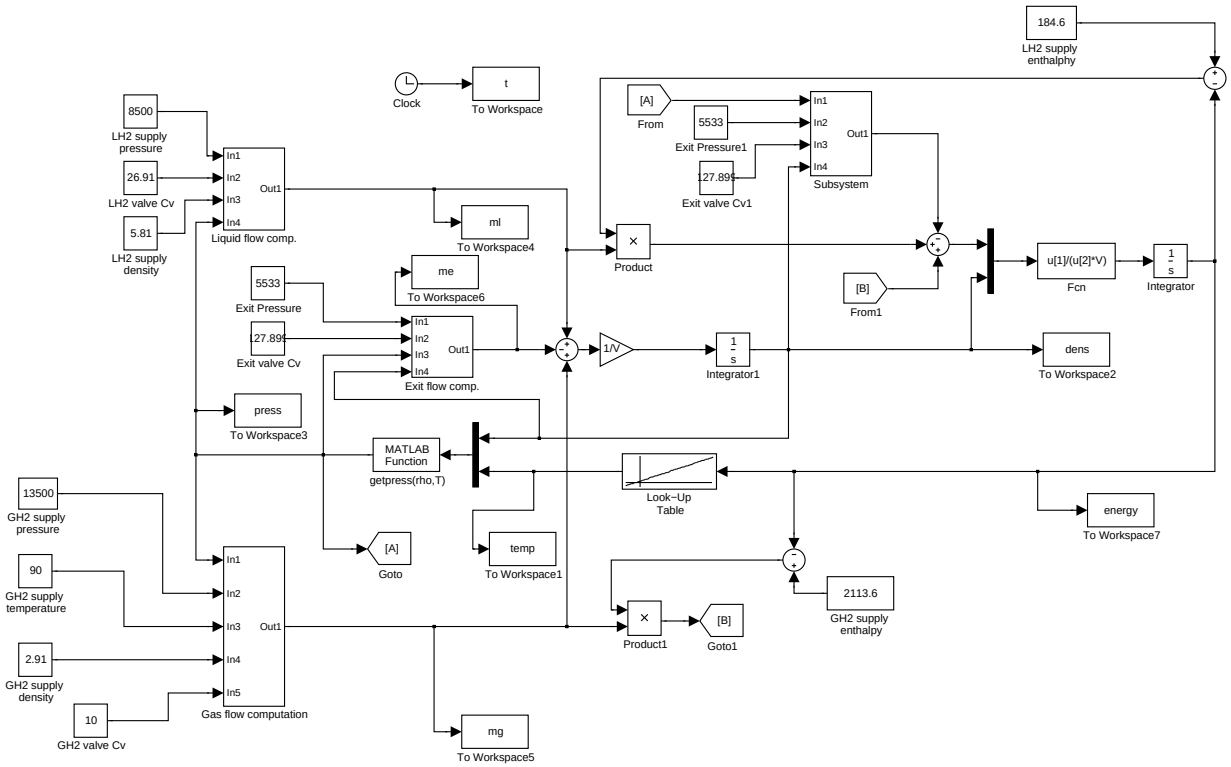

Figure 2.3: Mixer Simulation - Method 1

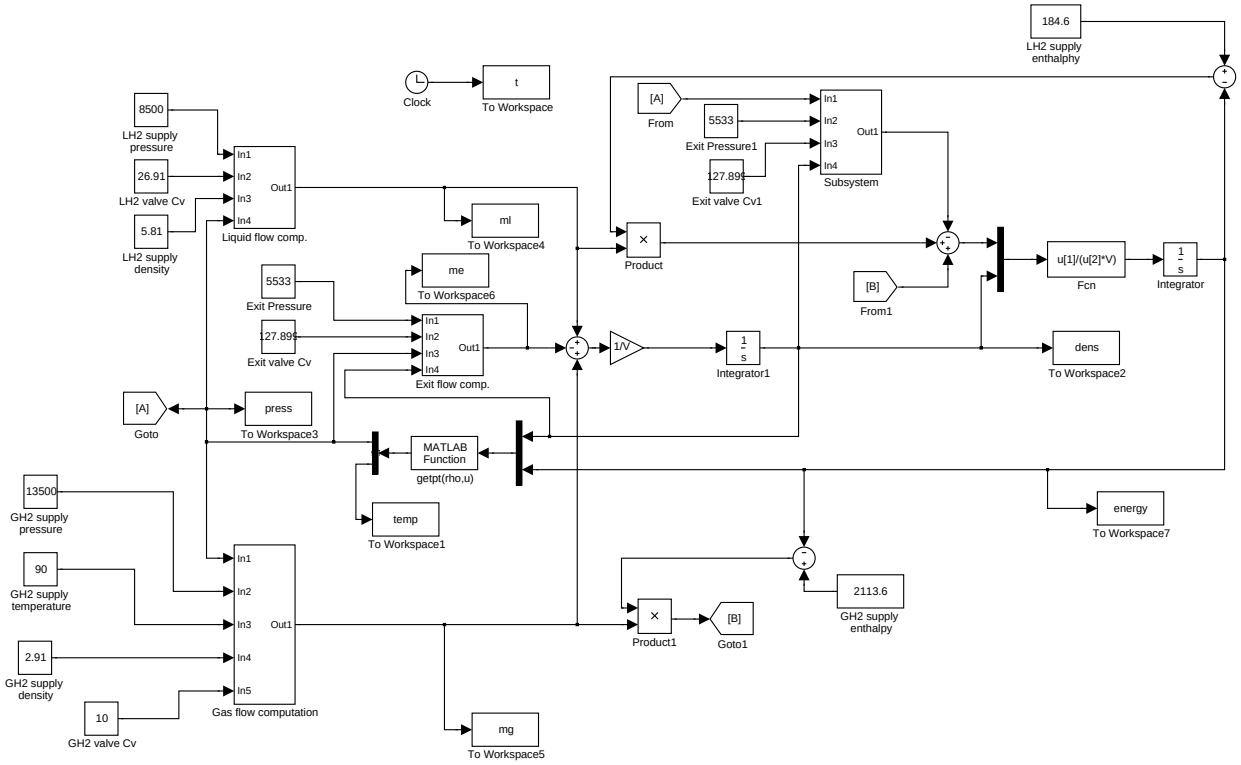

Figure 2.4: Mixer Simulation - Method 2

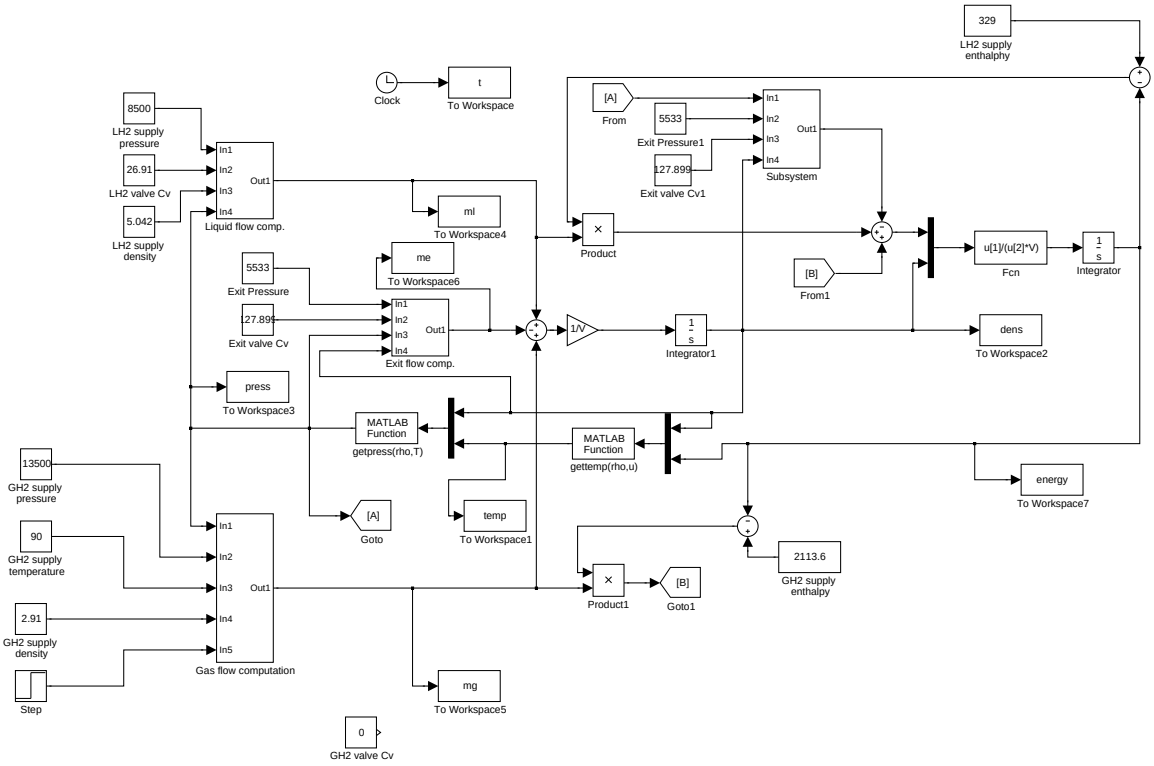

Figure 2.5: Mixer Simulation - Method 3

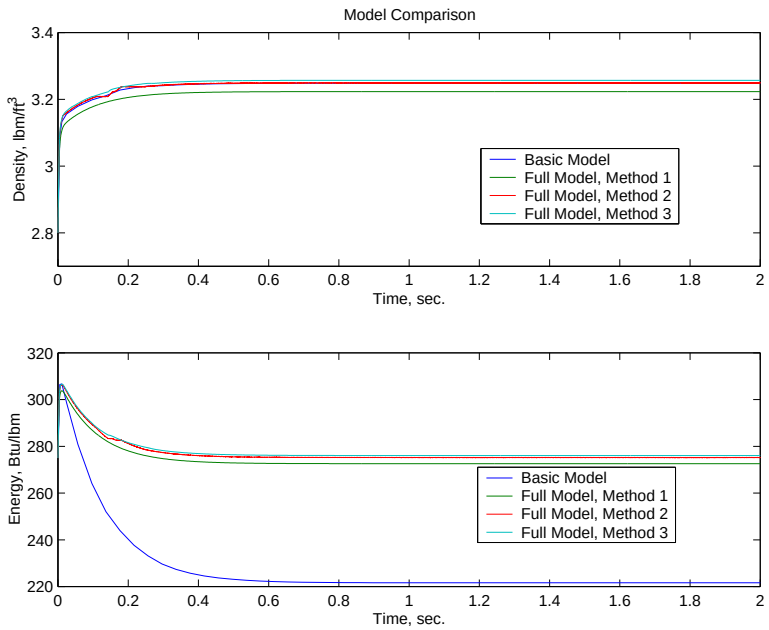

Figure 2.6: Mixer Simulation - Comparison of Methods

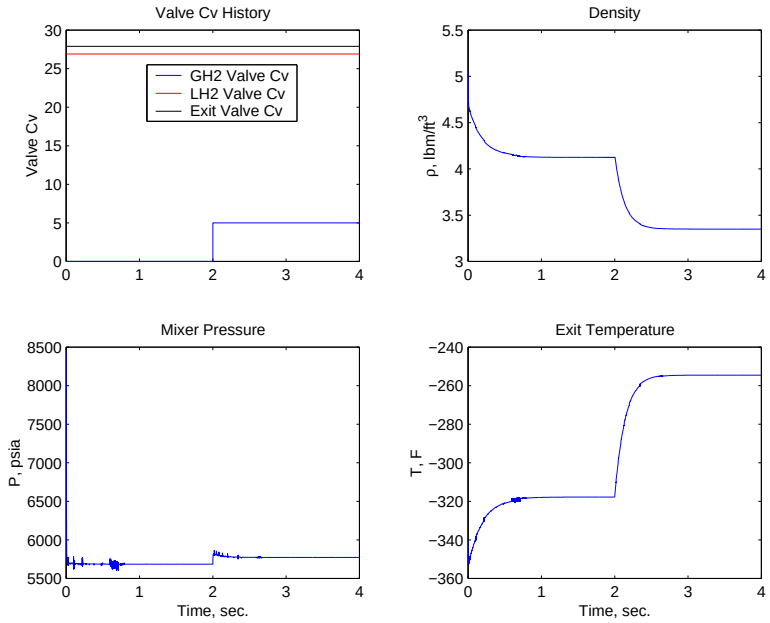

Figure 2.7: Mixer Simulation - Varying Cv

only LH2 flows through the mixer. Then, the GH2 valve is suddenly opened, resulting in a temperature increase of the exit flow.

2.3.8 Valve positions for a prescribed static operating condition

Having three independent controls in a two-state model allows the selection of steady values for the states, and, in addition, an extra degree of freedom is available. This degree of freedom can be used to fix the exit mass flow with the desired thermodynamic properties, as shown next. Supppose it is desired to have a given exit mass flow, with prescribed temperature (measured at the outlet of the exit valve). Let these quantities be denoted by W_e and T. The back pressure P_s at the outlet valve exit is assumed to be constant. The problem is to determine the valve coefficients that achieve this. Two degrees of freedom are used for W_e and T, and the third one is used to meet a desired mixer operating pressure, P. The back pressure P_s and T determine the enthalpy h, which is constant across the valve. Therefore, the enthalpy and mixer pressure at the exit valve inlet are known and, in turn, determine the mixer density from thermodynamic data. A static energy and material balance gives the required input flows that achieve a prescribed flow-exit enthalpy combination. The following formulas are straightforward to derive:

$$\begin{aligned} W_l &= \frac{W_e(h - h_g)}{h_l - h_g} \\ W_g &= \frac{W_e(h_l - h)}{h_l - h_g} \end{aligned} \tag{2.18}$$

where h_g and h_l are the gas and liquid supply enthalpies, respectively. Using the exit flow and the input equilibrium flows from Eq. 2.18, the three valve coefficients are determined from

Eq. (2.10) and (2.11). A Matlab program **mxr-cv.m** carries out the necessary computations. As an example, an operating condition is targeted. Then, the resulting C_v values are fed into the inverse program which computes the operating point. The operating conditions are recovered with good accuracy. Suppose the C_v values that achieve an exit flow of 80 lb/s at a temperature of $-300^{\circ}F$ with a mixer operating pressure of 7000 psia are sought. The values returned are

```
>> [Cvl,Cvg,Cve]=mxr_cv(-300,80,7000)

h =

  384.8930


Cvl =

   43.6348


Cvg =

    5.0234


Cve =

   56.9665
```

The equilibrium-finding program returns

```
>> solv_mxr_eq

ans =

Convergence achieved in 111 iterations


P =

  7.0023e+003


e =

  9.8624e-004
```

```
rho_cv =

    4.3345


h_th =

  386.4838


exit_flow =

   80.0122
```

Although system controllability will be analyzed rigorously in another section, the ability to select the operating point as shown above suggests that the system is indeed controllable.

2.4 Model Validation

The mathematical model of the mixer given by Eqs.(2.14) are valid regardless of the substance flowing through it. Preliminary tests of mixer operation at SSC have been performed with nitrogen as a working substance. One of such tests is used to verify the prediction capabilities of the model, together with its accesory programs giving pressure and temperature from given density and internal energy.

2.4.1 Test Sequence

The objective of the test is to obtain a desired temperature of the exit flow by means of the introduction of GN2 to the LN2 stream in the mixer. In the test configuration, the exit valve was replaced by an orifice. This does not represent a difficulty in using the model, since it can be assumed that the exit valve in the model remains open at a fixed position. The equivalent exit valve C_v is found from the experimental data. The mixed flow is released into the atmosphere. Valve openings are precalculated so that the mass flows match desired quantities, namely, $w_l = 22$ lbm/s, $w_g = 16$ lbm/s and, in steady state, $w_e = 38$ lbm/s. Pressure inside the mixer must also be maintained at a desired level, namely $P = 600$ psig. To achieve this, and as starting approach, the pressure is continuosly measured and used in a PID control loop around the gas valve *only*. The test sequence is as follows:

1. Open the LN2 valve to 4% to chill down pipes.
2. Pressurize the LN2 source to 1000 psig.
3. Ramp the LN2 valve to 40%.
4. Manually command the GN2 valve until a mixer pressure of 600 psig is reached.
5. Close both valves to 3%. (apparently, the previous steps were done to determine the opening of the GN2 valve to obtain 600 psig).

6. Ramp the LN2 valve back to 40%.
7. Ramp the GN2 valve to approx. 40% and close the PID control of mixer pressure. Since the valve opening is close to the already determined value, a relatively bumpless transfer occurs.
8. Close the valves and terminate the test.

The following data where gathered at all times during the test:

- LN2 and GN2 valve positions.
- LN2 and GN2 inlet pressures (upstream of the valves).
- LN2 and GN2 inlet temperatures (upstream of the valves).
- Mixer pressure.
- Mixer temperatue.

Note that the flows were not measured, but calculated from pressure differences, fluid properties and valve positions. The duration of the test data is 2400 seconds, with data sampled every 0.02 seconds. This results in data records containing more than 100000 points. For simulation in a PC to be practical, the data must be reduced. Data was processed using Matlab's **resample** command, which decimates and filters the data according to user specifications. Resampling and filtering was applied to yield data records having little more than 1000 points each.

2.4.2 Model Simulation

The valve positions and inlet fluid properties of the test are shown in Fig. 2.8. The sudden drop in temperature observed for the LN2 was not handled by any of the numerical methods available in SIMULINK. Since significant valve activity begins after the drop, where LN2 temperature is practically constant, this constant value is used as an input at all times. Note that this is possible to do given that the mixer response is in the order of seconds. The other resampled data is directly fed to the mixer model using the "From Workspace" blocks in SIMULINK. The time horizon for the simulation was restricted to the first 920 seconds, which contain the most useful information. It is important to note that some numerical problems were obtained due to interaction of SIMULINK's integration routine ode45 (Runge-Kutta 45) and the property program **yourprops.m**. After several attempts, it was determined that a reliable simulation is obtained using the following parameters:

- Integration Method: Variable-step ODE23 (Bogacki-Shampine).
- Maximum step size: 0.05
- Initial step size: 0.001
- Relative tolerance: 0.001
- Absolute tolerance: determined by SIMULINK.
- Refine factor: 2

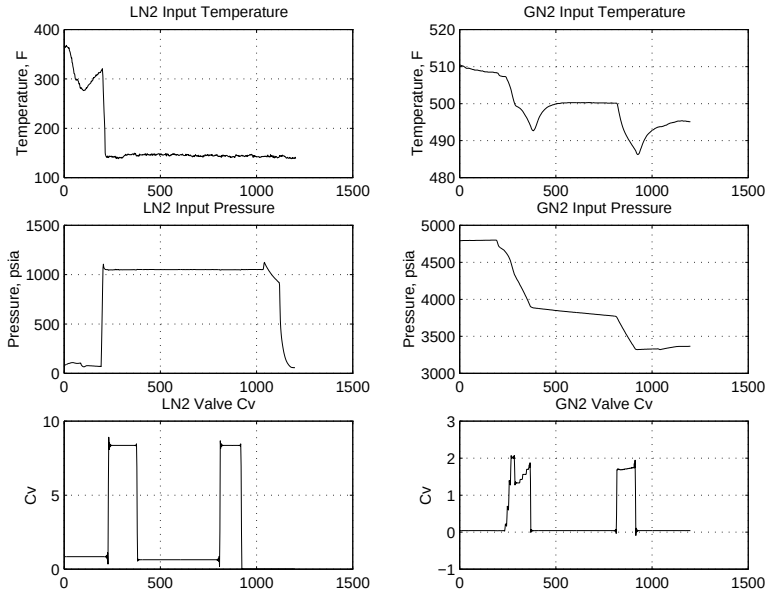

Figure 2.8: Valve positions and inlet fluid properties during validation test.

2.4.3 Model Calibration

The data measured during the test shows pressures that fall below zero. This may be attributable to instrument offset which becomes important when actual pressures are low. It is to be noted that the mathematical model will not produce negative absolute pressures. This induces a slight discrepancy between measured and simulated values. Also, the current version of **yourprops.m** handles pressures starting at 20 psia. This value was used as atmospheric pressure during simulation, and it also constitutes a small discrepancy. The valve models are calibrated to reproduce the calculated steady flows given by the test operators. The mixer pressure of 614.7 psia and temperature of $-222^{\circ}F$ corresponds to a density of 17.287 lbm/s. With the flow formula of Eq. (2.10) and the 38 lbm/sec exit flow it is obtained that the equivalent C_{ve} of the orifice is 21.2. This was later adjusted to $C_{ve} = 19$ to match experimental data. Similarly, it is obtained that $C_{vg} = 1.7$ and $C_{vl} = 8.35$ for 37/

2.4.4 Results

Fig. 2.9 shows the resulting state trajectories and flows, along with an error variable which ensures that there were no errors in **yourprops.m**. Figs. 2.10 and 2.11 constitute the validation. In view of the expected discrepancies explained above, it can be said that the agreement is very good.

2.4.5 Immediate Improvements to the Model

The following improvements can be made to have a better prediction capability (listed in order of expected effectiveness):

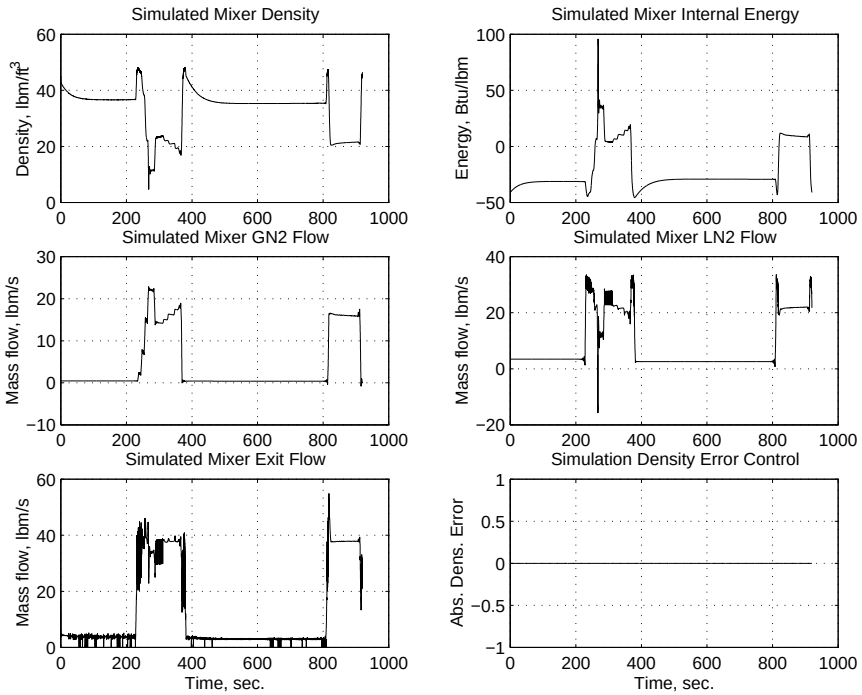

Figure 2.9: Simulated mixer states.

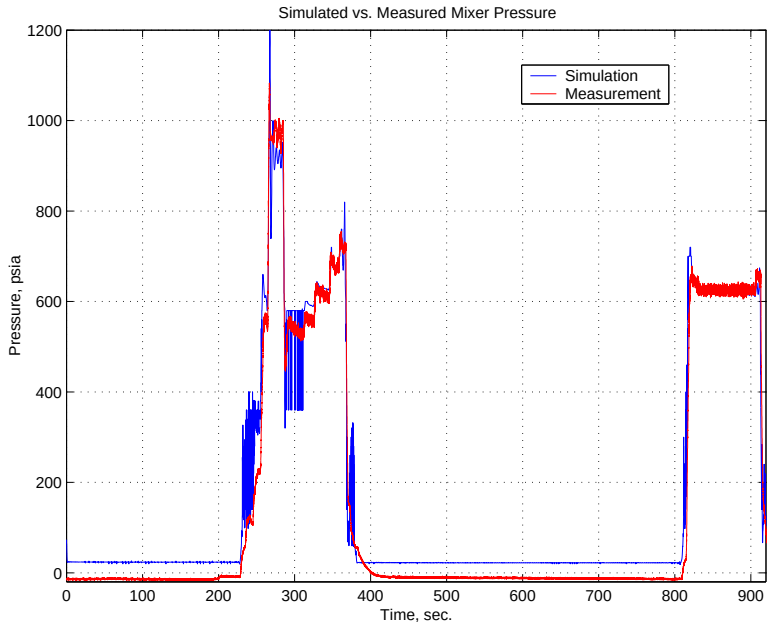

Figure 2.10: Simulated and measured mixer pressure.

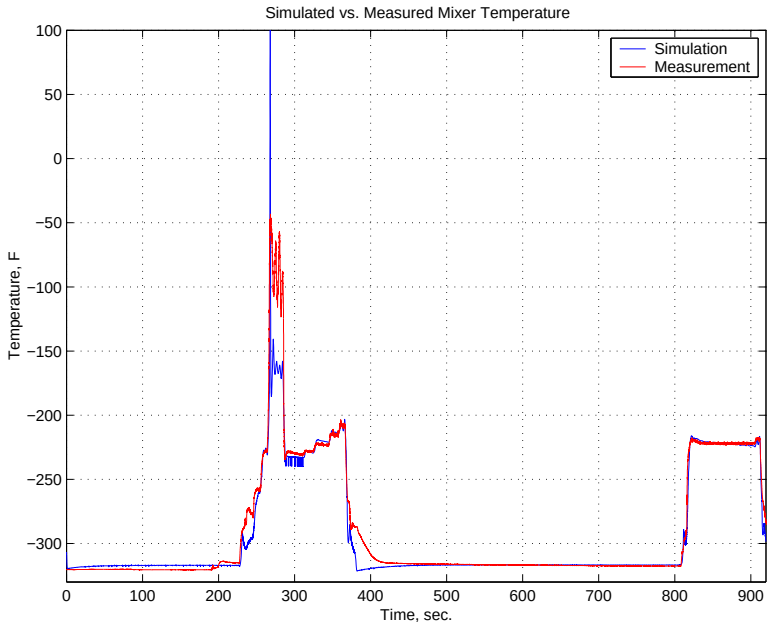

Figure 2.11: Simulated and measured mixer temperature.

- Expand the pressure range of the **yourprops** program to include near-zero pressure. This will allow to set the atmospheric pressure in the simulation to the correct value.
- Obtain the true value of the bottom pressure of the mixer that was obtained during the test. Shift the data and recalibrate the Cv values.
- Include first-order lag dynamics in the valve models.

The model can be further refined by performing flow experiments with the valves in order to determine more accurate descriptions. Also, the current model uses valve Cv as a primary input variable. Valve dynamics can be further studied to replace the control inputs in the model by *commanded* valve position, which are electrical signals to be used in an actual controller.

Chapter 3

Feedback Linearization Analysis

Of the control techniques that are suitable for the model structure, feedback linearization is the simplest and most direct. The technique, however, may have disadvantages. Specifically, the complexity introduced by the cancellation of all nonlinear dynamics may be to high for a realistic implementation with limited computational resources. The other significant disadvantage is that all state measurements are required. Peaking of control signals is also a factor of concern, especially when actuator saturation and rate limitations are present. The technique, however, is worth examining, since essential features of the model appear during the analysis.

3.1 Output Definitions

Mixer operation requires tracking of prescribed output mass flow and temperature profiles. As seen in a previous section, the extra degree of freedom of the system can be used to specify the mixer operating pressure in addition to temperature and mass rate of the out flow, given that the output pressure P_s is known and constant. While this is true for equilibrium conditions, it will now be assumed that simultaneous tracking of the three quantities is also possible. Note that this amounts to specifying a desired output vector whose components are temperature at the exit valve outlet, mixer pressure, and exit mass flow rate. All of the above quantities are rather complicated functions of the state $[\rho \quad u]^T$. In order to simplify matters, the following observations are made: specifying the temperature at the exit valve outlet determines the enthalpy, since P_s is known and constant. The enthalpy, in turn, is constant across the valve, and therefore matches that of the mixer. If mixer density is specified according to the enthalpy in a way such that the resulting pressure matches the desired pressure profile, then density can be used as a desired output. Since the prescribed density and enthalpy also determine the internal energy, the latter can be used as another desired output. The third output, the mass flow rate, is kept as a function of the states. Summarizing, the outputs are defined as

$$y = \begin{bmatrix} \rho \\ u \\ C_3\sqrt{(P(\rho,u)-P_s)\rho}C_{ve} \end{bmatrix} \tag{3.1}$$

The corresponding desired quantities are precomputed from the desired pressure, temperature and mass flow rate profiles as follows:

1. With P_s and the prescribed output temperature profile, find the enthalpy profile.

2. With the enthalpy and mixer pressure profiles, find the internal energy and density profiles.

3. The desired mass flow rate profile is used directly.

3.2 Relative Degree and Input Integration

The model of Eqs. 2.14 along with the outputs defined above can be compactly written as

$$\begin{aligned} \dot{\rho} &= f_1(P(\rho,u),\rho)C_{vl} + f_2(P(\rho,u),\rho)C_{vg} + f_3(P(\rho,u),\rho)C_{ve} && (3.2)\\ \dot{u} &= g_1(P(\rho,u),\rho,u)C_{vl} + g_2(P(\rho,u),\rho,u)C_{vg} + g_3(P(\rho,u),\rho,u)C_{ve} && (3.3)\\ y &= [\rho \quad u \quad -Vf_3(P(\rho,u),\rho)C_{ve}]^T && (3.4) \end{aligned}$$

where the function definitions are chosen to match Eqs. (2.14) and (3.1) and V is the constant mixer volume. The model has certain characteristic which prevents direct application of input/output linearization theory. It is seen that the third component of y is statically related to one of the control inputs, namely C_{ve}. This implies that the partial relative degree of y_3 is zero. Conceivably, one could use a time-explicit control of the form

$$C_{ve}(t,\rho,u) = -\frac{y_{3d}}{Vf_3(P(\rho,u),\rho)}$$

to attain perfect tracking of the output mass flow rate and use the two remaining controls to force the flow to have the desired pressure and temperature. This approach suffers from two drawbacks: the most serious one lies in the fact that the resulting reduced two-input, two-output system may be rendered non-minimum phase by the choice of $C_{ve}(t,\rho,u)$. Even if the reduced system is minimum-phase, the lack of robustness of a feedforward law is still questionable.

One way to get around this problem altogether is to augment the exit valve channel with an integrator, that is, let:

$$\dot{C}_{ve} = v$$

where v is a new control input. Now C_{ve} is regarded as a state, and the resulting system is of third order, with three inputs and outputs. If the arguments of functions g_i and f_i are dropped from the notation, the new system equations become:

$$\begin{aligned} \dot{\rho} &= f_1C_{vl} + f_2C_{vg} + f_3C_{ve} && (3.5)\\ \dot{u} &= g_1C_{vl} + g_2C_{vg} + g_3C_{ve} && (3.6)\\ \dot{C}_{ve} &= v && (3.7)\\ y &= [\rho \quad u \quad -Vf_3C_{ve}]^T && (3.8) \end{aligned}$$

Upon differentiating the outputs once, it is seen that the partial relative degrees are all 1:

$$\dot{y}_1 = f_1 C_{vl} + f_2 C_{vg} + f_3 C_{ve} \tag{3.9}$$

$$\dot{y}_2 = g_1 C_{vl} + g_2 C_{vg} + g_3 C_{ve} \tag{3.10}$$

$$\begin{aligned}\dot{y}_3 = & -V \left[v f_3 + C_{ve} \left(\frac{\partial f_3}{\partial P} \frac{\partial P}{\partial \rho} (f_1 C_{vl} + f_2 C_{vg} + f_3 C_{ve}) + \right.\right. \\ & + \frac{\partial f_3}{\partial P} \frac{\partial P}{\partial u} (g_1 C_{vl} + g_2 C_{vg} + g_3 C_{ve}) \\ & + \left.\left. \frac{\partial f_3}{\partial \rho} (f_1 C_{vl} + f_2 C_{vg} + f_3 C_{ve}) \right) \right]\end{aligned} \tag{3.11}$$

Upon rearranging, the output derivatives can be expressed compactly as

$$\begin{bmatrix} \dot{y}_1 \\ \dot{y}_2 \\ \dot{y}_3 \end{bmatrix} = \begin{bmatrix} f_3 C_{ve} \\ g_3 C_{ve} \\ -V C_{ve}^2 [\frac{\partial f_3}{\partial P} (\frac{\partial P}{\partial \rho} f_3 + \frac{\partial P}{\partial u} g_3) + \frac{\partial f_3}{\partial \rho} f_3] \end{bmatrix}$$

$$+ \begin{bmatrix} f_1 & f_2 & 0 \\ g_1 & g_2 & 0 \\ -V C_{ve} [\frac{\partial f_3}{\partial P} (\frac{\partial P}{\partial \rho} f_1 + \frac{\partial P}{\partial u} g_1) + \frac{\partial f_3}{\partial \rho} f_1] & -V C_{ve} [\frac{\partial f_3}{\partial P} (\frac{\partial P}{\partial \rho} f_2 + \frac{\partial P}{\partial u} g_2) + \frac{\partial f_3}{\partial \rho} f_2] & -V f_3 \end{bmatrix} \begin{bmatrix} C_{vl} \\ C_{vg} \\ v \end{bmatrix}$$

or,

$$\dot{y} = D + E w$$

Provided E is invertible in a region Ω of the state space, the feedback law

$$w = E^{-1}(\dot{y}_d - \Gamma(y - y_d) - D) \tag{3.12}$$

achieves exact linearization of the system, with tracking error dynamics given by

$$(\dot{y} - \dot{y}_d) + \Gamma(y - y_d) = 0$$

If Γ is chosen as a diagonal positive-definite matrix, the resulting control law is called "decoupling control", since the dynamics of the outputs are decoupled. If the appropriate function definitions are substituted, the forms of the E and D matrices are as follows:

$$\begin{aligned} f_1 &= C_1' \sqrt{(P_l - P)\rho_l} \\ f_2 &= C_2', \text{ if } P_g \geq 2P \\ f_2 &= C_4' \sqrt{P_g^2 - P^2}, \text{ if } P_g < 2P \\ f_3 &= C_3' \sqrt{(P - P_s)\rho} \\ g_1 &= C_1' \sqrt{(P_l - P)\rho_l} \left(\frac{h_l - u}{\rho} \right) \\ g_3 &= C_3'' \sqrt{\frac{P - P_s}{\rho}} \frac{P}{\rho} \end{aligned}$$

$$D = \begin{bmatrix} C_3' \sqrt{(P - P_s)\rho} C_{ve} \\ C_3'' \sqrt{\frac{P - P_s}{\rho}} \frac{P}{\rho} C_{ve} \\ -\frac{V C_{ve}^2 C_3'^2}{2} \left[\rho \frac{\partial P}{\partial \rho} + 0.185 \frac{P}{\rho} \frac{\partial P}{\partial u} + (P - P_s) \right] \end{bmatrix}$$

$$E = \begin{bmatrix} C_1'\sqrt{(P_l - P)\rho_l} & f_2 & 0 \\ C_1'\sqrt{(P_l - P)\rho_l}\left(\frac{h_l - u}{\rho}\right) & f_2\left(\frac{h_g - u}{\rho}\right) & 0 \\ -\frac{VC_{ve}C_1'C_3'\sqrt{(P_l-P)\rho_l}}{2\sqrt{(P-P_s)\rho}}\left[\rho\frac{\partial P}{\partial \rho} + (h_l - u)\frac{\partial P}{\partial u} + (P - P_s)\right] & -\frac{VC_{ve}f_2C_3'}{2\sqrt{(P-P_s)\rho}}\left[\rho\frac{\partial P}{\partial \rho} + (h_g - u)\frac{\partial P}{\partial u} + (P - P_s)\right] & -VC_3'\sqrt{(P - P_s)\rho} \end{bmatrix}$$

where the constants C_1', C_2', C_3' and C_4' are related to those of Eq. 2.14 by $C_1' = C_1/V$, $C_2' = C_2\sqrt{T_g}\rho_g/V$, $C_3' = -C_3/V$, $C_3'' = 0.185C_3'$ and $C_4' = C_4\sqrt{T_g}\rho_g/V$.

3.3 Input-Output Linearizability of Augmented Model

The ability to construct a feedback linearization controller hinges, firstly, on stable zero dynamics of the augmented system, and, secondly, on the invertibility of matrix E.

3.3.1 Invertibility of E

By inspection, it is readily seen that the first two rows of E are linearly independent provided $h_g \neq h_l$. This has a direct physical interpretation: if the two fluids have the same thermal properties (i.e., enthalpies), the ability to change the thermal properties of the mixture by changing the relative flows is lost. Gas and liquid enthalpies are different for the expected operating conditions. The third row is linearly independent from the first two if $P - P_s > 0$, which is also true for the mixer. Therefore E is invertible over the whole range of expected mixer operating conditions.

3.3.2 Zero Dynamics of the Augmented Model

As it is known, the zero dynamics is preserved under input transformations. This implies that one may examine the non-augmented model for zero dynamics and draw conclusions about the augmented model's zero dynamics. Suppose the exit flow is to be held constant at a value Y_{30}. The only way in which this can be achieved is by letting

$$C_{ve}(t) = -\frac{Y_{30}}{Vf_3(t)} \tag{3.13}$$

at all times. Differentiating the other two outputs and equating them to zero results in

$$C_{vl}(t) = \frac{1}{f_1(t)}\left(-f_2(t)C_{vg}(t) + \frac{Y_{30}}{V}\right) \tag{3.14}$$

$$C_{vg}(t) = -\frac{1}{g_2(t)}\left(g_1(t)C_{vl}(t) + \frac{g_3(t)Y_{30}}{Vf_3(t)}\right) \tag{3.15}$$

Upon substitution and rearrangement, it is seen that there exist three uniquely defined control inputs which hold the outputs constant. Since two of the outputs coincide with the states, it trivially follows that they are kept bounded, and therefore the system has stable zero dynamics (i.e., the system is *minimum-phase*). The control inputs are given by Eq. (3.13) and, dropping the time notation,

$$C_{vg} = \frac{\frac{Y_{30}f_1}{V}\left(\frac{g_3}{f_3} - \frac{g_1}{f_1}\right)}{f_1g_2 - g_1f_2} \tag{3.16}$$

$$C_{vl} = \frac{Y_{30}}{Vf_1}\left[1 - \frac{f_1f_2}{f_1g_2 - g_1f_2}\left(\frac{g_3}{f_3} - \frac{g_1}{f_1}\right)\right] \tag{3.17}$$

Note that the above formulas can be used to find the valve positions at which the system has a prescribed outflow and a pair of thermodynamic properties. Therefore it produces the same results as the program **mxr-cv** described earlier.

3.4 Implementation Issues

Aside from the computational burden introduced by the inversion of E at each time step, the control law requires knowledge of the partial derivatives $\frac{\partial P}{\partial \rho}$ and $\frac{\partial P}{\partial u}$ at all times. This significantly increases the complexity of the controller, since not only $P(\rho, u)$ is required as a table, but two extra tables are required which contain the partial derivatives. The complexity is somewhat reduced by noticing that one of such partial derivatives has a very small value for the range of properties of Hydrogen considered. In fact, all thermodynamic data in use for mixer simulations consists of a table of densities and internal energies as a function of pressure and temperature. That is,

$$\rho = \rho(P, T)$$

and

$$u = u(P, T)$$

The data for Hydrogen between 2000 and 13500 psia and -400 and 200°F reveals that

$$\left.\frac{\partial u}{\partial T}\right|_P >> \left.\frac{\partial \rho}{\partial T}\right|_P \tag{3.18}$$

For the above pressure and temperature ranges, it is possible to show from the data that given density and internal energy, one can recover the pressure and temperature. That is,

$$P = P(\rho, u)$$

and

$$T = T(\rho, u)$$

are functions of two variables. Noting that P and T are independent variables we have

$$\frac{\partial P}{\partial T} = \frac{\partial P}{\partial \rho}\frac{\partial \rho}{\partial T} + \frac{\partial P}{\partial u}\frac{\partial u}{\partial T} = 0$$

and making use of Eq. 3.18 it is seen that

$$\frac{\partial P}{\partial u} \approx 0$$

Thus the above partial derivative is set to zero in matrices D and E. The other partial derivative can be found as

$$\frac{\partial P}{\partial \rho} = \frac{1}{\frac{\partial \rho}{\partial P}}$$

The derivative on the right is readily found from the data matrices.

Even though it is unlikely that the control resources available can accommodate even one partial derivative, a simulation study using derivative information is carried out next. It provides a basis for comparison of other designs, since the feedback linearization controller with full information is expected to give excellent performance.

Parameter	Value	Units
P_l	8500	psia
T_l	-340	$^\circ F$
P_g	13500	psia
T_g	90	$^\circ F$
P_s	5533	psia
ρ_o	3.85	lbm/ft^3
u_o	180	Btu/lbm

Table 3.1: Feedback Linearization Parameters

3.5 Simulation Study of the Feedback Linearization Controller

The purpose of the study is to test the suitability of the partial derivative approximations and to provide insight about the limits to attainable performance. Initial simulations will hold plant parameters constant and assume that valves open instantaneously. Then the thermodynamic properties of the supply fluids will be perturbed to reflect actual operating conditions. First order dynamics and saturation will be imposed on the valves and the performance of the nominal controller evaluated.

3.5.1 Nominal performance

Table 3.1 summarizes the parameters used in the simulations. The decoupled control gains were set as 10 for the density, 10 for the energy and 5 for the exit flow. The controller has exact knowledge of these parameters, except the initial conditions. The objective in Simulation 1 is to transfer the mixer from the initial conditions to a pressure of 6000 psia, exit temperature of $-200^\circ F$ and exit flow of 40 lbm/s. With the known and fixed back pressure it is determined that the mixer states must be transferred to $\rho = 2.93\ lbm/ft^3$ and $u = 400.9$ Btu/lbm for the pressure and exit temperature to converge to their desired values. The reference states and flow are specified as constants, leaving the trajectories to be determined by the controller. In Simulation 2, the mixer is asked to reach the previous equilibrium point and then raise the exit temperature to $0^\circ F$ and the pressure to 7000 psia, while reducing the exit flow to 10 lbm/s. This corresponds to lowering the density to $\rho = 2.143$ and raising the energy to $u = 995.9$. This time, the states and the flow are required to track ramp functions which transfer from old to new values in 5 seconds. Figs. 3.1 and 3.2 show the results of Simulations 1 and 2, respectively. The steady values required are exactly achieved. However, the transient response of the exit flow in the simulations has overshoot. This may be reduced by modifying the control gains, but perhaps at the expense of slowing down the response.

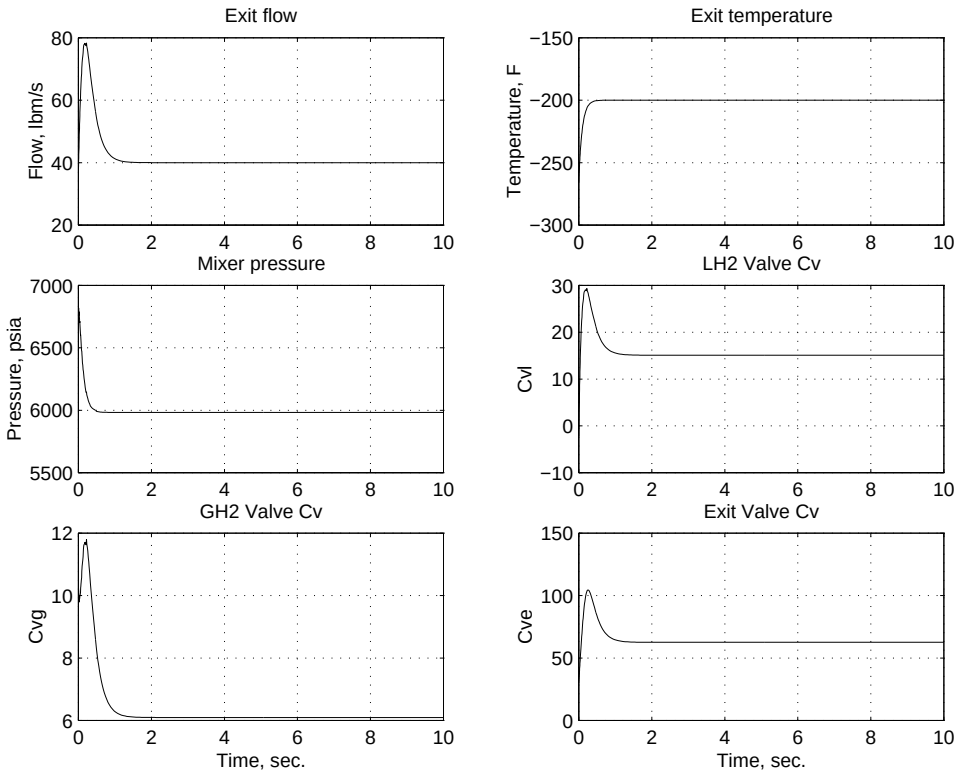

Figure 3.1: Simulation of Feedback Linearization Controller

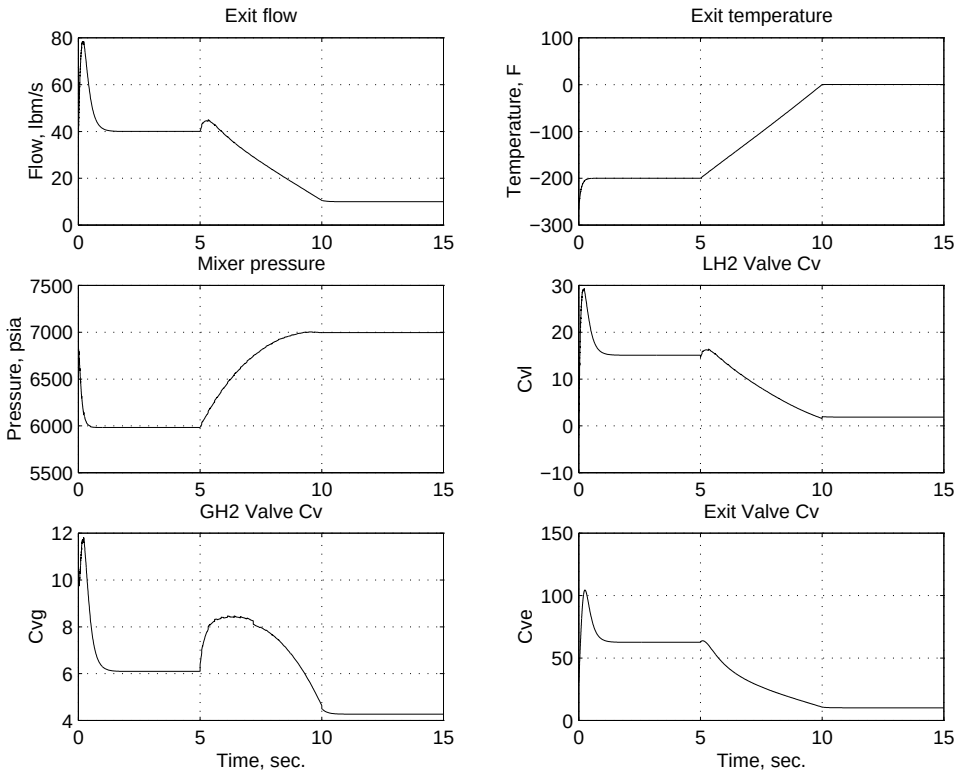

Figure 3.2: Simulation of Feedback Linearization Controller

Chapter 4

Sliding Mode Control of the Mixer with Valve Dynamics

4.1 Mixer Model with Valve Dynamics

The developments of the previous sections assume that there is direct and instantaneous command over the valve opening coefficients, which are taken as control inputs. In reality, a C_v coefficient is the response of the valve to a given command. The valves have their own analog controller, which makes the valve behave as a first order linear system with certain gain and time constant. Thus, it is assumed that the valve models are given by

$$\dot{C}_v = A_c C_v + B_c \zeta \tag{4.1}$$

where $A_c = \text{diag}(-1/\tau_1,\ -1/\tau_2,\ -1/\tau_3)$, $B_c = [\beta_1\ \beta_2\ \beta_3]^T$, τ_i are the time constants of the liquid, gas and exit valves and β_i are their respective gains, $\zeta = [\zeta_1\ \zeta_2\ \zeta_3]^T$ is the vector of control inputs to the liquid, gas and exit valves, and $C_v = [C_{vl}\ C_{vg}\ C_{ve}]^T$ is the vector of valve opening coefficients. The C_v coefficients now become states in the model equations, which can be written as

$$\begin{aligned}
\dot{\rho} &= \frac{1}{V} C_v^T f && (4.2)\\
\dot{u} &= \frac{1}{V} C_v^T A_p f && (4.3)\\
\dot{C}_v &= A_c C_v + B_c \zeta && (4.4)\\
y &= [\rho\ \ u\ \ C_{ve} f_e]^T && (4.5)
\end{aligned}$$

where $f = [f_1\ \ f_2\ \ -f_e]^T$ and $A_p = \text{diag}(\frac{h_l - u}{\rho},\ \frac{h_g - u}{\rho},\ 0.185\frac{P}{\rho^2})$. The feedback linearization controller presented earlier has several disadvantages which limit its applicability in the real system. One of the most salient disadvantages is its lack of robustness due to dependence on an accurate model and constancy of parameters. Both can be handled by means of Sliding Mode Control, a technique which is specifically tailored to work with multivariable systems with certain types of distrubances and parameter variations. In the specific case of the mixer, the most significant unmodeled effect is the heat transfer with the environment. Although possible to model in principle, a quantitative description of the heat transfer through mixer

walls involves awkward convection correlations with parameters which are heavily dependent on temperature and flow characteristics. The convection coefficients can be extremely uncertain and often have to be found through iteration, even for the steady heat transfer calculations. For control purposes, it is far more convenient to treat the heat transfer (and other unmodeled energy losses) as a lumped and unknown bounded disturbance. A bound on the external heat transfer is relatively easy to find. As it will be shown in the next sections, the heat transfer appears in the equations as a matched disturbance, to which the system can be made insensitive through Sliding Mode Control. The feedback linearization controller of the previous sections was derived with the implicit assumption that the pressure and temperature of the fluids reaching the mixer are constant. While a feedback linearization controller can be derived that takes into account those variations, it would require knowledge of the inlet thermodynamic properties at all times, and what is worse, the derivatives of the properties would also be required. Performance tradeoffs and limitations are expected, however, due to the intrinsic limitations of valve actuators in the system.

4.2 A Pressure-Density Model with Heat Transfer Disturbance: Ideal Gases

It is convenient to start the study of Sliding Mode controllers by simplifying the mixer model. The model will be simplified by assuming that the fluid reaching the inlet valves is an ideal gas, which obeys the well-known state equation

$$P = \rho R T$$

where R is the ideal gas constant in ft^3-lbf/in^2-lbm-R, T is the temperature in degrees Rankine, P is the pressure in psi and ρ is the density in lbm/ft^3, for English units. For SI units, the choices are also straightforward. It is convenient to write the equations in term of a pressure state instead of internal energy, since the flow rates can be directly computed from the state variables without further reference to thermodynamic data. For the case of the ideal gas, the following identities and definitions are in order

$$h = C_p T = \frac{P C_p}{\rho R} \tag{4.6}$$

$$u = C_v T = \frac{P C_v}{\rho R} \tag{4.7}$$

$$k = \frac{C_p}{C_v} \tag{4.8}$$

$$R = C_p - C_v \tag{4.9}$$

where C_p and C_v are the constant pressure and constant volume heat capacities, respectively, and k is the heat capacity ratio. Using these definitions and identities, and performing manipulations, the A_p matrix of Eq. (4.3) can be written as

$$A_p = \text{diag}\left[\frac{Rh_1}{C_v},\ \frac{Rh_2}{C_v},\ \frac{kP}{\rho}\right] \tag{4.10}$$

The A_p matrix is dependent on the state, as it can be seen in the above formula. The heat transfer disturbance is directly included in the basic energy balance of Eq. 2.4, where the subindices have been modified to reflect the ideal gas assumption:

$$\dot{m}u + \dot{u}m = \dot{m}_1 h_1 + \dot{m}_2 h_2 - \dot{m}_e h_e + Q$$

where Q denotes the heat transfer rate, expressed in Btu/sec or in Watts, according to the system of units. The energy balance equation can be written in terms of the pressure derivative as

$$\dot{P} = \frac{1}{V}\left(\frac{Rh_1}{C_v}\dot{m}_1 + \frac{Rh_2}{C_v}\dot{m}_2 - k\frac{P}{\rho}\dot{m}_e + \frac{RQ}{C_v}\right)$$

Using the above definitions and identities, the final form of the ideal gas mixer model with heat transfer disturbance is given by

$$\dot{\rho} = \frac{1}{V}C_v^T f \tag{4.11}$$

$$\dot{u} = \frac{1}{V}C_v^T A_p f + \frac{R}{VC_v}Q \tag{4.12}$$

$$\dot{C}_v = A_c C_v + B_c \zeta \tag{4.13}$$

$$y = [\rho \;\; u \;\; C_{ve} f_e]^T \tag{4.14}$$

with A_p given by Eq. 4.10.

4.2.1 Equilibrium Points

It is convenient to start the study of model properties by considering its equilibrium points. It is of particular interest to characterize the equilibrium points which correspond to positive flows and positive valve openings. This information is of crucial importance in the operation of the mixer, for the model may allow for operating conditions which are not of practical interest, such as those necessitating reverse flows. Note that the equilibrium analysis alone is not sufficient to guarantee that a particular operating condition is reachable with given system resources and without violating physical constraints during transient conditions.

4.2.2 Sliding Mode Control Design

Having established the stability of the zero dynamics, it is now possible to follow the steps of a standard sliding mode controller design. The first step is to write the 5th-order system in terms of output derivatives. Differentiating the first output twice leads to

$$\ddot{y}_1 = \frac{C_v^T}{V}\left(A_c f + \frac{df}{dt}\right) + \frac{\zeta^T B_c f}{V}$$

where

$$\frac{df}{dt} = \left[\frac{df_1}{dt} \;\; \frac{df_2}{dt} \;\; -\frac{df_e}{dt}\right]^T$$

Similarly, differentiating the second output twice gives

$$\ddot{y}_2 = \frac{C_v^T}{V}\left[\left(AcAp + \frac{dA_p}{dt}\right) f + A_p \frac{df}{dt}\right] + \frac{\zeta^T B_c A_p f}{V} + \frac{R}{VC_v}\dot{Q}$$

The third output, however, needs to be differentiating only once for the control to appear:

$$\dot{y}_3 = C_{ve}\frac{df_e}{dt} + (-\frac{1}{\tau_3}C_{ve} + \beta_3\zeta_3)f_e$$

The sliding manifolds are chosen to yield linear tracking errors when the sliding regime has been reached. Specifically, choose

$$\begin{aligned} s_1 &= \dot{\rho}_d - \dot{\rho} + c_\rho(\rho_d - \rho) && (4.15)\\ s_2 &= \dot{P}_d - \dot{P} + c_P(P_d - P) && (4.16)\\ s_3 &= c_w(w_d - C_{ve}f_e) && (4.17) \end{aligned}$$

where ρ_d, P_d and w_d denote the desired trajectories for the density, pressure and exit mass flow outputs, respectively, and c_ρ, c_P and c_w are sliding coefficients. It is desired that the s_1, s_2 and s_3 reach zero after some finite time and remain zero despite of the heat transfer disturbance. Choosing Lyapunov functions

$$V_i = \frac{1}{2}s_i^2$$

for $i = 1, 2, 3$, it is sufficient to ensure that $\dot{V}_i < 0$ at all times to guarantee the convergence of s_i. To reach zero in finite time, a commonly used choice is to enforce

$$\dot{V}_i = s_i\dot{s}_i \leq -\eta_i|s_i| \quad (4.18)$$

It can be shown [30] that the above implies that s_i reaches zero in a time t_i given by

$$t_i \leq \frac{|s_i(t=0)|}{\eta_i}$$

Now, the derivatives of the sliding functions can be obtained as

$$\begin{aligned} \dot{s}_1 &= \ddot{\rho}_d + c_\rho\left(\dot{\rho}_d - \frac{1}{V}C_v^T f\right) - \frac{\zeta^T B_c f}{V} - \frac{C_v^T}{V}\left(A_c f + \frac{df}{dt}\right)\\ \dot{s}_2 &= \ddot{P}_d - \frac{C_v^T}{V}\left[\left(A_c A_p + \frac{dA_p}{dt}\right)f + A_p\frac{df}{dt}\right] - \frac{\zeta^T B_c A_p f}{V} - \frac{R}{VC_v}\dot{Q} + c_P\left(\dot{P}_d - \frac{1}{V}C_v^T A_p f - \frac{RQ}{VC_v}\right)\\ \dot{s}_3 &= c_w\left[\dot{w}_d - \left(-\frac{1}{\tau 3}C_{ve} + \beta_3\zeta_3\right)f_e - C_{ve}\frac{df_e}{dt}\right] \end{aligned}$$

Enforcement of Eq. (4.18) can be achieved by using the equality for s_1 and s_3, since the heat transfer uncertainty is not involved in the expressions, that is, let $s_i\dot{s}_i = -\eta_i|s_i|$ for $i = 1, 2$. This is equivalent to $\dot{s}_i = -\eta_i\text{sign}(s_i)$. For s_2 the equality cannot be guaranteed, since it would require knowledge of Q and $\dot{Q}$. The Sliding Mode Controller will rely, however, on the knowledge of a bound for these quantities and on the ability to increase the sliding gain η_2 to counteract the disturbance. Enforcing $\dot{s}_i = -\eta_i\text{sign}(s_i)$ for $i = 1, 3$ leads to

$$\begin{aligned} \frac{\zeta^T B_c f}{V} &= \Gamma_1 && (4.19)\\ \zeta^T G f &= \Gamma_3 && (4.20) \end{aligned}$$

where

$$\Gamma_1 = \ddot{\rho}_d + c_\rho \dot{\rho}_d + \eta_1 \text{sign}(s_1) - \frac{C_v^T}{V}\left((A_c + c_\rho I)f + \frac{df}{dt}\right)$$

$$\Gamma_3 = c_w\left(\dot{w}_d + \frac{1}{\tau_3}C_{ve}f_e - C_{ve}\frac{df_e}{dt}\right) + \eta_3 \text{sign}(s_3)$$

and G is a 3-by-3 matrix with zeros in every entry, except for $G(3,3) = -c_w\beta_3$. For the remaining sliding variable, we choose

$$\frac{\zeta^T B_c A_p f}{V} = \Gamma_2 \tag{4.21}$$

where

$$\Gamma_2 = \ddot{P}_d + c_P\dot{P}_d + \eta_2 \text{sign}(s_2) - \frac{C_v^T}{V}\left[\left((A_c + c_P I)A_p + \frac{dA_p}{dt}\right)f + A_p\frac{df}{dt}\right]$$

so that

$$\dot{s}_2 = -\eta_2 \text{sign}(s_2) - \frac{R\dot{Q}}{VC_v} - \frac{c_p R}{VC_v}Q$$

We want

$$s_2\dot{s}_2 \leq -\eta_2'|s_2| \tag{4.22}$$

with $\eta_2' > 0$. Let

$$\eta_2 = \eta_2' + \frac{R\bar{Q}}{VC_v}$$

where $\bar{Q}$ is a known bound such that

$$|\dot{Q} + c_P Q| < \bar{Q}$$

at all times. Then it is straightforward to show that Eq. (4.22) is satisfied. Since $\eta_2' > 0$, it is thus sufficient to choose

$$\eta_2 > \frac{R\bar{Q}}{VC_v} \tag{4.23}$$

. The equations that yield the control input, Eqs. (4.19), (4.21) and (4.20) can be compactly expressed in matrix form as a system of equations which is linear in ζ:

$$\begin{bmatrix} \frac{f^T B_c}{V} \\ \frac{f^T A_p B_c}{V} \\ f^T G \end{bmatrix} \zeta = \begin{bmatrix} \Gamma_1 \\ \Gamma_2 \\ \Gamma_3 \end{bmatrix} \tag{4.24}$$

Invertibility of the system matrix is related to the zero dynamics and to the existence of feasible trajectories, which is currently under study.

Parameter	Value	Units
P_1	6.894	MPa
T_l	311.1	$^\circ K$
P_2	5.516	MPa
T_2	422.22	$^\circ K$
P_s	206.842	kPa
R	296.8	J/kg$^\circ K$
C_p	1041.6	J/kg$^\circ K$
k	1.398	n.a
P_0	3.447	MPa
ρ_0	48.05	kg/m^3
$C_{v1,2,3}$	10	n.a
$\tau_{1,2,3}$	0.1	sec
β_1	1	n.a
β_2	2	n.a
β_3	3	n.a
V	0.07079	m^3
c	2.40428 $\times 10^{-5}$	n.a

Table 4.1: System Parameters for Sliding Mode Controller Simulation

4.2.3 Simulation Example

In this example, we choose the SI system of units with Nitrogen as the working gas and the following design specifications:

- Obtain a steady exit flow of 10 kg/s with a mixer operating pressure of 4 MPa.
- The temperature of the exit flow must be $337^\circ K = 64^\circ C$.
- The heat transfer disturbance is is $Q = 10\sin(10t)$.
- The steady operating point must be reached in less than 25 seconds, for known initial conditions given in Table 4.1.
- Valve chattering must not be observed.

Other system parameters are summarized in Table 4.1. The value of c in Table 4.1 is the appropriate one for the valve flow formula in SI units. The formula for liquids has been chosen for simplicity and illustration purposes.

Sliding Mode Controller Design The values of w_d and P_d are directly taken from the design specifications. It is necessary to calculate the value of ρ_d which will result in the desired exit temperature. For this, we have that the isoenthalpic process at the exit valve is also isothermal, since it is assumed that C_p is constant. Therefore we choose $\rho_d = \frac{P_d}{RT_d} = 40\text{kg/m}^3$. In order to meet the settling time requirement, we choose $c_\rho = c_P = c_w = 100$, $\eta_1 = \eta_3 = 120$ and $\eta_2 = 2.4062 \times 10^6$. With the known initial conditions and setting $\dot{\rho}_d = \ddot{\rho}_d = \dot{P}_d = \ddot{P}_d =$

$\dot{w}_d = 0$ we obtain the reaching times:

$$\begin{aligned} t_{r1} &\leq \frac{|s_1(t=0)|}{\eta_1} = 7.08sec \\ t_{r2} &\leq \frac{|s_2(t=0)|}{\eta_2} = 19.5sec \\ t_{r3} &\leq \frac{|s_3(t=0)|}{\eta_3} = 5.83sec \end{aligned}$$

The overall settling time will be given by the sliding surface reaching time plus the settling time during sliding, which is given by $t_{s1} = t_{s2} = t_{s3} = 4/100 = 0.04sec.$. The above gain choices thus satisfy the settling time requirements. Finally, we check that the controller can attain its objective despite the presence of the heat transfer disturbance. The value of $\bar{Q}$ is computed as

$$\bar{Q} = |\dot{Q} + c_P Q| = 1100$$

We see that the selection of η_2 is appropriate, since

$$\eta_2 = 2.4062 \times 10^6 > \frac{\bar{Q}R}{VC_v}$$

To avoid chattering, the signum functions present in the control law are replaced by finite slope approximations consisting of saturation functions:

$$\text{sign}(s_i) \approx \text{sat}(s_i/\phi_i)$$

where

$$\text{sat}(x) = \begin{cases} x & \text{if } |x| \leq 1 \\ 1 & \text{if } x > 1 \\ -1 & \text{otherwise} \end{cases} \tag{4.25}$$

For the simulation example, the values $\phi_1 = \phi_3 = 10$ and $\phi_2 = 1 \times 10^4$ were chosen. Figures 4.1, 4.2 and 4.3 show the simulation results. As it can be seen, the control objectives are satisfied. The second valve position history, however, is physically meaningless, since it contains a time interval when the valve opening is negative. Avoidance of reverse flows and negative valve positions was not specified in the control problem. This simulation motivates for further study into admissible trajectories and controllers which produce them.

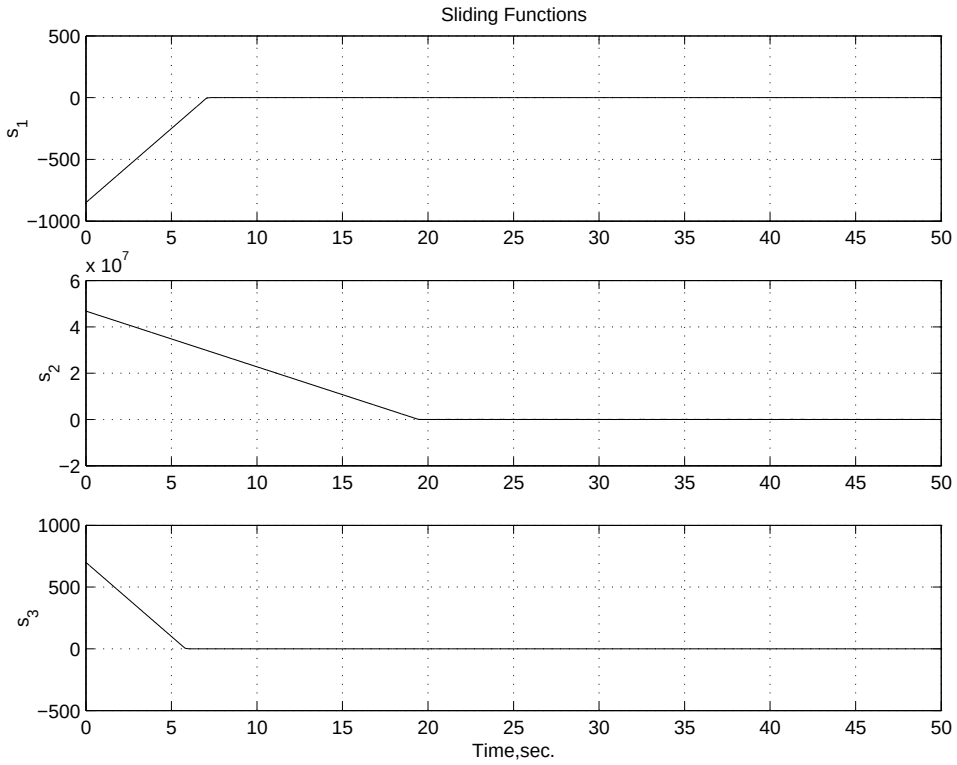

Figure 4.1: Simulation of Sliding Mode Controller - Sliding Variables

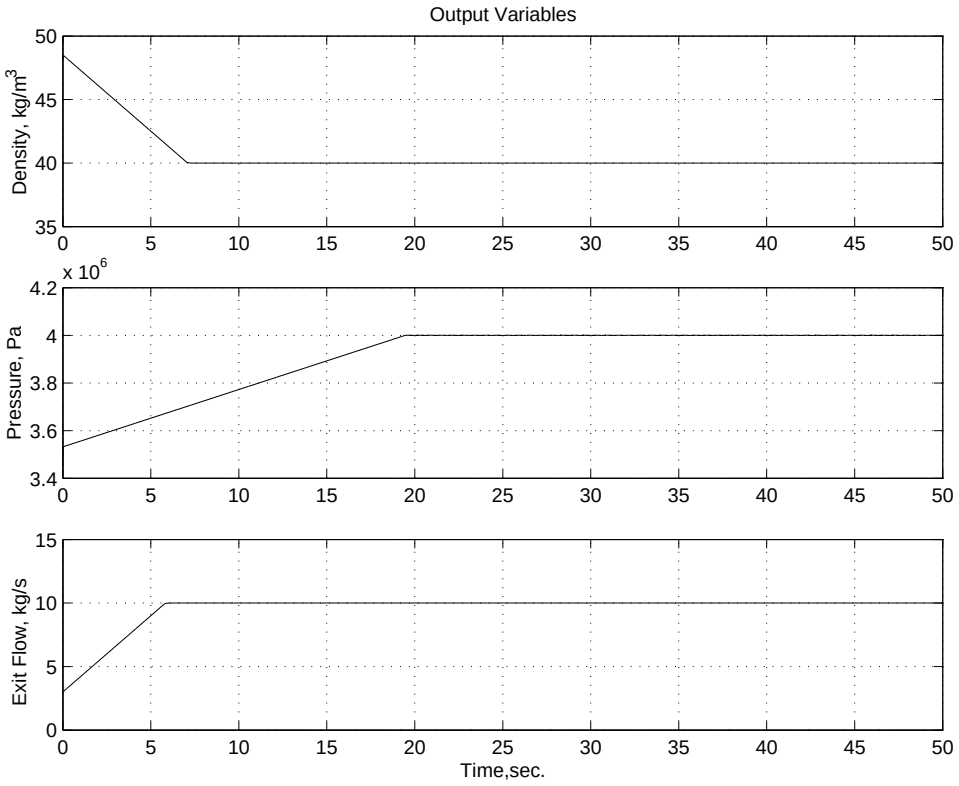

Figure 4.2: Simulation of Sliding Mode Controller - Output Variables

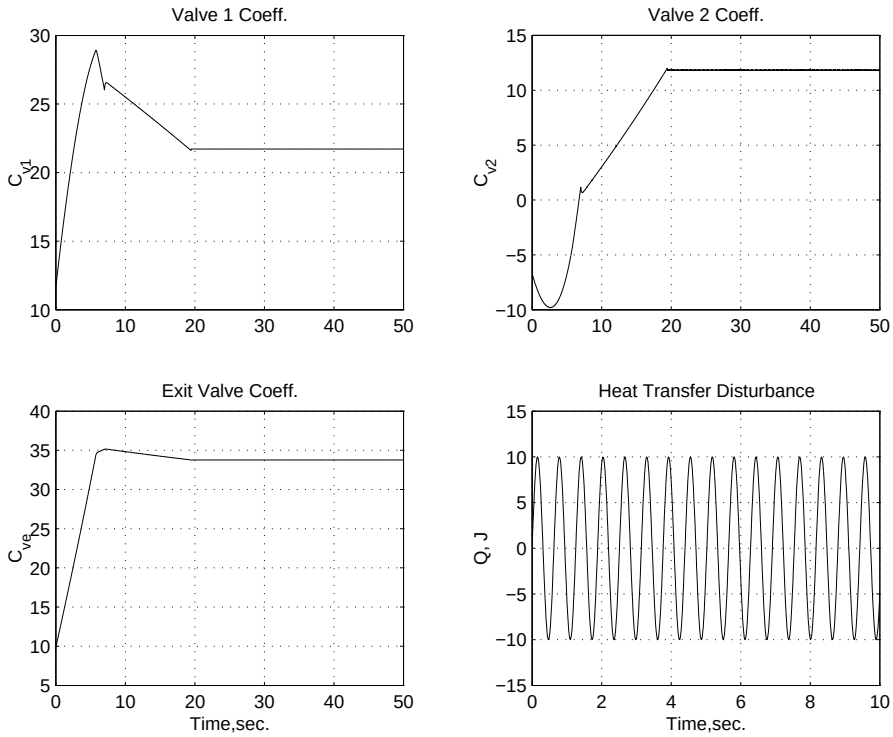

Figure 4.3: Simulation of Sliding Mode Controller - Control Variables and Disturbance

Chapter 5

Constrained Sliding Mode Control Design Using Robustly Positively Invariant Cylinders

5.1 Introduction

A practical solution to the robust control problem of the mixer under constraints requires an examination of invariant set theory. Valve positions are physically restricted to be nonnegative and bounded by certain constant value related to allowable stem travel. In the model derived above, such positions are state variables, while the *commanded* positions are control inputs. It is therefore important to examine conditions and design methods which guarantee that the controlled states belong to certain predetermined operating set, even under uncertainty and disturbances. In mathematical control theory, such operating sets are termed *invariant*, and several kinds of invariance are defined. A comprehensive survey of set invariance in control theory is out of the scope of this report, however some definitions will be required. For details, please refer to [4, 8, 20]. Much of the work in set invariance concerns linear systems and ellipsoidal or polyhedral operating sets. New theory is developed and introduced here for linear and a class of nonlinear systems under Sliding Mode Control. The invariant sets under consideration here are hyper-cylinders which project orthogonally as ellipsoids in a reduced dimension space.

5.2 Basic Theory of Robust Positive Invariance

Although the systems to which the main results of this article apply are linear, the results of this section apply to more general systems, possibly time-varying. The explicit dependence on time has been dropped from the notation, however. Given a dynamic system described by $\dot{x} = f(x(t))$, having a unique solution $x(t)$ in a subset $\Omega \subset \mathbb{R}^n$, the set $\mathcal{S} \subset \Omega$ is said to be *positively invariant* (PI) for the system if for every initial state $x_o \in \mathcal{S}$, the solution $x(t)$ belongs to $\mathcal{S}$ for $t > 0$. For the uncertain system $\dot{x} = f(x(t), w(t))$ where $w(t)$ is an input known to belong to some set $\mathcal{W}$, $\mathcal{S}$ is said to be *robustly positively invariant* (RPI) for the system if for all $x_o \in \mathcal{S}$ and for all $w(t) \in \mathcal{W}$ the solution $x(t)$ belongs to $\mathcal{S}$ for $t > 0$. The widely known result

due to Nagumo [17] provides a necessary and sufficient condition for the invariance of a set $\mathcal{S}$ in terms of its *tangent* cone, also known as Bouligand *contingent cone*. A precise definition of tangent cone is given, for instance, in [4] and the reader is referred to it for details. For our purposes, it will suffice to state what the tangent cones of particular sets are, and to cite some relevant properties. The notation $\mathcal{C}_{\mathcal{S}}(x)$ will be used for the tangent cone of set $\mathcal{S}$ at a point $x \in \mathbb{R}^n$. The notations A^c, $\bar{A}$, ∂A and $A \subset B$ indicate, as usual, the complement, closure and boundary of A, and that A is a subset (not necessarily proper) of B, respectively. The extended real line is denoted here as $\mathbb{R}^* = \mathbb{R} \cup \{\infty\} \cup \{-\infty\}$.

Theorem 1 (Nagumo [17]). *Consider the system $\dot{x} = f(x(t))$ having a unique solution for each initial condition in a set Ω. Let $\mathcal{S} \subset \Omega$ be a closed and convex set. Then $\mathcal{S}$ is PI for the system if and only if $f(x) \in \mathcal{C}_{\mathcal{S}}(x)$ for all $x \in \partial\mathcal{S}$.*

Mechanically interpreted, the theorem formalizes the intuitive notion of invariance being attained when the velocity vectors $\dot{x}$ at the boundary of the set all point into, or are tangent to $\mathcal{S}$. The following important extension of Nagumo's result is given in [1] and concerns robust positive invariance.

Theorem 2. *Consider the uncertain system $\dot{x} = f(x(t), w(t))$ where the uncertain input $w(t)$ has values in $\mathcal{W}$ for all $t \geq 0$. Assume that the system posesses a unique solution for all initial conditions $x_0 \in \Omega$ and all $w(t) \in \mathcal{W}$. Then the convex and closed set $\mathcal{S} \subset \Omega$ is RPI if and only if $f(x, w) \in \mathcal{C}_{\mathcal{S}}(x)$ for all $x \in \partial\mathcal{S}$ and for all $w \in \mathcal{W}$.*

A few useful properties of tangent cones are now stated.

Property 5.2.1 ([1, 12]). *If A and B are closed and convex sets such that $0 \in int(A - B)$, then $\mathcal{C}_{A\cap B}(x) = \mathcal{C}_A(x) \cap \mathcal{C}_B(x)$ for all $x \in A \cap B$.*

Property 5.2.2 ([1, 4]). *If A is convex, then $\mathcal{C}_A(x)$ is convex for all $x \in A$.*

It is also a fact [1, 4] that if $x \in \text{int}(A)$ then $\mathcal{C}_A(x) = \mathbb{R}^n$. To end this section, we show that, for certain class of systems, and when the uncertain input belongs to a closed interval, it is sufficient to check for positive invariance of the system at extreme values of the input.

Theorem 3. *Consider a system that is linear in the uncertainty, e.g., $\dot{x} = f(x(t), w(t)) = g(x(t)) + Bw(t)$ where $w(t) \in \mathcal{I} = [\underline{w}\ ,\ \overline{w}]$. Assume that the system posesses a unique solution for all initial conditions $x_0 \in \Omega$ and all $w(t) \in \mathcal{I}$. Then $\mathcal{S} \subset \Omega$ is RPI if and only if it is PI for $\dot{x} = f(x(t), \underline{w})$ and for $\dot{x} = f(x(t), \overline{w})$.*

Proof. Suppose $\mathcal{S}$ is positively invariant for $\dot{x} = f(x(t), \underline{w})$ and for $f(x(t), \overline{w})$. Then, by Theorem 1, $f(x, \underline{w}) \in \mathcal{C}_{\mathcal{S}}(x)$ and $f(x, \overline{w}) \in \mathcal{C}_{\mathcal{S}}(x)$ for all $x \in \partial\mathcal{S}$. Let $w \in \mathcal{I}$. Then $w = \alpha\overline{w} + (1-\alpha)\underline{w}$ for some $\alpha \in [0, 1]$ and thus $f(x, w) = \alpha f(x, \overline{w}) + (1-\alpha) f(x, \underline{w})$. Since $\mathcal{C}_{\mathcal{S}}(x)$ is convex whenever S is convex, we conclude that $f(x, w) \in \mathcal{C}_{\mathcal{S}}(x)$ for all $x \in \partial\mathcal{S}$ and for all $w \in \mathcal{I}$. By Theorem 2, $\mathcal{S}$ is RPI. The reverse implication is trivial. □

5.3 Sliding Mode Control of Linear Systems

Sliding Mode Control (SMC) is a widely studied technique [10, 30, 31] that achieves total insensitivity of the controlled variables to certain kinds of disturbances and parameter uncertainties.

In this section we briefly introduce the salient characteristics of linear systems under SMC. Consider the single-input, linear and time-invariant system

$$\dot{x} = Ax + Bu(t) + D\delta(t) \tag{5.1}$$

where A is an n-by-n matrix, B and D are column vectors, $x \in \mathbb{R}^n$, u is the scalar control input and $\delta(t)$ is a scalar, unknown disturbance. It is assumed that the pair (A, B) is controllable and that the matching condition

$$\text{rank}[B|D] = \text{rank}(B)$$

is satisfied, so that the system can be rewritten as

$$\dot{x} = Ax + B(u(t) + \zeta(t)) \tag{5.2}$$

Assume that $\delta(t)$ is bounded so that $\zeta(t) \in \mathcal{Z}$ for all $t \geq 0$, where $\mathcal{Z} = [-\bar{\zeta}, \bar{\zeta}]$. In order to specify a sliding mode control law with linear sliding manifold, let T be a nonsingular matrix such that $T^{-1}B = [0\ 0 ...|\ 1]^T$ and such that A_{11} is a nonsingular $n-1$ by $n-1$ matrix, where A_{ij} for $i, j = 1, 2$ are the partition blocks of $T^{-1}AT$ such that A_{22} is scalar. Such transformation can always be found. Note that taking T as the transformation matrix for the control canonical form is not a good choice, since in that case the first column of A_{11} is zero. A method to find such a transformation is given in the appendix. Define a coordinate transformation $x = Tz$ and write the system equations in the new coordinates as

$$\dot{z} = T^{-1}ATz + [0 \mid 1]^T(u(t) + \zeta(t))$$

Consider the sliding manifold $s = Gx = GTz = [G_1 \mid G_2]z$. Without loss of generality, consider that $G_2 = 1$. The control law

$$u(t) = -A_{21}z_1 - A_{22}z_2 - G_1(A_{11}z_1 + A_{12}z_2) - \eta\ \text{sgn}(s) \tag{5.3}$$

results in the closed-loop dynamics described by

$$\begin{aligned} \dot{z}_1 &= A_{11}z_1 + A_{12}z_2 \\ \dot{z}_2 &= -G_1A_{11}z_1 - G_1A_{12}z_2 - \eta\ \text{sign}(s) + \zeta(t) \\ s &= G_1z_1 + z_2 \end{aligned}$$

It can be easily shown any choice of G under the above constraints on T, and such that $G_2 = 1$, results in $GB = 1$. It is likewise straightforward to show that the closed-loop dynamics in the original coordinates is described by

$$\dot{x} = (I - BG)Ax - B\eta\ \text{sign}(s) + B\zeta(t) \tag{5.4}$$

Using $V = s^2$ as a Lyapunov function shows that if $\eta > \bar{\zeta}$ then control law (5.3) results in the state reaching the plane $s = 0$ in finite time and remaining there indefinitely despite the presence of the disturbance [10, 30, 31]. Evolution of the closed-loop system (5.4) for $s = 0$ is independent of the disturbance and described by the reduced dynamics

$$\dot{z}_1 = A_wz_1 \tag{5.5}$$

where

$$A_w = A_{11} - A_{12}G_1 \tag{5.6}$$

Thus, a stable sliding mode is obtained by choosing G_1 such that A_w has eigenvalues with negative real parts (A_w is Hurwitz). It can be shown that the controllability of (A, B) guarantees that the eigenvalues of A_w may be freely placed using G_1. For the remainder of this article, it will be assumed that A_w is Hurwitz, $\eta > \bar{\zeta}$ and that a unique solution to the closed-loop SMC differential equation (5.4) exists for every initial condition in $\mathbb{R}^n$.

5.3.1 A Useful Decomposition of the Closed-Loop Dynamics

The Lyapunov function $V = s^2$ induces an obvious family of invariant sets, namely the sets $S_\gamma = \{z \in \mathbb{R}^n : |s(z)| \leq \gamma\}$ for $\gamma \geq 0$ are all positively invariant. These sets are "naturally" invariant for systems under SMC. A coordinate transformation is introduced here that decouples the motion towards $s = 0$ from the overall convergence to the origin. This decomposition will suggest a cylindrical shape for positively invariant sets.

Lemma 5.3.1. *There exists a coordinate transformation $x = Jw$ with J nonsingular in which the closed-loop dynamics (5.4) is expressed as*

$$\begin{cases} \left[\begin{array}{c} \dot{w}_1 \\ \hline \dot{w}_2 \end{array}\right] = \left[\begin{array}{c|c} A_w & 0 \\ \hline 0 & 0 \end{array}\right] \left[\begin{array}{c} w_1 \\ \hline w_2 \end{array}\right] + \left[\begin{array}{c} B_1 \\ \hline B_2 \end{array}\right] (\eta sign(s) - \zeta(t)) \\ \\ s = G_w w_2 \end{cases} \tag{5.7}$$

where $B_w \triangleq [B_1|B_2]^T = -J^{-1}B$ and $G_w = -G_1 A_{11}^{-1} A_{12} + 1$. Moreover, $B_2 G_w = -1$.

The proof to Lemma 5.3.1 is done directly by specifying J and is shown in the appendix. Note that s is just proportional to the scalar w_2 and independent of w_1. An immediate observation is that an arbitrary (possibly infinite) real interval is RPI for the dynamics of w_2. The result is formalized in the following

Lemma 5.3.2. *For any initial condition $[w_{10}^T \mid w_{20}]^T \in \mathbb{R}^n$, where w_{20} belongs to the possibly infinite interval $[a, b] \ni 0$, the trajectory $w(t)$ of the closed-loop system (5.7) is such that for all $w_2(t) \in [a, b]$ for all $t > 0$, that is, $[a, b]$ is RPI for the dynamics of w_2.*

Lemma 5.3.2 follows directly from Lemma 5.3.1 by using the conditions $B_2(-G_1 A_{11}^{-1} A_{12} + 1) = -1 < 0$ and $\eta > \bar{\zeta}$ in establishing the monotonic decrease of $|s|$ (and that of $|w_2|$) at both sides of $s = 0$. With the aid of Lemma 5.3.2 it is now possible to specify cylindrical positive-invariant sets with fairly general cross sections. Introduce the notation

$$\mathcal{H}_{\mathcal{S}_o}[a, b] = \left\{ [w_1^T | w_2]^T \in \mathbb{R}^n \ : \ w_1 \in \mathcal{S}_o, \ w_2 \in [a, b] \right\}$$

The set $\mathcal{S}_o$ is termed the cylinder's *cross section*. The following result follows directly from Lemma 5.3.2:

Theorem 4. *Let $\mathcal{S}_o \subset \mathbb{R}^{n-1}$ be a compact and convex set containing the origin . Suppose $\mathcal{S}_o$ is RPI for the system $\dot{w}_1 = A_w w_1 + B_1 \zeta'(t)$, where A_w is Hurwitz and $|\zeta'(t)| \leq \eta + \bar{\zeta}$ for all $t \geq 0$. Then all cylinders $\mathcal{H}_{\mathcal{S}_o}[a, b]$ such that $0 \in [a, b]$ are RPI for the closed-loop dynamics of (5.7).*

From now on, a compact and convex cross section will be assumed in the notation for cylinders. Also, the notation $\mathcal{H}_{\mathcal{S}_o}$ is used for the family of cylinders $\mathcal{H}_{\mathcal{S}_o} = \{\mathcal{H}_{\mathcal{S}_o}[a, b] \ : \ 0 \in [a, b], \ a, b \in \mathbb{R}^*\}$.

5.4 State-Constrained Invariant Sets

Robust positive invariance of a set $\mathcal{S}$ alone is not sufficient to guarantee that the state of the controlled system will not exceed prescribed bounds given by a set G (except in the uninteresting case $\mathcal{S} \subset G$). Consideration here is restricted to linear state constraints.

Definition 5.4.1. *A linear state constraint set is defined as $G = \cap G_i$ for $i = 1, 2..m$, where $G_i = \{w \in \mathbb{R}^n \ : \ \Gamma_i w \leq 1\}$. Γ_i are row vectors such that G is a convex set containing the origin in its interior.*

Note that ∂G_i, the boundary of G_i, is the set of points such that $\Gamma_i w = 1$. In the context of SMC under state constraints, G is assumed to be the constraint set in w coordinates. That is, to each linear constraint $\Gamma_{ix} x \leq 1$ for the original system there corresponds a constraint $\Gamma_{ix} J x = \Gamma_i w \leq 1$. Since J is nonsingular, it is straightforward to see that G is a convex if and only if the original constraint set in x coordinates is so. Furthermore, assume that $\Gamma_{ix} B \neq 0$ for $i = 1, 2..m$. This basic feasibility assumption for the problem goes beyond controllability of the pair (A, B) [9]. At this point it is convenient to state that the tangent cone to a linear state constraint $\Gamma_i w \leq 1$ is given by $\Gamma_i w \leq 0$. In connection with the uncertain system $\dot{w} = f(w, \zeta(t))$, where $\zeta \in \mathcal{Z}$ for all $t \geq 0$, introduce the following sets:

$$\begin{aligned} G_i^+ &= \{w \in \mathbb{R}^n \ : \ \Gamma_i f(w, \zeta) > 0 \text{ for some } \zeta \in \mathcal{Z}\} \\ G_i^- &= \{w \in \mathbb{R}^n \ : \ \Gamma_i f(w, \zeta) < 0 \text{ for all } \zeta \in \mathcal{Z}\} \end{aligned} \tag{5.8}$$

The next result concerns the invariance of the intersection of a state constraint set and an RPI set. It generalizes Theorem 1 from [20], in that the system is not restricted to be linear under state feedback, the positively invariant set does not have to be an ellipsoid, disturbance is allowed and the constraints may be asymmetric.

Theorem 5. *Let $M \subset \mathbb{R}^n$ be a compact and convex set which is RPI for a system $\dot{w} = f(w, \zeta(t))$, where $\zeta(t) \in \mathcal{Z}$ for $t \geq 0$. Let $G = \cap G_i, i = 1, 2..m$ be a linear state constraint set as in Def. 5.4.1. Assume, further, that $0 \in int(M - G)$. Denote $\mathcal{S} = M \cap G$. Then $\mathcal{S}$ is robustly positively invariant for the system if and only if $\mathcal{S} \cap \partial G_i \cap G_i^+ = \emptyset$ for $i = 1, 2...m$.*

The proof of Th. 5 is shown in the appendix. Since G is compact, the following quantities are well-defined:

$$\overline{w}_2 = \max_{w \in G} w_2 \tag{5.9}$$

$$\underline{w}_2 = \min_{w \in G} w_2 \tag{5.10}$$

Note that $\underline{w}_2 < 0 < \overline{w}_2$, since $0 \in \text{int}(G)$. The following Corollary provides a sufficient condition for robust positive invariance that leads to computation.

Corollary 5.4.1. *Let the family of cylinders $\mathcal{H}_{\mathcal{S}_o}$ be RPI for the SMC dynamics (5.7). Let G be a constraint set such that $0 \in int(G - \mathcal{H}_{\mathcal{S}_o})$. Then $\mathcal{S} = \mathcal{H}_{\mathcal{S}_o} \cap G$ is RPI for (5.7) if $\mathcal{H}_{\mathcal{S}_o}[\underline{w}_2, \overline{w}_2] \cap \partial G_i \cap \partial G_i^+ = \emptyset \ \forall i = 1, 2...m$.*

For the remainder of the development consider

$$f(w,\zeta) \triangleq [A_w w_1 + B_1(\eta \text{sign}(G_w w_2) - \zeta) \mid B_2(\eta \text{sign}(G_w w_2) - \zeta)]^T \tag{5.11}$$

Eq. (5.11) defines $f(w,\zeta)$ as the value of $\dot{w}$ in the SMC closed-loop dynamics for a constant disturbance value. The following technical results are useful in the proof of Corollary 5.4.1:

Lemma 5.4.1. *Let the family of cylinders $\mathcal{H}_{\mathcal{S}_o}$ be RPI for the SMC dynamics (5.7). Let a linear state constraint G_i be such that $\partial G_i \cap \mathcal{H}_{\mathcal{S}_o}[\underline{w}_2, \overline{w}_2] \neq \emptyset$. Then $\exists w \in \mathcal{H}_{\mathcal{S}_o}[\underline{w}_2, \overline{w}_2] \cap \partial G_i$ such that $\Gamma_i f(w,\zeta) < 0 \; \forall \, \zeta \in \mathcal{Z}$*

Proposition 5.4.1. *Suppose $\Gamma_i = [\Gamma_{i1} \mid \Gamma_{i2}]$, where $\Gamma_{i1} A_w \neq 0$. Then the collection of subsets $\left\{ int(G_i^+), int(G_i^-), \partial G_i^+ \right\}$ corresponding to $f(w,\zeta)$ of Eq. (5.11) is a partition of $\mathbb{R}^n$. Furthermore,*

$$\partial G_i^+ = \{w \in \mathbb{R}^n \; : \; \Gamma_i f(w,\zeta^*) = 0 \; , \; w_2 \neq 0\} \cup \left\{ \left[w_1^T \mid 0 \right]^T \in \mathbb{R}^n \; : \; |\Gamma_{i1} A_w w_1 - \Gamma_i B_w \zeta^*| \leq |\Gamma_i B_w| \eta \right\}$$

where $\zeta^* = -sign(\Gamma_i B_w)\bar{\zeta}$.

The proof of Lemma 5.4.1 and Proposition 5.4.1 are shown in the appendix.

Proof of Corollary 5.4.1. By hypothesis, and using Proposition 5.4.1, we have that either $\mathcal{H}_{\mathcal{S}_o}[\underline{w}_2, \overline{w}_2] \cap \partial G_i \subset \text{int}(G_i^+)$ or $\mathcal{H}_{\mathcal{S}_o}[\underline{w}_2, \overline{w}_2] \cap \partial G_i \subset \text{int}(G_i^-)$. For the first possibility we have that

$$\mathcal{H}_{\mathcal{S}_o}[\underline{w}_2, \overline{w}_2] \cap \partial G_i \subset \text{int}(G_i^+) \subset G_i^+$$

Then, for all $w \in \mathcal{H}_{\mathcal{S}_o}[\underline{w}_2, \overline{w}_2] \cap \partial G_i$, $\exists \zeta \in \mathcal{Z}$ such that $\Gamma_i f(w,\zeta) > 0$, contradicting Lemma 5.4.1. Therefore it must be that $\mathcal{H}_{\mathcal{S}_o}[\underline{w}_2, \overline{w}_2] \cap \partial G_i \subset \text{int}(G_i^-)$. But $\text{int}(G_i^-) \cap G_i^+ = \emptyset$, therefore $\mathcal{H}_{\mathcal{S}_o}[\underline{w}_2, \overline{w}_2] \cap \partial G_i \cap G_i^+ = \emptyset$. Finally, since $\mathcal{S} \subset \mathcal{H}_{\mathcal{S}_o}(-\infty, \infty)$ we have $\mathcal{S} \cap \partial G_i \cap G_i^+ = \emptyset$. The Corollary now follows from Th. 5. □

5.5 Cylinders with Ellipsoidal Cross Sections

The results presented above apply to a fairly large class of cylinder cross sections $\mathcal{S}_o$. Ellipsoidal invariant sets are extensively used in computations due to the correspondence to quadratic Lyapunov functions and their simplicity in relation to the also commonly used polyhedral sets. Ellipsoidal sets, however, can be conservative. The semi-ellipsoidal sets introduced by O'Dell for linear systems under state feedback achieve a good compromise between simplicity and conservativeness. A semi-ellipsoidal set is obtained by intersecting a linear state constraint set and an ellipsoidal invariant set [19, 20]. In this section we restrict $\mathcal{S}_o$ to be ellipsoidal and develop results leading to calculations for constrained SMC design. As seen in the previous sections, a cylinder is required to be RPI for it to yield an RPI set upon intersection with the state constraints. By Th. 4, we see that the cylinder cross section is required to be itself RPI for a linear system driven by a bounded disturbance. Moreover, by Th. 3, it is sufficient to establish invariance for extreme disturbance values.

5.5.1 RPI Cylinders

Consider the system

$$\dot{w}_1 = A_w w_1 + B_1 \zeta'(t) \tag{5.12}$$

where $\zeta' \in [-\bar{\zeta}',\ \bar{\zeta}']$. We wish to find conditions under which the ellipsoidal set $\mathcal{E} = \{w_1 \in \mathbb{R}^{n-1} : w_1^T P w_1 \leq 1\}$ is RPI for the dynamics (5.12). To this effect, note that [4] the tangent cone of $\mathcal{E}$ at its boundary $\partial\mathcal{E}$ is given by $\mathcal{C}_{\mathcal{E}}(w_1) = \{y : 2w_1^T P y \leq 0\}$. Nagumo's condition results in

$$2w_1^T P(A_w w_1 + B_1 \zeta'(t)) \leq 0 \text{ along } w_1^T P w_1 = 1 \tag{5.13}$$

Conditions on P for (5.13) to hold can be derived following two approaches. One involves linear matrix inequalities (LMI) and it lends itself to ellipsoid volume optimization. The other approach has a simpler form and provides the maximum sum of disturbance bound and switching gain alowable for a particular ellipsoid.

5.5.2 LMI Approach

Nagumo's condition (5.13) is equivalent to a *quadratic boundedness* requirement, which, as shown in [5], can be equivalently expressed by the LMI

$$\begin{bmatrix} PA_w + A_w^T P + \alpha P & \bar{\zeta}' P B_1 \\ \bar{\zeta}' B_1^T P & -\alpha I \end{bmatrix} \leq 0 \tag{5.14}$$

where $P = P' > 0$ is sought.

Lemma 5.5.1. *The set $\mathcal{E} = \{w_1 \in \mathbb{R}^n : w_1^T P w_1 \leq 1\}$ is RPI for system (5.12) there exist a symmetric, positive-definite matrix P and a scalar $\alpha > 0$ such that the LMI (5.14) holds.*

Note that LMI (5.14) is always feasible, since A_w is Hurwitz. Moreover, only values of α less than the maximum decay rate need to be considered, that is, α satisfies $0 < \alpha < 2|\mathrm{Re}(\bar{\lambda})|$, where $\bar{\lambda}$ is that eigenvalue of A_w with the largest real part in absolute value [5]. The above matrix inequality can be readily solved using, for instance, the Matlab LMI Toolbox.

5.5.3 Critical Switching Gain

A computationally simpler alternative is obtained by using Theorem 3. Positive invariance is now required for the two autonomous systems that result when either $-\bar{\zeta}'$ or $\bar{\zeta}'$ is used. In view of the symmetry of P, Nagumo's condition can be restated as

$$\begin{aligned} w_1^T(A_w^T P + P A_w) w_1 \pm 2\bar{\zeta}' B_1^T P w_1 &\leq 0 \\ \text{along} \quad w_1^T P w_1 &= 1 \end{aligned} \tag{5.15}$$

Define

$$A_w^T P + P A_w = -Q$$

It is straightforward to prove that a necessary condition for (5.15) to hold for some $P > 0$ is that $Q > 0$. Thus we may assume that P is the unique symmetric, positive-definite solution to the above Lyapunov equation for arbitrary $Q > 0$, guaranteed to exist due to A_w

being Hurwitz. Given $Q = Q' > 0$ and $P = P' > 0$, there exists some $\beta > 0$ such that $w_1^T(A_w^T P + P A_w)w_1 = -w_1^T Q w_1 \leq -\beta w_1^T P w_1$ for all $w_1 \in \partial\mathcal{E}$. The quantity β is bounded by $\bar{\beta} = \min\ w_1^T Q w_1 \ : \ w_1 \in \partial\mathcal{E}$. The bound $\bar{\beta}$ is readily obtained by Lagrange multipliers and given by

$$\bar{\beta} = \frac{v^T Q v}{\gamma^2} \tag{5.16}$$

where $\gamma^2 = v^T P v$ and v is that eigenvector of $P^{-1}Q$ yielding the least value for the right hand side of Eq. (5.16). Knowing $\bar{\beta}$ it now follows that inequality (5.15) holds in $\partial\mathcal{E}$ if $\pm 2\bar{\zeta}' B_1^T P w_1 \leq \bar{\beta}$. Moreover, since $\bar{\beta} > 0$, we consider

$$\begin{aligned} 2\bar{\zeta}'|B_1^T P w_1| &\leq \bar{\beta} \\ \text{along} \quad w_1^T P w_1 &= 1 \end{aligned} \tag{5.17}$$

To obtain a condition equivalent to (5.17) we solve

$$\begin{aligned} \max\ 2\bar{\zeta}'|B_1^T P w_1| \quad &\text{s.t.} \\ w_1^T P w_1 &= 1 \end{aligned}$$

This is readily solved using Lagrange multipliers. The maximum is $2\bar{\zeta}'\sqrt{B_1^T P B_1}$, which must be less than $\bar{\beta}$. The resulting invariance condition can be also shown to be necessary, and it is summarized in the following

Lemma 5.5.2. *The set $\mathcal{E} = \{w_1 \in \mathbb{R}^n : w_1^T P w_1 \leq 1\}$ is RPI for system (5.12) if and only if there exist symmetric, positive-definite matrices P and Q such that*

$$\begin{aligned} A_w^T P + P A_w &= -Q \text{ and} \\ \bar{\zeta}' \leq \frac{\bar{\beta}}{2\sqrt{B_1^T P B_1}} & \end{aligned}$$

with $\bar{\beta}$ defined in (5.16).

Lemmas 5.5.2 and 5.5.1 lead to computation of invariant cylinders for SMC, as summarized in the next result.

Theorem 6. *Let $\mathcal{E} = \{w_1 \in \mathbb{R}^n : w_1^T P w_1 \leq 1\}$. The family of cylinders $\mathcal{H}_\mathcal{E}$ is RPI for the SMC closed-loop dynamics of Eq. (5.7) if and only if there exist symmetric, positive-definite matrices Q and P and a scalar $\alpha > 0$ such that Lemma 5.5.2 or Lemma 5.5.1 are satisfied, where $\bar{\beta}$ is defined in (5.16) and $\bar{\zeta}' = \eta + \bar{\zeta}$, with $\eta > \bar{\zeta}$.*

Th. 6 is a direct consequence of Theorems 4 and 3.

5.5.4 State-Constrained RPI Cylinders

In this section we apply Corollary 5.4.1 to cylinders with ellipsoidal cross sections and provide results leading to design calculations. The shape of the set ∂G_i^+ and the partition it induces is schematically depicted in Fig. 5.1 for $n = 3$, as viewed from a plane perpendicular to the planes

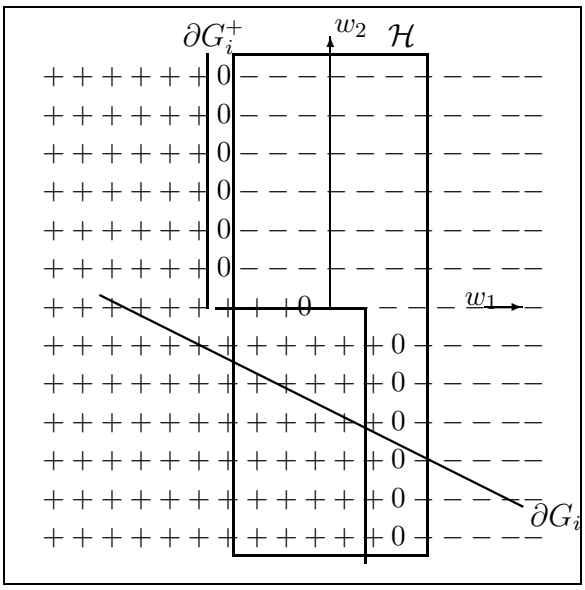

Figure 5.1: The set ∂G_i^+ and the partition it induces.

$\Gamma_{i1}A_w$ =constant. The constraint shown would not satisfy Corollary 5.4.1, since it intersects ∂G_i^+ inside the cylinder. One way to satisfy the condition in the Corollary is to find the point w^* of $\partial G_i^+ \cap \partial G_i$ (if any) for which $w_1^T P w_1$ is minimum and enforce $w_1^{T*} P w_1^* > 1$. In other words, we wish to solve the optimization problem

$$\begin{aligned} &\min_{w_2 \in \mathbb{R}} w_1^T P w_1 \quad \text{s.t.} \\ &\left[w_1^T \mid w_2\right]^T \in \partial G_i^+ \cap \partial G_i \end{aligned} \tag{5.18}$$

The set ∂G_i can intersect ∂G_i^+ at the half planes $\Gamma_{i1}A_w w_1 = -(\Gamma_i B_w)(\pm\eta - \zeta^*)$ or at $w_2 = 0$. Therefore we solve separate optimization problems for each case and enforce $w_1^{T*} P w_1^* \geq 1$ in all of them. Noting that the portion of ∂G_i^+ contained in $w_2 = 0$ is defined by $|\Gamma_{i1}A_w w_1 - \Gamma_i B_w \zeta^*| \leq |\Gamma_i B_w|\eta$ we see that the optimization problems to be solved are

$$\begin{aligned} &\min_{w_2 \neq 0} w_1^T P w_1 \quad \text{s.t.} \\ \Gamma_{i1}A_w w_1 &= -(\Gamma_i B_w)(\eta \ \text{sign}(G_w w_2) - \zeta^*) \\ \Gamma_{i1} w_1 &+ \Gamma_{i2} w_2 = 1 \end{aligned}$$

and

$$\begin{aligned} &\min w_1^T P w_1 \quad \text{s.t.} \\ &\Gamma_{i1} w_1 = 1 \\ &|\Gamma_{i1}A_w w_1 - \Gamma_i B_w \zeta^*| \leq |\Gamma_i B_w|\eta \end{aligned} \tag{5.19}$$

Both optimization problems require solving the more general problems

$$\begin{aligned} \min x^T P x \quad & \text{s.t.} \\ F_1 x &= a \\ F_2 x &= b \end{aligned}$$

and

$$\begin{aligned} \min x^T P x \quad & \text{s.t.} \\ F x &= c \end{aligned}$$

For the first problem, a unique solution x^* is readily obtained by Lagrange multipliers, provided that F_1 and F_2 are nonzero and non-parallel. The solution is such that $x^{*T} P x^* = [a\, b] M^{-1} [a \mid b]^T$, where

$$M = \left[\frac{F_1}{F_2} \right] P^{-1} [F_1^T \mid F_2^T]$$

For the second problem the solution is $x^* = cF^T/(FP^{-1}F^T)$ provided $F \neq 0$. It is straightforward to see that M is a symmetric, positive definite two-by-two matrix. Details of the solution to the optimization problems are contained in the appendix. Verification of Corollary 5.4.1 is achieved through the decision procedure shown in Tables 5.5.4 and 5.5.4. The tables are used with the following variables:

$$\begin{aligned} w^+_{2,crit} &= \frac{\bar{M}_{22} - \bar{M}_{12}\Gamma_i B_w(\eta - \zeta^*)}{\Gamma_{i2}\bar{M}_{22}} \\ w^-_{2,crit} &= \frac{\bar{M}_{22} - \bar{M}_{12}\Gamma_i B_w(-\eta - \zeta^*)}{\Gamma_{i2}\bar{M}_{22}} \\ \tilde{w}^+_2 &= \frac{1}{\Gamma_{i2}} \left(1 + \frac{\Gamma_i B_w(\eta - \zeta^*)}{\alpha} \right) \\ \tilde{w}^-_2 &= \frac{1}{\Gamma_{i2}} \left(1 + \frac{\Gamma_i B_w(-\eta - \zeta^*)}{\alpha} \right) \\ \hat{w}_1 &= \frac{P^{-1}\Gamma_{i1}^T}{\Gamma_{i1}P^{-1}\Gamma_{i1}^T} \\ v_1 &= [-\Gamma_i B_w(\eta - \zeta^*) \;\; 1] \\ v_2 &= [\Gamma_i B_w(\eta + \zeta^*) \; 1] \\ v_3 &= [|\Gamma_i B_w|(\eta - \bar{\zeta}) \;\; 1] \\ v_4 &= [-|\Gamma_i B_w|(\eta + \bar{\zeta}) \; 1] \end{aligned}$$

where $\bar{M}_{ij}$ are the entries of M^{-1} and M_{ij} are those of M.

5.5.5 Design Philosophy and Control Constraints

Unlike [20, 19], The method presented here uses a fixed sliding manifold, which is equivalent to fixing a state feedback gain in [19, 20]. That is we do not seek the largest RPI cylinder, as this may be achieved with sliding coefficients that do not satisfy other design requirements. In

Label	Condition
C1	$(\eta - \zeta^*)^2 > \frac{M_{11}}{(\Gamma_i B_w)^2}$
C2	$(\eta + \zeta^*)^2 > \frac{M_{11}}{(\Gamma_i B_w)^2}$
C3	$v_1 M^{-1} v_1^T > 1$
C4	$v_2 M^{-1} v_2^T > 1$
C5	$\left(\frac{\Gamma_i B_w (\eta - \zeta^*)}{\alpha}\right)^2 > M_{22}$
C6	$\left(\frac{\Gamma_i B_w (\eta + \zeta^*)}{\alpha}\right)^2 > M_{22}$
C7	$\Gamma_{i1} P^{-1} \Gamma_{i1}^T < 1$
C8	$v_3 M^{-1} v_3^T > 1$
C9	$v_4 M^{-1} v_4^T > 1$

Table 5.1: Condition Table

Case	Subcase	Condition
$\Gamma_{i1} A_w \nparallel \Gamma_{i1}$	$G_w w_{2,crit}^+ > 0$ and $\Gamma_{i2} \neq 0$	C1
	$G_w w_{2,crit}^+ \leq 0$ or $\Gamma_{i2} = 0$	C3
	$G_w w_{2,crit}^- < 0$ and $\Gamma_{i2} \neq 0$	C2
	$G_w w_{2,crit}^- \geq 0$ or $\Gamma_{i2} = 0$	C4
	$\lvert\Gamma_{i1} A_w \hat{w}_1 - \Gamma_i B_w \zeta^*\rvert \leq \lvert\Gamma_i B_w\rvert \eta$	C7
	$\lvert\Gamma_{i1} A_w \hat{w}_1 - \Gamma_i B_w \zeta^*\rvert > \lvert\Gamma_i B_w\rvert \eta$	C8 and C9
	otherwise	constraint satisfied
$\Gamma_{i1} A_w = \alpha \Gamma_{i1}$	$G_w \tilde{w}_2^+ > 0$ and $\Gamma_{i2} \neq 0$	C5
	$G_w \tilde{w}_2^- < 0$ and $\Gamma_{i2} \neq 0$	C6
	$\Gamma_{i2} = 0$ and $\eta = \lvert\zeta^* - \alpha/(\Gamma_i B_w)\rvert$	C7
	$\lvert\alpha - \Gamma_i B_w \zeta^*\rvert \leq \lvert\Gamma_i B_w\rvert \eta$	C7
	otherwise	constraint satisfied

Table 5.2: Decision Table

this case, the method requires that the SMC design be partially completed before addressing the constraints. More specifically, the sliding hyperplane needs to be chosen *a priori*. Then the decision procedure is applied to determine an allowable combination of switching gain and invariant set. Nominal performance of the sliding motion is thus guaranteed. Several refinements can be incorporated to aid the solution of LMI (5.14). For instance, one may rule out large ellipsoids, e.g., those whose interior contains the constraint set. This is accomplished by enforcing $P > kI$, where k is a suitable positive scalar to be determined from constraint geometry. The volume of the ellipsoid can be maximized under $P > kI$ and the LMI constraint. The problem formulation in this case becomes:

$$\begin{aligned} &\min \ \text{trace}\,(P) \quad \text{s.t.} \\ &\begin{bmatrix} PA_w + A_w^T P + \alpha P & \bar{\zeta}' P B_1 \\ \bar{\zeta}' B_1^T P & -\alpha I \end{bmatrix} \leq 0 \\ &P > kI \end{aligned}$$

Control constraints are easily incorporated in the design. In fact, the control law of Eq. (5.3) can be expressed in x-coordinates as

$$u = -GAx - \eta \ \text{sign}(s)$$

Thus, it is straightforward to show, using the triangle inequality, that a control constraint of the form $|u| \leq \bar{u}$ can be accommodated by introducing the additional state constraints $\Gamma_u w \leq 1$ and $-\Gamma_u w \leq 1$, where

$$\Gamma_u = \frac{GAJ}{\bar{u} - \eta}$$

5.6 Numerical Example

Consider the following controllable pair:

$$A = \begin{bmatrix} -1 & 0 & 0 \\ 1 & -2 & -1 \\ 0 & 1 & 0 \end{bmatrix}; \quad B = \begin{bmatrix} 1 \\ 0 \\ 1 \end{bmatrix}$$

Consider that the constraints in x-coordinates are given by a parallelepiped containing the origin in its interior. The rows Γ_x specify individual constraints:

$$\Gamma = \begin{bmatrix} 0.8 & 0.32 & -0.16 \\ -1 & -0.4 & 0.2 \\ 0 & 0.96 & 0.32 \\ 0 & -1.2 & -0.4 \\ 0 & 0.4 & 0.8 \\ 0 & -0.5 & -1 \end{bmatrix}$$

Suppose that the disturbance is given by $\zeta(t) = 0.2 \sin(10t)$. An appropriate set of transformation matrices is given by

$$T = \begin{bmatrix} 1 & -1 & 1 \\ 0 & 1 & 0 \\ 0 & -1 & 1 \end{bmatrix}; \quad K = \begin{bmatrix} 1 & 0 & -1 \\ 0 & 1 & -0.5 \\ 0 & 0.5 & 1 \end{bmatrix}; \quad J = \begin{bmatrix} 1 & -0.5 & 0.5 \\ 0 & 1 & -0.5 \\ 0 & -0.5 & 1.5 \end{bmatrix}$$

The transformed constraints are obtained as the rows of $\Gamma_x J$:

$$\Gamma_x J = \Gamma = \begin{bmatrix} 0.8 & 0 & 0 \\ -1 & 0 & 0 \\ 0 & 0.8 & 0 \\ 0 & -1 & 0 \\ 0 & 0 & 1 \\ 0 & 0 & -1.25 \end{bmatrix}$$

Note that the constraints are not symmetric in either x or w coordinates. Using the transformation $x = TKw = Jw$, matrix A_{11} has two negative eigenvalues. Choosing to place the poles of A_w at $[-1.5 \pm 0.5i]$ results in $G_1 = [0 \ -0.5]$, which corresponds to $G = [0 \ 0.5 \ 1]$ in the original x-coordinates. The range for α is $(0, 3)$. Choosing an arbitrary fixed $\alpha = 2.1$, we solve the volume optimization problem using $k = 0.5$ and $\eta + \bar{\zeta} = 1$. The solution is a matrix P with $[0.8284, 0.6581]$ is the diagonal and -0.2278 in the off-diagonal. Choosing $\eta = 0.8$ satisfies the decision procedure for constraint qualification and thus the intersection of the cylinder and state constraints in w-coordinates is RPI. Of course, the intersection of the transformed cylinder and constraints in x-coordinates is also RPI. Using the alternative method with the same P matrix, we obtain $\beta = 2.3324$ and

$$\eta_{crit} + \bar{\zeta} = \frac{\beta}{2\sqrt{B_1^T P_w B_1}} = 1.6667$$

Then we may choose, for instance, $\eta = 1.4$ for ellipsoidal invariance alone, but the second constraint would be violated. Figure 5.2 sketches the shape of constrained cylinder in w-coordinates. Figure 5.3 sketches, in x-coordinates, the trajectories projected onto the $x_3 = 0$ plane, and the constraints and transformed cylinder section at $x_3 = 0$.

5.7 Nonlinear Systems

Certain kinds of nonlinear system under Sliding Mode Control with linear manifolds have reaching dynamics similar to that of linear systems. SI nonlinear systems in integrator-cascade form are a direct example. Certain minimum-phase, nonlinear MIMO systems under tracking control via sliding modes result in decoupled tracking error dynamics which can be also treated with the methods described here. In the case of the mixer, such decoupling is possible and the output tracking error behaves as

$$\ddot{e}_\rho + c_\rho \dot{e}_\rho = -\eta_1 \ \text{sign}(s_1)$$
$$\ddot{e}_P + c_P \dot{e}_P = -\eta_2 \ \text{sign}(s_2)$$
$$\dot{e}_w + c_w e_w = -\eta_3 \ \text{sign}(s_3)$$

where the subindices indicate density, pressure and flow. It is clear that positively invariant sets can be found for the tracking errors by considering each equation independently and using the methods described above. Valve positions, however, do not appear explicitly in the above input/output equations, as they constitute internal states. An analysis of the mixer nonlinear dynamics is required to determine if valve positions can be used in a linear state-space realization of the above error dynamics. If that were possible, the methods of this work could be directly applied.

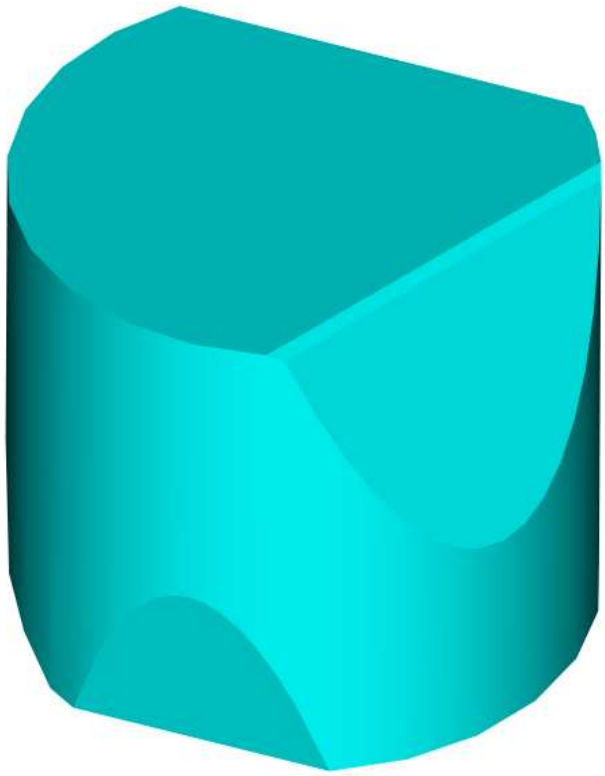

Figure 5.2: RPI State constrained-cylinder

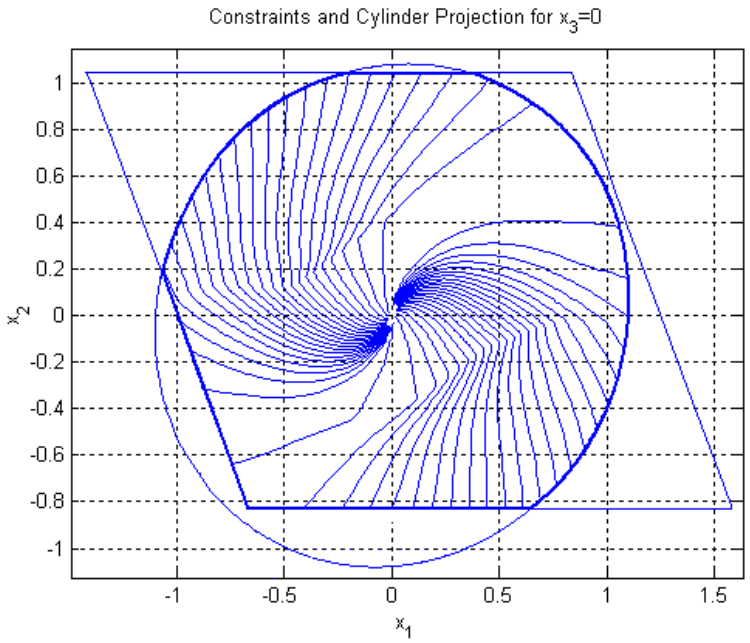

Figure 5.3: Projected trajectories, cylinder and constraints onto $x_3 = 0$

5.7.1 Nonlinear Systems in Integrator Cascade Form

Consider the single-input system

$$\begin{aligned} \dot{x}_1 &= x_2 \\ &\vdots \\ \dot{x}_{n-1} &= x_n \\ \dot{x}_n &= f(x) + g(x)u \end{aligned} \tag{5.20}$$

where $g(x) \neq 0$ in a convex region of $\mathbb{R}^n$ containing the origin. As in the linear case, let the sliding function be defined by $s = Gx$. Suppose the control input u is such that

$$\dot{s} = -\eta \ \text{sign}(s)$$

with $\eta > 0$. Assume w.l.o.g. that the n-th component of G is 1. Then the closed-loop dynamics can be expressed as

$$\begin{cases} \begin{bmatrix} \dot{x}_1 \\ \vdots \\ \dot{x}_{n-1} \\ \dot{x}_n \end{bmatrix} = \begin{bmatrix} 0 & 1 & \dots & 0 \\ \vdots & \dots & & \vdots \\ 0 & 0 & \dots & 1 \\ 0 & -G_1 & \dots & -G_{n-1} \end{bmatrix} \begin{bmatrix} x_1 \\ \vdots \\ x_{n-1} \\ x_n \end{bmatrix} - \begin{bmatrix} 0 \\ \vdots \\ 0 \\ 1 \end{bmatrix} \eta \ \text{sign}(s) \\ \\ s = Gx \end{cases} \tag{5.21}$$

When sliding occurs, $\dot{x}_n = -[G_1 \ G_2 \ ...G_{n-1}].[x_2 \ ...x_n]^T$ and the last state equation in (5.21) is redundant with the sliding condition $\dot{s} = 0$. The reduced dynamics is described by

$$\begin{bmatrix} \dot{x}_1 \\ \vdots \\ \dot{x}_{n-2} \\ \dot{x}_{n-1} \end{bmatrix} = \begin{bmatrix} 0 & 1 & \dots & 0 \\ \vdots & \dots & & \vdots \\ 0 & 0 & \dots & 1 \\ -G_1 & -G_2 & \dots & -G_{n-1} \end{bmatrix} \begin{bmatrix} x_1 \\ \vdots \\ x_{n-2} \\ x_{n-1} \end{bmatrix} \tag{5.22}$$

Define the constant matrix in Eq. (5.22) as A_w. This matrix has the standard controllability form, and it is clear how to choose the first $n-1$ coefficients of G to achieve a stable sliding mode. In the following, it will be assumed that A_w is Hurwitz. As in the linear case, we seek a coordinate transformation which reveals the defective structure of the constant matrix in Eq.(5.21). The existence of such transformation is ascertained in the following

Lemma 5.7.1. *There exists a coordinate transformation $x = Jw$ with J nonsingular in which the closed-loop dynamics (5.21) are expressed as*

$$\begin{cases} \left[\begin{array}{c} \dot{w}_1 \\ \hline \dot{w}_2 \end{array}\right] = \left[\begin{array}{c|c} A_w & 0 \\ \hline 0 & 0 \end{array}\right] \left[\begin{array}{c} w_1 \\ \hline w_2 \end{array}\right] + \left[\begin{array}{c} B_1 \\ \hline -1 \end{array}\right] \eta sign(s) \\ \\ s = w_n \end{cases} \tag{5.23}$$

where $B_1 = [0 \ .... \ 1]^T$.

One possible form of J that verifies Lemma 5.7.1 is given by

$$J^{-1} = \begin{bmatrix} 0 & 1 & \dots & 0 \\ \vdots & \dots & \vdots & \\ 0 & 0 & \vdots & 1 \\ G_1 & G_2 & \dots & 1 \end{bmatrix} \tag{5.24}$$

Once the system is written in w-coordinates, it is straightforward to find invariant tunnels with the methods of previous sections.

5.8 Application: Invariant Intervals for Mixer Outputs

Under the sliding mode control law of Eq.(4.24), it is clear that the tracking error dynamics is given by

$$\ddot{e}_\rho + c_\rho \dot{e}_\rho = -\eta_1 \text{ sign}(s_1) \tag{5.25}$$
$$\ddot{e}_P + c_P \dot{e}_P = -\eta_2 \text{ sign}(s_2) \tag{5.26}$$
$$\dot{e}_w + c_w e_w = -\eta_3 \text{ sign}(s_3) \tag{5.27}$$

The developed theory can be directly applied to obtain conditions under which a given interval is positively invariant. This is particularly useful in the case of the pressure. If mixer pressure is outside the range of supply and discharge pressures, flow reversals and control singularities may result. As it will be seen next, enforcing invariant intervals for the pressure will also have beneficial effects on tracking performance. Note that absolute temperatures are always positive, thus enforcing a positive pressure interval will necessarily result in a positive density state at all times and physical feasibility of the control scheme is maintained.

5.8.1 Invariant Pressure Intervals

It is straightforward to see that the closed-loop dynamics (5.26) is equivalent to a double integrator plant under sliding mode control with manifold

$$s_2 = \dot{e}_P + c_P e$$

Thus the theory presented earlier is immediatly applicable with matrices

$$A = \begin{bmatrix} 0 & 1 \\ 0 & 0 \end{bmatrix} \; ; \; B = \begin{bmatrix} 0 \\ 0 \end{bmatrix} \; ; \; G = [c_p \;\; 1]$$

The objective is to guarantee that $P_s < P < P_1$, where it has been assumed, w.l.o.g., that $P_1 = \min(P_1, P_2)$. This can be achieved by setting a margin $\delta > 0$ such that $|P_d - P| = |e_P| < \delta$ and by restricting the reference pressure to satisfy $P_d \leq P_1 - \delta$ and $P_d \geq P_s + \delta$. Note that this is in fact a performance requirement, since bounds are being placed on the tracking error $|e_P|$. Although the theory so far developed will yield invariant sets of simple description in *some*

set of coordinates, it turns out that, in this case, positively invariant intervals in the original coordinates are also directly obtained. The transformations T and K and J are chosen as

$$T = \begin{bmatrix} 1 & 0 \\ 1 & 1 \end{bmatrix} \; ; \; K = \begin{bmatrix} 1 & -1 \\ -(c_P+1) & 1 \end{bmatrix} \; ; \; J = \begin{bmatrix} 1 & -1 \\ -c_P & 0 \end{bmatrix} \tag{5.28}$$

The reaching dynamics is expressed in w-coordinates as

$$\begin{aligned} \dot{w}_1 &= -c_P w_1 + \frac{1}{c_P}\eta \, \text{sign}(s) \\ \dot{w}_2 &= \frac{1}{c_P}\eta \, \text{sign}(s) \\ s &= -10 w_2 \end{aligned}$$

Since $|e| = c_P|w_1|$, it can be readily established that the interval defined by $|e| < \delta$ is positively invariant if

$$\eta \leq \frac{c_P^3}{\delta}$$

Chapter 6

A Graphical User Interface for Mixer Simulations

The fairly complete modeling and control analysis effort for the mixer must be complemented with a simulation environment. The purpose of this activity is to develop and program a Graphical User Interface (GUI) for mixer simulations using the validated model and its controls. The objective is to generate a GUI which allows simulations and control tuning without advanced knowledge in control theory or mathematical models, so that operations personnel can benefit from the results of this research. While the programming details are left out for not constituting a research activity, some of the design criteria and a basic functional description of the GUI follow. Although some packages like EASY5 and GFSSP [14] are available that incorporate the basic laws of fluid flow and thermodynamics, the objective here is to construct a simulation environment that trades off generality by increased flexibility, modularity and ease of use in test stands and associated technologies. Key innovations are cited below

1. Use of advanced concepts in modeling and control: Test stands and related subsystems are fairly predictable and governed by basic laws of thermodynamics and fluid flow. Therefore reliable dynamic models are possible to construct. Models generally consist of systems of nonlinear ordinary differential equations. Model properties that are relevant to actual system operation can be inferred through mathematical analysis of the model. The determination and tuning of control strategies can be likewise carried out with the aid of modern control theories. The currently available hardware does not permit implementation of advanced concepts in real-time operations. That is, most real-time control processing is implemented in programmable logic controllers (PLC). Advances in processing speed and hardware/software architectures by 2006 will be suitable for the deployment of advanced concepts in modeling and control.

2. Modularity and expandability: Isolated subsystems are modeled in a modular fashion. Each model has a number of inputs and outputs and corresponding connection rules. Modularity allows the simulation of individual subsystems by feeding them with predefined data, or of larger systems by interconnecting the inputs and outputs of various subsystems according to connection rules. Modules may be added indefinitely to create expanded systems. An important advantage of a modular set of models is that a working

simulation is available as soon as the first module is complete, thus making possible a concurrent use and development of the simulation tool.

3. Flexibility and user-friendliness: Programs such as EASY5 and GFSSP [14] can, in principle, be customized to meet simulation needs for test stand facilities. They, however, lack the flexibility that the proposed environments will provide. Both packages require a trained and experienced user. Moreover, including feedback loops may require the writing of code. The proposed simulation environments will present graphical user interfaces (GUI) that mask the mathematics governing the model in a black-box approach. A user needs to be familiar with the actual test stand only, not with a particular scripting language.

4. Accuracy: The incorporation of the latest modeling and control technologies in the models and simulation environments will produce more accurate simulations. Future test requirements will demand higher accuracies than those possible with current prediction and control schemes. The modeling work proposed here will satisfy future demands for higher prediction accuracy. Accurate simulations and model validation has a direct impact in design and operation of test stands, and both activities will need to be done more effectively than today.

5. Integration: The proposed simulation tools will link with health management technologies (HMT) directly. The simulations will provide inputs to HMT and get important information about system changes from HMT.

6.1 Functional Description

The front interface is shown in Fig. 6.1. A brief description of GUI functions follows.

- Input Fluid Properties: The user enters either a constant pressure and temperature for the GH2 and LH2 or clicks on the From File button to import two ASCII-formatted data files.

- Mixer Parameters: The simulation must start with some pressure and temperature of the fluid inside the mixer. These constants, along with the volume of the mixer in cubic feet are entered.

- Exit Pressure: The model considers the pressure past the exit valve a boundary condition, that is, it must be supplied as a parameter. The user has the option of specifying a constant pressure by directly typing it in the box, or using a time-varying pressure from a file.

- Control Valves: Each control valve is defined in the same way. The user clicks on the Parameters button and enters the value of the flow coefficient when the valve is fully open, the time constant, and the gain between percent opening and commanded opening (in percent per volt). In this version, the relationships between flow coefficient, percent opening and commanded opening are taken as linear. The user then clicks on the Source button and specifies how the particular valve will be operated. The choices are to leave the

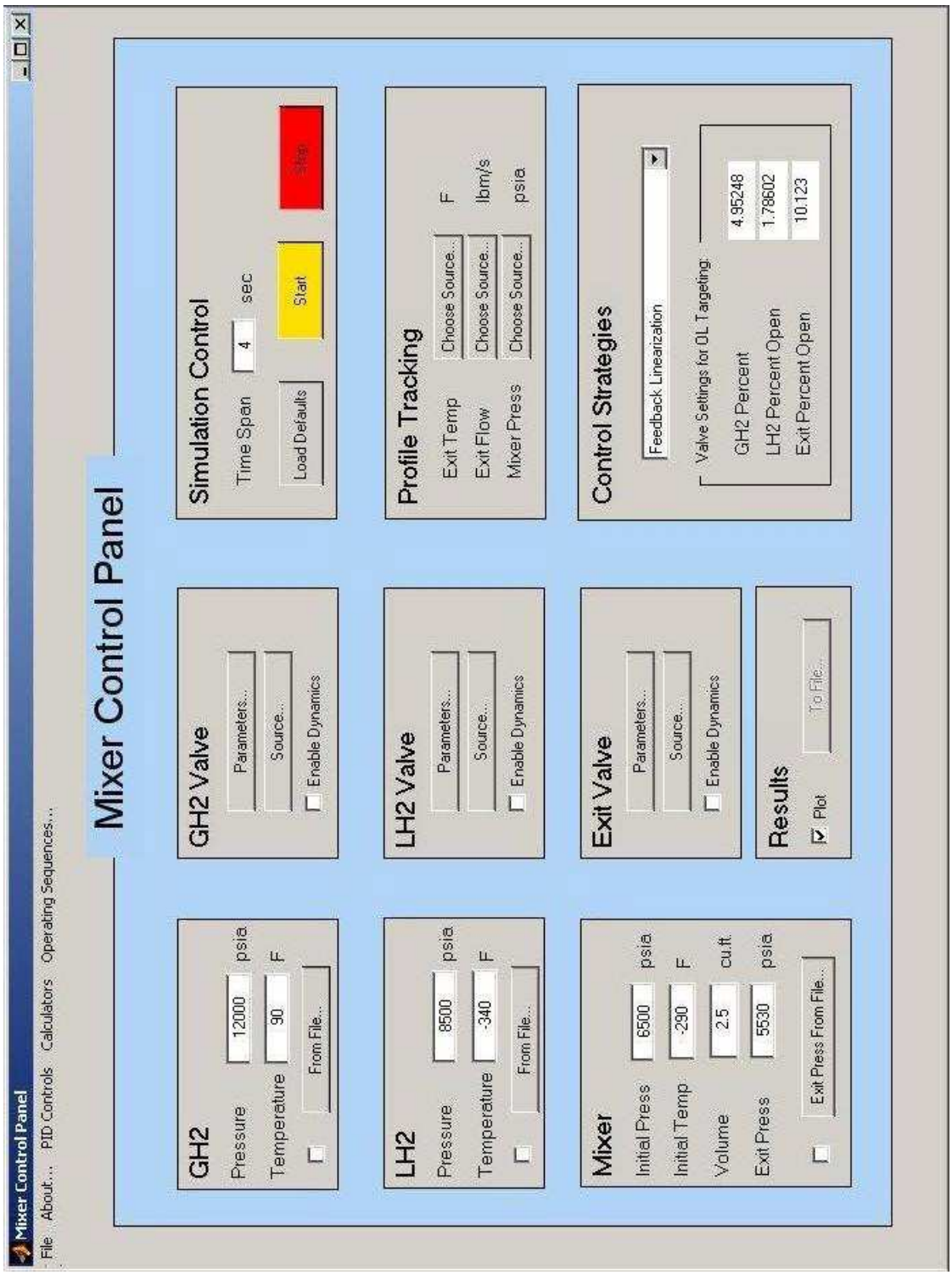

Figure 6.1: The front interface

percent opening fixed by typing a value between 0 and 100 in the Constant box, to specify a ramp by entering the appropriate values, or to import a valve opening history from a file. The file must be in ASCII format and contain two columns of data, the first one containing time and the second one containing the corresponding percentage opening. If the Enable Dynamics box is checked, a first order transfer function with the specified gain and time constant is assumed between commanded and actual valve openings. Otherwise, the GUI takes a zero time constant and sets the gain to one.

- Profile Tracking: This area is used to enter desired output profiles when operating under feedback control. The user chooses the outputs to be constant setpoints, ramps, or arbitrary profiles imported from a data file.

- Control Strategies: The user selects a control option from a pull-down list. The following options are available:

    1. Pressure PI Control (GH2 Valve Only): This simulates the automatic stage of the control mode often used at the test stands. A feedback loop is formed by measuring mixer pressure and using the tracking error in a proportional-integral law. The GH2 valve is actuated, while the LH2 and exit valves remain at fixed positions. The proportional and integral gains are selected in the PI Controls pull-down menu at the top-level interface.
    2. Multi Input PI Control: This control law simultaneously actuates the three valves. It is based on the work done by Barbieri [3]. The control law was derived based on local linearization of the model equations. It is useful for regulation close to a steady setpoint or for commanding the output variables in small ranges.
    3. Feedback Linearization: This control law simultaneously actuates the three valves. It is based on the work done by Richter [26]. The control law may be used for regulation or tracking over wide ranges of the output variables. The gains involved in the control law are hidden from the user in this version.
    4. Manual Valve Control: If this option is selected, simulation proceeds in open-loop, using the valve profiles specified in the Control Valves area
    5. Operating Sequence: This option allows to schedule switching between control strategies during a simulation. Simulation may be initiated, for instance, in manual mode. When switching criteria are met, the control mode is switched to one of the automatic options. The automatic mode may be then released and operation may be switched to a shutdown procedure. Switching criteria is entered as time values or values for combinations of process variables.

6.1.1 Calculator Functions

In addition to the dynamic simulation modes, the GUI operates as a steady-state calculator, namely two functions are incorporated:

- Setpoint Targeting: The GUI calculates the constant valve openings required to obtain the steady output values specified as Constant in the Profile Tracking area. The results are displayed in the text boxes.

- Operating Point: This operation is the inverse of Setpoint Targeting. It calculates the steady mixer pressure, exit flow and exit temperature that result when the control valves are left at the constant openings specified in the Control Valves area.

6.1.2 Operating Sequences

Actual mixer operation is frequently done according to a schedule where switching between manual and closed-loop controls may occur. In one of the typical operating modes, the mixer is first manually brought close to a desired operating point and a feedback controller is then engaged. The Operating Sequence feature allows to simulate such modes. The user specifies control strategies, control objectives and manual valve actions using the interface. Upon selecting the Operating Sequence mode, the user is prompted for a condition to be satisfied for the current control settings to be effective. The user enters the condition as a Matlab string, for example `'(t>2) & (abs(P-7000))<=10'` specifying that the current control settings become active if the pressure is between 6990 and 7010 psia and the time is greater than 2 seconds. The GUI then records the settings and adds them to a schedule. An arbitrary number of events can be scheduled. If Operating Sequence is selected as a control strategy, then the simulation proceeds according to schedule.

6.1.3 Simulation Control and Results

In this version, the user has control over the simulation time span, and can start and stop a simulation by clicking on the appropriate button. The simulation is performed by Simulink. Advanced users may access the file containing the simulation diagram and modify parameters such as numerical method, time steps and tolerances. If the Plot check box is enabled, the simulation results are displayed in windows, from where they may be printed.

Chapter 7

Pressurization and Collapse in Cryogenic Tanks

The high oxidizer and fuel pressures typically required by engine and component testing are achieved by means of a run-tank equipped with a pressurization mechanism. A typical spherical run tank is depicted in Figure 7. The tank is partially filled with the liquid propellant to be pressurized. The space above the liquid surface is occupied by a gaseous pressurant, typically Nitrogen for LOX run tanks and Hydrogen for LH2 run tanks. The gas contained in the tank is known as *ullage*. There exist several methods of pressurization [28], broadly classified into self-pressurization and external pressurization. Self-pressurizing systems use the vapor produced by the boil-off of the liquid propellant due to heat transfer. In this project we concentrate on external pressurization systems, which rely on an independent source of pressurant gas. In this configuration, the liquid is pressurized by controlled injection of pressurant from high pressure bottles. A control valve is installed between the upper portion of the tank and the storage bottles. This valve serves as primary control element for the tank pressurization. The pressure is usually controlled with a PI loop as shown in Figure 7.2. Pressure collapse of cryogen propellant during pressurization has been identified as an effect that often leads to down time and test disruptions. Physically, the collapse occurs when the incoming stream of warm gas is violently cooled by contact with the cryogenic liquid. The sudden drop in temperature creates a pressure drop which counteracts pressure build-up from the added mass. Depending on key parameters such as incoming flow rate and temperature and degree of mixing, the two competing effects result in an initial pressure build-up followed by collapse. In some cases, pressure recovery is observed. The phenomenon is worsened by control valve saturation and the subsequent integrator windup in the PI loop. The purpose of this section is to construct the simplest possible dynamic model, consisting of ordinary differential equations, that captures the collapse phenomenon qualitatively and with an acceptable degree of numerical accuracy against activation data. Once the model is validated and refined, it is desired to study the effects of the control loop on the collapse phenomenon, initially by simulation with various PI gains (including actual gains) followed by an in-depth analysis to determine if a properly designed controller can mitigate the collapse effect.

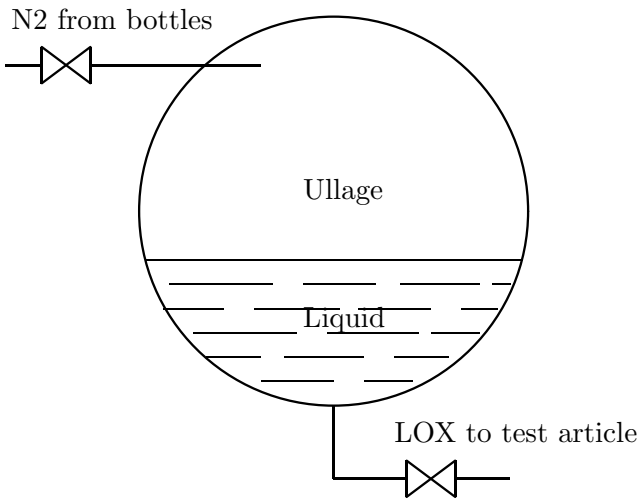

Figure 7.1: Oxygen run tank schematic

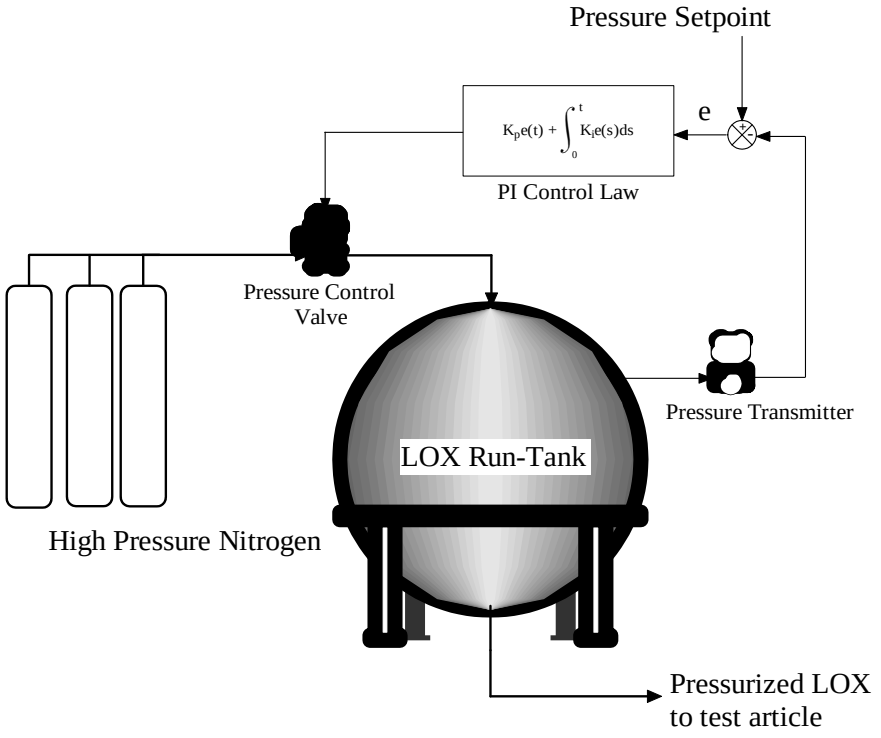

Figure 7.2: Run-Tank Pressurization System

7.1 Simplest Model for Tank Pressurization

A fairly detailed model of the run-tank that feeds the mixer was developed by Follet and Taylor [7] and programmed in EASY5/ROCETS for simulation studies. While the model is adequate to predict the behavior of variables related to tank operation, it introduces complexity that makes it difficult to use it for controller design purposes. Specifically, the calculation of heat transfer through tank walls and between the vapor-liquid interface is what introduces complexity in the form of cumbersome mathematical expressions and iterative procedures. As stated by the authors in page 6 of [7], the heat transfer correlations use Rayleigh numbers that exceed the recommended limiting values, possibly introducing errors. In the following model, the heat transfer through tank walls is set to zero, while the exchange of heat between the phases is not explicitly considered in the equations, for the energy balance equation uses the whole tank as a control volume. Mass conservation is still applied separately to the liquid and vapor phases, and the assumption that there is no net exchange of mass through the vapor-liquid interface is also used. The model in [7] uses the same assumption with good results. The proposed control model will be compared to the existing model in its prediction capabilities. The basic governing equations can be obtained from conservation of mass and the First Law of Thermodynamics for a control volume with transient terms. Refer to Figure 7.2 for a depiction of the pressurization system. The following assumptions are made in the derivation of the first model:

- The tank is adiabatic.
- A single coefficient is used to describe the heat transfer between gas and liquid under all conditions of stirring and mixing. The coefficient, however may be allowed to vary during pressurization.
- No gas is condensed.
- The inlet valve behaves isoenthalpically.
- The ullage and liquid pressures are equal at all times.
- The bulk temperature of the liquid does not change during pressurization.

Denote the source gas mass flow rate and enthalpy by w and h_1, respectively. Let T, ρ, P and u denote the ullage gas temperature, density, pressure and internal energy. Let T_c be the bulk temperature of liquid and $\dot{V}(t)$ denote the instantaneous volume the liquid in the tank, so that the work done by the ullage is given by $\dot{V}(t)P$. The energy and mass balances for the ullage give the following system of differential equations:

$$\dot{\rho} = \frac{1}{V(t)}\left\{w(t) - \dot{V}(t)P\right\} \tag{7.1}$$

$$\dot{u} = \frac{1}{V(t)\rho}\left\{-\dot{V}(t)P + w(t)(h_1 - u) - \eta(T - T_c)\right\} \tag{7.2}$$

where η is a heat transfer coefficient which encompasses all mixing effects. Note that all quantities -except T_c- are time-varying, however the explicit time dependence notation has been used for $V(t)$ and $w(t)$ only, to emphasize that they are exogenous inputs to the dynamic system.

According to [28, 15], η can be calculated from a natural convection correlation involving the Prandtl and Grashoff numbers of the ullage gas:

$$\begin{aligned} \eta &= h_c A, \text{ where:} \\ h_c &= K_h C \frac{K_f}{d} (\text{Gr Pr})^n \end{aligned} \tag{7.3}$$

K_h, C and n are constants, K_f is the thermal conductivity of the ullage, d is a characteristic length, A is the area of the liquid-ullage interface, and Gr and Pr are the Grashoff and Prandtl numbers, respectively. The above equations already show a basic qualitative description of the competing effects: as more mass enters the tank with rate w, the internal energy increases due to the second summand in Eq. (7.2). However, the third summand is negative whenever the ullage gas is warmer than the liquid, creating a counteracting effect. The interplay of these contributions to the energy derivative depends on the operating parameters, mainly η, T_c and w. Although the description given in [28] is mostly academic, it is possible to leave η as an unknown function of to be identified from experimental data. The identification of η is listed as future work in Section 8.1. Note also that the pressure P and temperature T of the ullage are functions of the state variables ρ and u, as are the variables participating in the calculation of η and $w(t)$, making Eqs. (7.1) and (7.2) a self-contained system of differential equations.

Chapter 8

Conclusions and Future Directions for Research

Tenure lasted 31 months, during which a significant amount of results relevant to rocket test stand modeling, simulation and control have been produced. Moreover, the research activity has inspired novel theoretical work in the area of constrained control and has revealed new directions for research at the intersection of control theory, thermodynamics and fluid flow.

8.1 Work in Progress and Future Work

Modeling work on test stand subsystems can benefit from the development of an efficient thermodynamic property library for Matlab, relying on correlations instead of table look-ups and interpolation. Such work has been completed for Oxygen and will be continued for Hydrogen and Nitrogen.

The theoretical developments in constrained sliding mode control need to be expanded to include the multivariable case, to consider tracking problems and to incorporate a chattering reduction mechanism which is compatible to the cylinder methodology. The boundary layer approach of Slotine [30] seems appropriate, as the boundary layer itself enjoys invariance properties. The tracking errors in the mixer problem have linear dynamics falling in the framework of the cylinder approach, however the possibility of applying the theory to constraints in the C_v coefficients is still unclear. That is, the theory can be used to limit the ranges of thermodynamic variables, but the fundamental issue of valve position constraints is yet to be solved.

Work on the run tank model requires experimental data tailored to the needs of the project. It remains unclear at this point if the data routinely collected during tests is adequate for system identification and parameter estimation procedures. Upon a successful validation of the run tank model, its interconnection with the mixer can be modeled.

Work on the GUI can continue by developing an interface for the validated run tank model. Ultimately, a collection of GUIs developed for independent subsystems can be brought together in a GUI suite which facilitates large-scale simulations. While the GUI presented here is prototypical, future versions need to address the issue of execution speed, which is already low, even for the mixer alone. Compilation of modules and routines into dynamic run-time libraries may improve execution speed. Substitution of the look-up routines for thermodynamic properties by

efficient ones based on correlations is also expected to significantly improve execution speed.

Bibliography

[1] J.P. Aubin and A. Cellina. *Differential Inclusions*. Springer-Verlag, 1988.

[2] E. Barbieri. Small signal modelling and control of the hydrogen mixer for facility E-1. Technical report, Final Report, ASEE Summer Faculty Program, 2001.

[3] E. Barbieri and et. al. Small-signal point to point tracking of a propellant mixer. In *American Control Conference*, pages 2845–2850, 2003.

[4] F. Blanchini. Set invariance in control. *Automatica*, 35:1747–1767, 1999.

[5] M. Brockman and M. Corless. Quadratic boundedness of nominally linear systems. *International Journal of Control*, 71(6):1105–1117, 1998.

[6] Y.S. Chou and et.al. Robust controller design for uncertain nonlinear system via feedback linearization. *Chemical Engineering Science*, 50(9):1429–1439, 1995.

[7] R.F. Follet and R.P. Taylor. CTF dynamic fluid flow modeling program. Technical report, Contract Number NAS13-564, Delivery Order 83, 1996.

[8] P. Gutman and P. Hagander. A new design of constrained controllers for linear systems. *IEEE Transactions on Automatic Control*, AC-30:22–33, 1985.

[9] M. Innocenti and M. Falorni. State constrained sliding mode controllers. In *American Control Conference*, pages 104–108, 1998.

[10] U. Itkis. *Control Systems of Variable Structure*. John Wiley, 1977.

[11] T. Kailath. *Linear Systems*. Prentice-Hall, 1980.

[12] V. Krivan. On the intersection of contingent cones. *Journal of Optimization Theory and Applications*, 70(2):397–404, 1991.

[13] M. Krstc and Kanellakopoulos. *Nonlinear and Adaptive Control Design*. John Wiley, 1995.

[14] A. Majumdar. Generalized fluid system simulation program (gfssp). Technical report, Sverdrup Technologies, Report MG-99-290, 1999.

[15] A. Majumdar and T. Steadman. Numerical modeling of pressurization of a propellant tank. In *37th AIAA Aerospace Sciences Meeting Conference and Exhibit*, pages NV AIAA 99–0879, 1999.

[16] A. Michel and C. Herget. *Applied Algebra and Functional Analysis*. Dover, 1981.

[17] M. Nagumo. Über die Lage der Integralkurven gewöhnlicher Differentialgleichungen. *Proc. Physico-Mathematical Society of Japan*, 24:272–559, 1942.

[18] M.J. Nieuwstadt and R. Murray. Real time trajectory generation for differentially flat systems. *International Journal of Robust and Nonlinear Control*, 8(11):995–1020, 1998.

[19] B.D. O'Dell. *Ellipsoidal and Semiellipsoidal Controlled Invariant Sets for Constrained Linear Systems*. PhD thesis, Oklahoma State University, 1999.

[20] B.D. O'Dell. Semi-ellipsoidal controlled invariant sets for constrained linear systems. *ASME Journal on Dynamic Systems, Measurements and Control*, 124:98–103, 2002.

[21] H. Richter. Tracking of a thermodynamic process using a polytropic surface as sliding manifold. In *American Control Conference*, pages 197–201, 2003.

[22] H. Richter. Robust nonlinear control of a thermal mixing process. In *To be presented at the IEEE Conference in Control Applications, Taipei, Taiwan*, 2004.

[23] H. Richter, E. Barbieri, and F. Figueroa. Modelling and validation of a propellant mixer for controller design. *Accepted, Applied Mathematical Modelling*, 2004.

[24] H. Richter and *et.al.* A graphical user interface for modeling, simulation and control design of a propellant mixer, new technology item ssc-00213-1. *To appear, NASA Tech Briefs*, 2004.

[25] H. Richter and et. al. Modelling, simulation and control of a propellant mixer. In *AIAA/ASME/SAE/ASEE Joint Propulsion Conference and Exhibit*, 2003.

[26] H. Richter and et. al. Nonlinear modeling and control of a propellant mixer. In *American Control Conference*, pages 2839–2844, 2003.

[27] H. Richter and F. Figueroa. A matlab-based graphical user interface for simulation and control design of a propellant mixer. In *Accepted, AIAA/ASME/SAE/ASEE Joint Propulsion Conference and Exhibit*, 2004.

[28] E. Ring. *Rocket Propellant and Pressurization Systems*. Prentice-Hall Space Technology Series, 1964.

[29] J-H. She and et.al. Flow and temperature control of a tank by backstepping method. In *International Conference on Motion and Vibration Control*, 1998.

[30] J.J. Slotine and W. Li. *Applied Nonlinear Control*. Prentice-Hall, 1991.

[31] V.I. Utkin. *Sliding Modes in Control Optimization*. Springer-Verlag, 1992.

Appendix A

A.1 Construction of T

One of many ways to select T is presented here. Partition T congruently to A and B and write the requirements as

$$T_{11}b_1 + T_{12}b_2 = 0$$

$$T_{21}b_1 + T_{22}b_2 = 1$$

where the T_{ij} denote the block components of T^{-1} and b_1 and b_2 those of B. Denote the (1,1) component of $T^{-1}AT$ by A_{11}, as in Section 5.3 and let a_{ij} denote the components of A. Suppose, w.l.o.g., that the scalar b_2 is nonzero, which can be always achieved by re-labeling the states if necessary. Then select any invertible T_{11} and choose

$$T_{12} = -\frac{T_{11}b_1}{b_2}$$

Selection of T_{21} can be done so that the (1,1) block of $T^{-1}AT$ has desired eigenvalues, specifically, to make it nonsingular. In fact, using the block matrix inversion results from [11] and performing lengthy algebra it is possible to show that $A_{11} = T_{11}\tilde{A}_{11}T_{11}^{-1}$, where $\tilde{A}_{11} = \hat{A} - \hat{B}T_{21}$, with

$$\hat{A} = a_{11} - \frac{b_1 a_{21}}{b_2}$$

and

$$\hat{B} = \left[\left(a_{11} - \frac{b_1 a_{21}}{b_2}\right) b_1 + \left(a_{12} - \frac{b_1 a_{22}}{b_2}\right) b_2\right]$$

Thus T_{21} can be used to assign nonzero eigenvalues to $\tilde{A}_{11}$ with the restriction $T_{21}b_1 \neq 1$. Since A_{11} is similar to $\tilde{A}_{11}$, it is nonsingular. The selection of T is finished by choosing

$$T_{22} = \frac{1 - T_{21}b_1}{b_2}$$

Note that $T_{22} \neq 0$, therefore T is indeed invertible [11].

A.2 Proof of Lemma 5.3.1

Since

$$(I - BG)A = T \left[\begin{array}{c|c} A_{11} & A_{12} \\ \hline -G_1 A_{11} & -G_1 A_{12} \end{array}\right] T^{-1}$$

J can be chosen as TK where K is an invertible matrix such that

$$K^{-1} \left[\begin{array}{c|c} A_{11} & A_{12} \\ \hline -G_1 A_{11} & -G_1 A_{12} \end{array}\right] K = \left[\begin{array}{c|c} A_{11} - A_{12}G_1 & 0 \\ \hline 0 & 0 \end{array}\right]$$

Using the block matrix inversion results of [11] it can be shown that the following is a solution:

$$K = \left[\begin{array}{c|c} I & -A_{11}^{-1}A_{12} \\ \hline -G_1 & 1 \end{array}\right]$$

Note that invertibility of A_{11} is guaranteed by choice of T as explained in Section A.1. Moreover, with such choice of J we have that the sliding manifold coefficients are expressed in w-coordinates as

$$s = GJw = (GT)Kw = [G_1 \mid 1]\, Kw = \left[0 \mid -G_1 A_{11}^{-1} A_{12} + 1\right] w = G_w w_2$$

Also, B_2 can be readily found to be

$$B_2 = (G_1 A_{11}^{-1} A_{12} - 1)^{-1}$$

which results in $B_2 G_w = -1$.

A.3 Proof of Theorem 5

(*Sufficiency*). In view of Th. 2, we wish to show that $f(w,\zeta) \in \mathcal{C}_{\mathcal{S}}(w)\ \forall w \in \partial\mathcal{S}, \forall \zeta \in \mathcal{Z}$. It is possible to show, under the convexity and closure assumptions, that one can decompose the boundary of $\mathcal{S}$ as

$$\partial\mathcal{S} = (M \cap \partial G) \cup (\partial M \cap G)$$

First, we show that $f(w,\zeta) \in \mathcal{C}_{\mathcal{S}}(w)\ \forall\, w \in (M \cap \partial G)$. By hypothesis, $\Gamma_i f(w,\zeta) \leq 0\ \forall w \in \mathcal{S} \cap \partial G_i, \forall \zeta \in \mathcal{Z}, i = 1, 2..m$. Noting that $\bigcup(\mathcal{S} \cap \partial G_i) = M \cap \partial G$ we have that $f(w,\zeta) \in \mathcal{C}_G(w) \forall w \in (M \cap \partial G)$. Now, since $\partial G \cap M \subset M$ we have that, if $w \in \text{int}(M)$ then $\mathcal{C}_M(w) = \mathbb{R}^n$, thus $f(w,\zeta) \in \mathcal{C}_M(w)$, whereas if $w \in \partial M_o$ then $f(w,\zeta) \in \mathcal{C}_M(w)$ due to M being RPI. Therefore $f(w,\zeta) \in \mathcal{C}_M(w) \cap \mathcal{C}_G(w)\, \forall \partial G \cap M$. By assumption, $0 \in \text{int}(M - G)$. Then, by Property 5.2.1, $\mathcal{C}_M(w) \cap \mathcal{C}_G(w) = \mathcal{C}_{M \cap G}(w) = \mathcal{C}_{\mathcal{S}}(w)$. Thus $f(w,\zeta) \in \mathcal{C}_{\mathcal{S}}(w)\, \forall w \in (M \cap \partial G)$. Now we show that $f(w,\zeta) \in \mathcal{C}_{\mathcal{S}}\, \forall w \in (G \cap \partial M)$. M is RPI by assumption, therefore $f(w,\zeta) \in \mathcal{C}_M\, \forall w \in \partial M$, in particular $\forall w \in \partial M \cap G$. Since $\partial M \cap G \subset G$ we have that, if $w \in \text{int}(G)$ then $\mathcal{C}_G = \mathbb{R}^n$, thus $f(w,\zeta) \in \mathcal{C}_G(w)$, whereas if $w \in \partial G_i$ for some i then $w \in \partial M \cap \partial G_i \subset \partial G_i \cap M$, since M is closed. By hypothesis, it follows, as before, that $f(w,\zeta) \in \mathcal{C}_G(w)$. Thus $f(w,\zeta) \in \mathcal{C}_M(w) \cap \mathcal{C}_G(w) = \mathcal{C}_{\mathcal{S}}(w)\, \forall w \in \partial M \cap G$. We conclude that $f(w,\zeta) \in \mathcal{C}_{\mathcal{S}}\, \forall w \in \partial\mathcal{S}$, $\forall \zeta \in \mathcal{Z}$, and that $\mathcal{S}$ is therefore RPI.

(*Necessity*). Suppose $\mathcal{S}$ is RPI, and by contradiction, suppose $\exists w \in \mathcal{S} \cap \partial G_i, \exists \zeta \in \mathcal{Z}$ for some i such that $\Gamma_i f(w,\zeta) > 0$. Then $f(w,\zeta) \notin \mathcal{C}_{G_i}(w) \cap \mathcal{C}_M(w)$. So $\exists w \in \mathcal{S} \cap \partial G, \exists \zeta \in \mathcal{Z}$ such that $f(w,\zeta) \notin \mathcal{C}_G(w) \cap \mathcal{C}_M(w) = \mathcal{C}_{\mathcal{S}}(w)$. Since $\mathcal{S} \cap \partial G \subset \partial\mathcal{S}$ we have that $\exists w \in \partial\mathcal{S}, \exists \zeta \in \mathcal{Z}$ such that $f(w,\zeta) \notin \mathcal{C}_{\mathcal{S}}(w)$, contradicting that $\mathcal{S}$ is RPI.

A.4 Proof of Lemma 5.4.1

Partition Γ_i as $\Gamma_i = [\Gamma_{i1} \mid \Gamma_{i2}]$. Let $\partial G_i = \left\{[w_1^T \,|\, w_2]^T \in \mathbb{R}^n \,:\, \Gamma_{i1}w_1 + \Gamma_{i2}w2 = 1\right\}$. Suppose $\Gamma_{i2} \neq 0$. Then ∂G_i can be parameterized as $\left\{[w_1^T \,|\, w_2]^T \,:\, w_2 = \frac{1-\Gamma_{i1}w_1}{\Gamma_{i2}},\ w_1 \in \mathbb{R}^{n-1}\right\}$. Consider the set $V = \left\{w_2 \in \mathbb{R} \,:\, w_2 = \frac{1-\Gamma_{i1}w_1}{\Gamma_{i2}},\ w_1 \in \mathcal{S}_o\right\}$. The functional $h : \mathbb{R}^{n-1} \to \mathbb{R}$ given by $h(w_1) = \frac{-\Gamma_{i1}}{\Gamma_{i2}}w_1$ is bounded and therefore continuous in $\mathbb{R}^{n-1}$. Then $h(\mathcal{S}_o)$ is compact, since $\mathcal{S}_o \subset \mathbb{R}^{n-1}$ is compact [16]. Thus V, the translation of $h(\mathcal{S}_o)$ is also closed and bounded, i.e., V is a real closed interval posessing a minimum and a maximum. Note also that the maximum and minimum values of V are achieved at the boundary of $\mathcal{S}_o$. Denote by w_2^+ and w_2^- the half-spaces of $\mathbb{R}^n$ where $w_2 > 0$ and $w_2 < 0$, respectively. Denote by w_2^o the plane $w_2 = 0$. Consider, first, the case when $\partial G_i \cap \mathcal{H}_{\mathcal{S}_o}[\underline{w}_2, \overline{w}_2] \cap w_2^- = \emptyset$. Let $b = \min(V) > 0$. Note that $\overline{w}_2 \geq b > \underline{w}_2$. Then $\mathcal{H}_{\mathcal{S}_o}[\underline{w}_2, b]$ is RPI as a member of the family $\mathcal{H}_{\mathcal{S}_o}$. This implies, by Th. 2 that $f(w,\zeta) \in \mathcal{C}_{\mathcal{H}_{\mathcal{S}_o}[\underline{w}_2,b]}(w)\ \forall w \in \partial\mathcal{H}_{\mathcal{S}_o}[\underline{w}_2, b],\ \forall \zeta \in \mathcal{Z}$. Now, $\mathcal{H}_{\mathcal{S}_o}[\underline{w}_2, b] \subset G_i \cap \mathcal{H}_{\mathcal{S}_o}[\underline{w}_2, \overline{w}_2]$, thus $\mathcal{C}_{\mathcal{H}_{\mathcal{S}_o}[\underline{w}_2,b]}(w) \subset \mathcal{C}_{G\cap\mathcal{H}_{\mathcal{S}_o}[\underline{w}_2,\overline{w}_2]}(w)$ in particular for a point $w_b = [w_1^T \mid b] \in \partial\mathcal{H}_{\mathcal{S}_o}[\underline{w}_2, b]$, where $w_1 \in \partial\mathcal{S}_o$. So $f(w_b,\zeta) \in \mathcal{C}_{G\cap\mathcal{H}_{\mathcal{S}_o}[\underline{w}_2,\overline{w}_2]}(w_b) = \mathcal{C}_{G_i}(w_b) \cap \mathcal{C}_{\mathcal{H}_{\mathcal{S}_o}[\underline{w}_2,\overline{w}_2]}(w_b)$. Therefore $\Gamma_i f(w_b,\zeta) \leq 0$, with $w_b \in \partial G_i \cap \partial\mathcal{H}_{\mathcal{S}_o}[\underline{w}_2, \overline{w}_2] \subset \partial G_i \cap \mathcal{H}_{\mathcal{S}_o}[\underline{w}_2, \overline{w}_2]$. To prove the strict inequality, suppose, by contradiction, that $\Gamma_i f(w_b,\zeta) = 0$ for some $\zeta \in \mathcal{Z}$. This would require $\Gamma_{i2}B_2(\pm\eta - \zeta) = 0$, which is impossible, since $\zeta \leq \bar{\zeta} < \eta$. Thus w_b is a point satisfying the Lemma. The case when $\partial G_i \cap \mathcal{H}_{\mathcal{S}_o}[\underline{w}_2, \overline{w}_2] \cap w_2^+ = \emptyset$ is treated similarly, taking $b = \max(V)$, which is negative, and considering the cylinder $\mathcal{H}_{\mathcal{S}_o}[b, \overline{w}_2]$. Finally, consider the remaining possibilities of $\partial G_i \cap \mathcal{H}_{\mathcal{S}_o}[\underline{w}_2, \overline{w}_2] \cap w_2^o \neq \emptyset$ or $\Gamma_{i2} = 0$. In those cases, the intersection of ∂G_i with the cylinder and the sliding hyperplane $w_2 = 0$ is nonempty. System dynamics on the sliding hyperplane is given by $\dot{w}_1 = A_w w_1$. Consider the set resulting from the intersection of $\mathcal{S}_o$ and the closure of the complement of the state constraint restricted to $w_2 = 0$, that is, let $K = \mathcal{S}_o \cap \bar{G}_{oi}^c$, where $G_{oi}^c = \left\{w_1 \in \mathbb{R}^{n-1} \,:\, \Gamma_{i1}w_1 > 1\right\}$. It is easy to see that K is compact and convex and that it does not contain the origin. Suppose, by contradiction, that $\Gamma_{i1}\dot{w}_1 \geq 0\ \forall\ w_1 \in \partial G_{oi} \cap \mathcal{S}_o$. Then, following arguments similar to those used in the proof of Th. 5, it is possible to deduce that K is positively invariant for $\dot{w}_1 = A_w w_1$, which contradicts the asymptotic stability of the origin. Thus $\exists w_1 \in \partial G_{io} \cap \mathcal{S}_o$ such that $\Gamma_{oi}\dot{w}_1 < 0$, which in turns implies that $w = [w_1^T \mid 0] \in \partial G_i \cap \mathcal{H}_{\mathcal{S}_o}$ satisfies $\Gamma_i \dot{w} < 0$.

A.5 Proof of Proposition 5.4.1

For each $w \in \mathbb{R}^n$, consider the set $\alpha(w) = \{\Gamma_i f(w,\zeta) \,:\, \zeta \in \mathcal{Z}\}$. We show that $\max \alpha(w) = \Gamma_i f(w,\zeta^*)$, where $\zeta^* = \text{-sign}(\Gamma_i B_w)\bar{\zeta}$ and thus, $\Gamma_i f(w,\zeta^*) \geq \Gamma_i f(w,\zeta)\ \forall \zeta \in \mathcal{Z}$. First note that $\Gamma_i f(w,\zeta^*) \in \alpha(w)$ since $\zeta^* \in \mathcal{Z}$. For any $\zeta \in \mathcal{Z}$ we have that

$$\Gamma_i f(w,\zeta) = \Gamma_{i1}A_w w_1 + \Gamma_{i1}B_1(\eta\text{sign}(G_w w_2) - \zeta) + \Gamma_{i2}B_2(\eta\text{sign}(G_w w_2) - \zeta) = \Gamma_{i1}A_w w_1 + \Gamma_i B_w(\eta\text{sign}(G_w w_2) - \zeta)$$

and thus

$$\Gamma_i f(w,\zeta^*) - \Gamma_i f(w,\zeta) = |\Gamma_i B_w|\bar{\zeta} + \Gamma_i B_w \zeta$$

But since $|\zeta| \leq \bar{\zeta}$ we see that $\Gamma_i B_w \zeta \leq |\Gamma_i B_w||\zeta| = |\Gamma_i B_w \zeta| \leq |\Gamma_i B_w|\bar{\zeta}$ which shows that $|\Gamma_i B_w|\bar{\zeta} + \Gamma_i B_w \zeta \geq 0$ and therefore $\max \alpha(w) = \Gamma_i f(w,\zeta^*)$. To show that the collection of subsets is a partition we must show that the subsets are not empty, disjoint and that their

union equals $\mathbb{R}^n$. Assume, w.l.o.g., that $G_w > 0$. Take $w = [w_1^T \mid w_2]^T$ in the half-space $w_2 > 0$. Since $\Gamma_{i1} A_w \neq 0$ we have that $\Gamma_i f(w, \zeta^*) = 0$ is a half-hyperplane separating the half-space into open regions for which either $\Gamma_i f(w, \zeta^*) > 0$ or $\Gamma_i f(w, \zeta^*) < 0$. Any w contained in the positive region of the half-space belongs to G_i^+, thus $\text{int}(G_i^+) \neq \emptyset$. Similarly, any w contained in the negative side satisfies $\Gamma_i f(w, \zeta^*) = \max \alpha(w) < 0$. Then $\Gamma_i f(w, \zeta) < 0 \, \forall \zeta \in \mathcal{Z}$ and thus $w \in G_i^-$ and $\text{int}(G_i^-) \neq \emptyset$. Also, any point w on the half-hyperplane is an adherent point of $\text{int}(G_i^+)$ that is not contained in $\text{int}(G_i^+)$, thus $w \in \partial G_i^+ \neq \emptyset$. If we take the half-space $w_2 < 0$ we can likewise show that any point w on the corresponding half-hyperplane satisfies $w \in \partial G_i^+$. We have shown that $\partial G_i^+ \supset \left\{ [w_1^T \mid w_2]^T \in \mathbb{R}^n \, : \, \Gamma_i f(w, \zeta^*) = 0 \, , \, w_2 \neq 0 \right\}$. Now suppose $w_2 = 0$. We show that $\partial G_i^+ \supset \left\{ [w_1^T \mid 0]^T \in \mathbb{R}^n \, : \, |\Gamma_{i1} A_w w_1 - \Gamma_i B_w \zeta^*| \leq |\Gamma_i B_w| \eta \right\}$. Let $w_1 \in \mathbb{R}^n$ such that $|\Gamma_{i1} A_w w_1 - \Gamma_i B_w \zeta^*| \leq |\Gamma_i B_w| \eta$ and $\varepsilon > 0$ and consider the ball $\mathcal{B}([w_1^T \mid 0]^T), \varepsilon)$. Choose v_2 such that $|\Gamma_i B_w| \leq \Gamma_i B_w \text{sign}(G_w v_2)$ and $|v_2| < \varepsilon$, which can always be found. Consider the point $v = [w_1^T \mid v_2]^T$. Using the euclidean norm in $\mathbb{R}^n$ we see that $||v - [w_1^T \mid 0]^T|| = |v_2| < \varepsilon$, thus $v \in \mathcal{B}([w_1^T \mid 0]^T), \varepsilon)$. Moreover,

$$\Gamma_{i1} A_w w_1 - \Gamma_i B_w \zeta^* > -|\Gamma_i B_w| \eta \geq -\Gamma_i B_w \eta \text{sign}(G_w v_2)$$

which leads to $\Gamma_i f(v, \zeta^*) > 0$, so $v \in G_i^+$ and $w = [w_1^T | 0]^T$ is an adherent point of G_i^+. However, $w \notin \text{int}(G_i^+)$, for all the balls $\mathcal{B}([w_1^T \mid 0]^T), \varepsilon)$ also contain the point $v' = [w_1^T \mid -v_2]^T$, for which $\Gamma_i f(v', \zeta^*) \leq 0$. This implies $w \in \partial G_i^+$, showing the desired inclusion. We have thus shown that

$$\partial G_i^+ \supset \left\{ \left[w_1^T \mid w_2 \right]^T \in \mathbb{R}^n \, : \, \Gamma_i f(w, \zeta^*) = 0 \, , \, w_2 \neq 0 \right\} \cup \left\{ \left[w_1^T \mid 0 \right]^T \in \mathbb{R}^n \, : \, |\Gamma_{i1} A_w w_1 - \Gamma_i B_w \zeta^*| \leq |\Gamma_i B_w| \eta \right\}$$

Now we prove the reverse inclusion. Suppose that $w \in \partial G_i^+$ and that $\Gamma_i f(w, \zeta^*) < 0$. Then $\Gamma_i f(w, \zeta) < 0 \, \forall \zeta \in \mathcal{Z}$ and $w \in G_i^-$. Observing from the definition that $G_i^+ \cap G_i^- = \emptyset$, the only possibility is that $w \in \text{int}(G_i^+)$, which contradicts the hypothesis. Therefore $\Gamma_i f(w, \zeta^*) \geq 0$. If $\Gamma_i f(w, \zeta^*) = 0$ then we have proved the inclusion. The last possibility is that $\Gamma_i f(w, \zeta^*) > 0$. If we take w in either half-space $w_2 > 0$ or $w_2 < 0$ we see that the corresponding half-hyperplane separates the half-space into two open regions. Then w cannot be a boundary point for G_i^+. Thus it must be that $w_2 = 0$. By contradiction, suppose $|\Gamma_{i1} A_w w_1 - \Gamma_i B_w \zeta^*| > |\Gamma_i B_w| \eta$. Then take the open ball centered at w that contains all points $v = [v_1^T \mid v_2]^T$ for which $|\Gamma_{i1} A_w v_1 - \Gamma_i B_w \zeta^*| > |\Gamma_i B_w| \eta$. Take v in the ball and suppose $v_2 \neq 0$. Then $|\Gamma_i f(v, \zeta^*)| = |\Gamma_{i1} A_w v_1 + \Gamma_i B_w (\pm \eta - \zeta^*)| \geq ||\Gamma_{i1} A_w v_1 - \Gamma_i B_w \zeta^*| - |\Gamma_i B_w| \eta| > 0$. When $v_2 = 0$ we have that $|\Gamma_i f(v, \zeta^*)| = |\Gamma_{i1} A_w v_1 - \Gamma_i B_w \zeta^*| > |\Gamma_i B_w| > 0$. Since $\Gamma_i f(w, \zeta^*) > 0$ and w is in the ball, we see that $\Gamma_i f(v, \zeta^*) > 0$ and thus the ball is entirely contained in G_i^+. This contradicts w being a boundary point of G_i^+. Thus we have shown that $\partial G_i^+ = \left\{ [w_1^T \mid w_2]^T \in \mathbb{R}^n \, : \, \Gamma_i f(w, \zeta^*) = 0 \, , \, w_2 \neq 0 \right\} \cup \left\{ [w_1^T \mid 0]^T \in \mathbb{R}^n \, : \, |\Gamma_{i1} A_w w_1 - \Gamma_i B_w \zeta^*| \leq |\Gamma_i B_w| \eta \right\}$. We are now in a position to show that the sets are disjoint. From their definition, it is obvious that $\text{int}(G_i^+) \cap \text{int}(G_i^-) = \emptyset$. Also, $\partial G_i^+ \cap \text{int}(G_i^+) = \emptyset$. We now show that $\partial G_i^+ \cap \text{int}(G_i^-) = \emptyset$. Suppose $w \in \partial G_i^+$. Then $w \notin \text{int}(G_i^-)$, since every ball centered at w must contain points of $\text{int}(G_i^+)$ so there is no ball entirely contained in $\text{int}(G_i^-)$. It is now straightforward to show that $\text{int}(G_i^+) \cup \text{int}(G_i^-) \cup \partial G_i^+ \supset \mathbb{R}^n$.

Appendix B

B.1 Solution to Optimization Problems

B.1.1 Calculation of β (Section 5.5.1)

The problem is

$$\begin{aligned} &\min x^T Q x \quad \text{s.t.} \\ &x^T P x = 1 \end{aligned}$$

Define the augmented Lagrangian function as

$$\mathcal{L} = x^T Q x + \lambda (x^T P x - 1)$$

The first-order conditions are

$$\begin{aligned} \frac{\partial \mathcal{L}}{\partial x} &= 2Qx + 2\lambda P x = 0 \\ \frac{\partial \mathcal{L}}{\partial \lambda} &= x^T P x - 1 = 0 \end{aligned}$$

The first condition can be written as

$$(P^{-1}Q + \lambda I)x^* = 0$$

after multiplication by P^{-1}. Thus $-\lambda$ and x^* must be an eigenvalue-eigenvector pair for $P^{-1}Q$. A feasible solution set of vectors x^* is obtained by scaling the eigenvectors of $P^{-1}Q$ so that they "fit" in the ellipsoid defined by P. If x^*/γ is used, with $\gamma \in \mathbb{R}$, then the scaling factor γ must satisfy

$$x^{*T} P x^* = \gamma^2$$

All eigenvectors x^* of $P^{-1}Q$ are found, and β is chosen as

$$\beta = \min \frac{x^{*T} Q x^*}{x^{*T} P x^*}$$

B.1.2 Enforcement of Corollary 5.4.1

It is straightforward to note that if $\Gamma_{i1}A_w = 0$ or $\Gamma_i B_w = 0$ then the constraint is automatically satisfied. Assume $\Gamma_{i1}A_w \neq 0$ and $\Gamma_i B_w \neq 0$ and define the following variables:

$$\begin{aligned} M &= \left[\frac{F_1}{F_2}\right] P^{-1}[F_1^T \mid F_2^T] \\ F_1 &= \Gamma_{i1}A_w \\ F_2 &= \Gamma_{i1} \end{aligned}$$

Problem 1: $w_2 \neq 0$

First, suppose $\Gamma_{i1}A_w \nparallel \Gamma_{i1}$ and $\Gamma_{i2} \neq 0$. The problem to be solved is

$$\begin{gathered} \min w_1^T P w_1 \quad \text{s.t.} \\ F_1 w_1 = a \\ F_2 w_1 = b \end{gathered}$$

with $a = -(\Gamma_i B_w)(\eta \text{ sign}(G_w w_2) - \zeta^*)$ and $b = 1 - \Gamma_{i2}w_2$. The solution is readily obtained by Lagrange multipliers and results in a unique minimizing argument w_1^* such that

$$w_1^{*T} P w_1^* = [a\ b]\, M^{-1}\, [a\ b]^T = f_1(w_2)$$

Suppose $G_w w_2 > 0$. Function f_1 is clearly quadratic in w_2 and posesses a unique global minimum. Differentiating and equating to zero gives

$$\frac{df_1(w_2)}{dw_2} = 2\,[0\ \ -\Gamma_{i2}]\, M^{-1} \left[\begin{array}{c} -\Gamma_i B_w(\eta - \zeta^*) \\ 1 - \Gamma_{i2}w_2 \end{array}\right] = 0$$

This results in the linear equation

$$\Gamma_{i2}^2 \bar{M}_{22} w_2 = \Gamma_{i2}(\bar{M}_{22} - \bar{M}_{12}\Gamma_i B_w(\eta - \zeta^*))$$

where $\bar{M}_{ij}$ are the entries of M^{-1}. Note that $\bar{M}_{22} \neq 0$ since M is symmetric and positive-definite. Let $w_{2,crit}^+$ be the solution to the above equation:

$$w_{2,crit}^+ = \frac{\bar{M}_{22} - \bar{M}_{12}\Gamma_i B_w(\eta - \zeta^*)}{\Gamma_{i2}\bar{M}_{22}}$$

If $G_w w_{2,crit}^+ > 0$ and $w_{2,crit}^+ \in (\underline{w}_2, \overline{w}_2)$, the solution is valid and we enforce $vM^{-1}v^T > 1$, where $v = \Gamma_i B_w(\eta - \zeta^*)[-1\ \frac{\bar{M}_{12}}{\bar{M}_{22}}]$. After some algebra, this reduces to

$$(\eta - \zeta^*)^2 > \frac{M_{11}}{(\Gamma_i B_w)^2}$$

If $G_w w_{2,crit}+ \leq 0$ and $w_{2,crit}^+ \in (\underline{w}_2, \overline{w}_2)$, the minimum is obtained at $G_w w_2 = 0^+$ and the condition to enforce becomes $vM^{-1}v^T > 1$, with $v = [-\Gamma_i B_w(\eta - \zeta^*)\ 1]$. An entirely analogous procedure is followed for the case $G_w w_2 < 0$. Let

$$w_{2,crit}^- = \frac{\bar{M}_{22} - \bar{M}_{12}\Gamma_i B_w(-\eta - \zeta^*)}{\Gamma_{i2}\bar{M}_{22}}$$

If $G_w w_{2,crit}^- < 0$ and $w_{2,crit}^- \in (\underline{w}_2, \overline{w}_2)$, we enforce

$$(\eta + \zeta^*)^2 > \frac{M_{11}}{(\Gamma_i B_w)^2}$$

If $G_w w_{2,crit} - \geq 0$ and $w_{2,crit}^- \in (\underline{w}_2, \overline{w}_2)$, the condition to enforce becomes $vM^{-1}v^T > 1$, with $v = [\Gamma_i B_w(\eta + \zeta^*) \;\; 1]$. Now suppose $\Gamma_{i1} A_w \nparallel \Gamma_{i1}$ but $\Gamma_{i2} = 0$. Once a sign for $G_w w_2$ has been chosen, the function f_1 becomes constant. Therefore the condition to enforce becomes $vM^{-1}v^T > 1$ for both $v = [\Gamma_i B_w(\eta + \zeta^*) \;\; 1]$ and $v = [-\Gamma_i B_w(\eta - \zeta^*) \;\; 1]$. Now suppose $\Gamma_{i1} A_w = \alpha \Gamma_{i1}$ and $\Gamma_{i2} \neq 0$. Note that $\alpha < 0$ is the only possibility for A_w Hurwitz. In this case, we reduce the restrictions as follows. Substitution gives the equation

$$\alpha(1 - \Gamma_{i2} w_2) = -\Gamma_i B_w(\eta \, \mathrm{sign}(G_w w_2) - \zeta^*)$$

First we seek a solution for $G_w w_2 > 0$. Define

$$\tilde{w}_2^+ = \frac{1}{\Gamma_{i2}} \left(1 + \frac{\Gamma_i B_w(\eta - \zeta^*)}{\alpha} \right)$$

If $G_w \tilde{w}_2^+ > 0$ and $\tilde{w}_2^+ \in (\underline{w}_2, \overline{w}_2)$, then the solution is valid and the reduced optimization problem becomes

$$\min w_1^T P w_1 \quad \text{s.t.}$$
$$F_2 w_1 = -\frac{\Gamma_i B_w}{\alpha}(\eta - \zeta^*)$$

The unique solution w_1^* is readily obtained by Lagrange multipliers and is given by

$$w_1^* = -\frac{\Gamma_i B_w(\eta - \zeta^*) P^{-1} \Gamma_{i1}^T}{\Gamma_{i1} P^{-1} \Gamma_{i1}^T}$$

The condition to be enforced reduces to

$$\left(\frac{\Gamma_i B_w(\eta - \zeta^*)}{\alpha} \right)^2 > M_{22}$$

If $G_w \tilde{w}_2^+ \leq 0$ or $\tilde{w}_2^+ \notin (\underline{w}_2, \overline{w}_2)$ the solution is not valid and the constraints have empty intersection. An entirely analogous procedure is followed for the case $G_w w_2 < 0$. Let

$$\tilde{w}_2^- = \frac{1}{\Gamma_{i2}} \left(1 + \frac{\Gamma_i B_w(-\eta - \zeta^*)}{\alpha} \right)$$

If $G_w \tilde{w}_2^- < 0$ and $\tilde{w}_2^- \in (\underline{w}_2, \overline{w}_2)$ then the solution is valid and the condition to be enforced reduces to

$$\left(\frac{\Gamma_i B_w(\eta + \zeta^*)}{\alpha} \right)^2 > M_{22}$$

If $G_w \tilde{w}_2^- \geq 0$ or if $\tilde{w}_2^- \notin (\underline{w}_2, \overline{w}_2)$ then the solution is not valid and the constraints have empty intersection. Now suppose $\Gamma_{i1} A_w = \alpha \Gamma_{i1}$ and $\Gamma_{i2} = 0$. Then substitution gives the equation $\alpha = -\Gamma_i B_w(\eta \, \mathrm{sign}(G_w w_2) - \zeta^*)$. If $\eta = |\zeta^* - \alpha/(\Gamma_i B_w)|$ then the constraints reduce to $\Gamma_{i1} w_1 = 1$ and the problem becomes

$$\min w_1^T P w_1 \quad \text{s.t.}$$
$$F_2 w_1 = 1$$

The solution is straightforward and reduces to the enforcement of $\Gamma_{i1} P^{-1} \Gamma_{i1}^T < 1$.

Problem 2: $w_2 = 0$

The problem is

$$\begin{aligned} \min w_1^T P w_1 \quad & \text{s.t.} \\ \Gamma_{i1} w_1 &= 1 \\ |\Gamma_{i1} A_w w_1 - \Gamma_i B_w \zeta^*| &\le |\Gamma_i B w| \end{aligned}$$

The inequality can be written as

$$-|\Gamma_i B_w|(\eta + \bar{\zeta}) \le \Gamma_{i1} A_w w_1 \le |\Gamma_i B_w|(\eta - \bar{\zeta}) \tag{B.1}$$

Note that the interval specified for $\Gamma_{i1} A_w w_1$ is nonempty, since $\eta > 0$, $\bar{\zeta} > 0$ and $\eta > \bar{\zeta}$. The problem is of the form

$$\begin{aligned} \min w_1^T P w_1 \quad & \text{s.t.} \\ F_2 w_1 &= 1 \\ b \le F_1 w_1 &\le a \end{aligned}$$

with $a > b$, $F_2 \neq 0$. The associated problem

$$\begin{aligned} \min w_1^T P w_1 \quad & \text{s.t.} \\ F_2 w_1 &= 1 \end{aligned} \tag{B.2}$$

posesses a global and unique solution w_1^*. If the solution satisfies inequality (B.1) then w_1^* is a valid solution and must be used in the enforcement of $w_1^{*T} P w_1^* > 1$. If not, the following two problems must be solved

$$\begin{aligned} \min w_1^T P w_1 \quad & \text{s.t.} \\ F_2 w_1 &= 1 \\ F_1 w_1 &= a \end{aligned} \tag{B.3}$$

and

$$\begin{aligned} \min w_1^T P w_1 \quad & \text{s.t.} \\ F_2 w_1 &= 1 \\ F_1 w_1 &= b \end{aligned} \tag{B.4}$$

and $w_1^{*T} P w_1^* > 1$ must be satisfied by both solutions. Regardless of whether $\Gamma_{i1} A_w \parallel \Gamma_{i1}$, the solution to problem (B.2) is given by

$$w_1^* = \frac{P^{-1} \Gamma_{i1}^T}{\Gamma_{i1} P^{-1} \Gamma_{i1}^T}$$

If w_1^* satisfies inequality (B.1), then the condition to be enforced is $\Gamma_{i1} P^{-1} \Gamma_{i1}^T < 1$. If not, we solve problems (B.3) and (B.4) using $a = |\Gamma_i B_w|(\eta - \zeta^*)$ and $b = -|\Gamma_i B_w|(\eta + \zeta^*)$. Suppose first that $\Gamma_{i1} A_w \nparallel \Gamma_{i1}$. Then the solutions to problems (B.3) and (B.4) result in the condition to be enforced: $v M^{-1} v^T > 1$, for both $v = [|\Gamma_i B_w|(\eta - \bar{\zeta}) \;\; 1]$ and $v = [-|\Gamma_i B_w|(\eta + \bar{\zeta}) \;\; 1]$. Now suppose that $\Gamma_{i1} A_w = \alpha \Gamma_{i1}$. Substitution of this into the restrictions results in the equations $\alpha = |\Gamma_i B_w|(\eta - \bar{\zeta}) > 0$, which is impossible, and $\alpha = -|\Gamma_i B_w|(\eta + \bar{\zeta})$, which is incompatible with inequality (B.1).

Appendix C

C.1 Program Listings

The Matlab routines related to the GUI comprise thousands of lines of code. For this reason, only essential routines that obtain thermodynamic properties, evaluate equilibrium points and find valve positions for a steady operating target are listed.

C.1.1 Mixer Equilibrium Point

```
mxr_eq.m

%Graphical illustration of the mixer operating point. See report.

%Hanz Richter, PhD
%NASA - Stennis Space Center, 2002

%Set pressure range for plotting:
%Make sure:
%P>Ps
%Pl>P
%Pg>P

P=[5800:100:8000];

for i=1:length(P),
   if Pg>=2*P(i)
      f=2.423e-2*Pg;
   else
      f=2.857e-2*sqrt(Pg^2-P(i)^2);
   end;
   %Mixer density from steady mass balance:

   mdot_l=1.76e-2*Cvl*sqrt((Pl-P(i))*rho_l);
   mdot_g=f*Cvg*sqrt(Tg+460)*rho_g/Pg;
   rho_cv(i)=((mdot_l+mdot_g)/(1.76e-2*Cve))^2/(P(i)-Ps);

   %Enthalpy of above locus:
   %Find pressure column:
   pcol=2*(1+(P(i)-2000)/100);
   %Find density range:
   minrho=hydro(61,pcol-1);
   maxrho=hydro(1,pcol-1);
   %Interpolate enthalpy
   if (rho_cv(i)>=minrho) & (rho_cv(i)<=maxrho),
      h_th(i)=interp1(hydro(:,pcol-1),hydro(:,pcol),rho_cv(i));
else
      h_th(i)=NaN;
   end;

   %Finally, steady-state enthalpy:
    h_ss(i)=(mdot_l*hl+mdot_g*hg)/(mdot_l+mdot_g);
   %Create surface by extrusion of the above:
   Z(:,i)=h_ss(i)*ones(length(P),1);

end;
```

C.1.2 Valve Positions for Prescribed Operating Condition

```
%mxr_cv.m
```

```
%Calculates valve positions to achieve given exit flow and temperature, with
%given mixer operating pressure.

%****hydro_h and hydro_rho must be globalized and loaded in the workspace!!!*****

%Hanz Richter, PhD
%NASA - Stennis Space Center, 2002

function [Cvl,Cvg,Cve]=mxr_cv(T,we,P)

global hydro_h
global hydro_rho
global Ps
global V
global Pl
global Pg
global hl
global hg
global Tg
global Tl
global C1
global C3
global rho_g
global rho_l



%T: Desired temperature at exit valve outlet, deg. Fahrenheit
%we: Desired output massflow, lbm/sec.
%P: Desired mixer operating pressure (must ensure positive flow based on input and output pressures)


%Check pressures for positive flow:

if (P<=Ps) | (P>Pg) | (P>Pl),
   error('Reverse flow. Change pressures');
end;
%Find enthalpy from Ps and T by 2D interpolation on hydro_h (see hydro_desc.txt)
if (Ps<=2000) | (Ps>=13500) | (T<=-400) | (T>=200),
   error('Off-range');
end;
Pvect=[2000:100:13500];
Tvect=[-400:10:200];

h=interp2(Tvect,Pvect,hydro_h',T,Ps)

%Enthalpy accross exit valve is constant. Use it to find mixer density ( =at exit valve inlet)

%Generate interpolated enthalpy and density columns for given mixer pressure.
%Find bracketing pressures:
plow_index=max(find(Pvect<=P));
plow=2000+(plow_index-1)*100;
phigh=plow+100;
hsegment=hydro_h(:,[plow_index,plow_index+1]);
rhosegment=hydro_rho(:,[plow_index,plow_index+1]);
%Interpolated columns:
hdata=interp2(Tvect,[plow,phigh],hsegment',Tvect,P);
rhodata=interp2(Tvect,[plow,phigh],rhosegment',Tvect,P);

%Find the density for h:
if (h>max(hdata)) | (h<min(hdata)),
   error('Off-range');
end;

rho=interp1(hdata,rhodata,h)

%Find equilibrium flows (see report)
wl=we*(h-hg)/(hl-hg);
wg=we*(hl-h)/(hl-hg);

%Find exit Cv:
Cve=we/(C3*sqrt((P-Ps)*rho));

%Find gas Cv:
if Pg>=2*P
   f=2.423e-2*Pg;
else
   f=2.857e-2*sqrt(Pg^2-P^2);
end;
Cvg=wg/(f*sqrt(Tg+460)*rho_g/Pg);

%Find liquid Cv:
Cvl=wl/(C1*sqrt((Pl-P)*rho_l));
```

C.1.3 Thermodynamic Properties

```
thermo_props.m
%Hanz Richter, NASA 2002


%This function returns the temperature and pressure of nitrogen or hydrogen given density in lbm/ft^3 and
%internal energy in Btu/lbm.

%Final version (used to be called gettemp, getpress, and getprops1,2,3, and 4.

%July 18, 2002

function vect=thermo_props(rho,u,fluid)


switch lower(fluid)
case {'parahydrogen', '1'},

      global hydro_u_data
      global hydro_p_data
      global hydro_t_data
      global hydro_master_range

      u_data = hydro_u_data;
      p_data = hydro_p_data;
      t_data = hydro_t_data;
      master_range = hydro_master_range;
      rho_lower = .535;
      rho_step = 0.025;
      rho_upper = 6.31;
      u_lower = -88.8637;
      u_upper = 1559.8;
      nrows = 116;
      dens_interp_treshold=0.002;
energy_interp_treshold=0.1;
dens_perturb_step=0.02;   %these two control the error in original density
dens_tol=0.25;

   case {'nitrogen', '2'},

      global nitro_u_data
      global nitro_p_data
      global nitro_t_data
      global nitro_master_range

      u_data = nitro_u_data;
      p_data = nitro_p_data;
      t_data = nitro_t_data;
      master_range = nitro_master_range;
      rho_lower = .05;
      rho_step = 0.5;
      rho_upper = 54.55;
      u_upper = 224.1;
      u_lower = -59.4982;
      nrows = 250;
      dens_interp_treshold=0.01;
energy_interp_treshold=0.1;
dens_perturb_step=0.02;   %these two control the error in original density
dens_tol=0.25;

   otherwise,
      error('Invalid fluid');
end;

if (rho>rho_upper) | (rho<rho_lower),
   %off-range
   error('Density off-range')
end;
if (u>u_upper) | (u<u_lower),
   %off-range
   error('Energy off-range')
end;


last_resort=0;
interpolate_dens=1;
found=0;
dens_error=0;

while ~found & dens_error<dens_tol,

colnumber=floor((rho-rho_lower)/rho_step)+1; %find left bracket column

%First priority: check if the density is "close" to one of the nominal bracketing densities
   if abs(rho-(rho_lower+(colnumber-1)*rho_step))<=dens_interp_treshold,
      interpolate_dens=0;
```

```
   elseif abs(rho-(rho_lower+(colnumber)*rho_step))<=dens_interp_treshold,  %check the next column as well
      interpolate_dens=0;
      colnumber=colnumber+1;                                    %change the column
   end;
   if ~interpolate_dens,
      u_data_col=u_data(:,colnumber);
      p_data_col=p_data(:,colnumber);
      t_data_col=t_data(:,colnumber);
    %check if the density column contains a "close" energy match
    search_scope=master_range(colnumber);
    rownumber=nrows+max(find(abs(u_data_col(nrows-search_scope+1:nrows)-u)<=energy_interp_treshold))-search_scope;
if isempty(rownumber) | rownumber==nrows, %Now try for bracketing energy in the col:
        rownumber=nrows+max(find(u_data_col(nrows-search_scope+1:nrows)<=u))-search_scope;
        if isempty(rownumber) | rownumber==nrows,
        interpolate_dens=1;           %See if interpolation helps it.
        else
           p=interp1(u_data_col(rownumber:rownumber+1),p_data_col(rownumber:rownumber+1),u);
           t=interp1(u_data_col(rownumber:rownumber+1),t_data_col(rownumber:rownumber+1),u);
           found=1;
        end;
      else
         p=p_data_col(rownumber);
         t=t_data_col(rownumber);
         found=1;
      end;
   end;

 %Second priority: check if the interpolated density columns contain a "close" energy match
 if interpolate_dens,   %then colnumber should still be the left bracket
      colnumber=floor((rho-rho_lower)/rho_step)+1; %find left bracket column
      fraction=(rho-(rho_lower+(colnumber-1)*rho_step))/rho_step;
      u_data_col=u_data(:,colnumber)+fraction*(u_data(:,colnumber+1)-u_data(:,colnumber));
      p_data_col=p_data(:,colnumber)+fraction*(p_data(:,colnumber+1)-p_data(:,colnumber));
      t_data_col=t_data(:,colnumber)+fraction*(t_data(:,colnumber+1)-t_data(:,colnumber));
      %don't use the zeros in the interpolation:
      search_scope=min(master_range(colnumber),master_range(colnumber+1));
      %Try locate the energy in u_data_col within search_scope
%Remember data is stored at the bottom, and in ascending order
   %_master_range tells how many rows are useful from the bottom up.
      rownumber=nrows+max(find(abs(u_data_col(nrows-search_scope+1:nrows)-u)<=energy_interp_treshold))-search_scope;
      if isempty(rownumber) | rownumber==nrows, %Now try for bracketing energy in the interpolated col:
         rownumber=nrows+max(find(u_data_col(nrows-search_scope+1:nrows)<=u))-search_scope;
         if isempty(rownumber) | rownumber==nrows,  %In this case, go to last-resort procedure
         last_resort=1;
         else
            p=interp1(u_data_col(rownumber:rownumber+1),p_data_col(rownumber:rownumber+1),u);
            t=interp1(u_data_col(rownumber:rownumber+1),t_data_col(rownumber:rownumber+1),u);
            found=1;
         end;
      else
         p=p_data_col(rownumber);
         t=t_data_col(rownumber);
         found=1;
      end;
   end;
   if last_resort, %As a last resort, change the density and start over
      rho=rho+dens_perturb_step;
      dens_error=dens_perturb_step+dens_error;
   end;
end;

if found,
vect=[t p dens_error];
else
   rho
   u
   dens_error
   error('Pair really off-range');
end;
```

C.2 Feedback Linearization Controller

```
function w=feedback_lin_control(x)

%x contains [cve y,yd,ydd,P,T,pars,en]

%y and yd are arranged as [rho, u, exit_massflow]^T
%P is pressure measurement
%T is temperature measurement
%pars is a vector containing [pl,hl,rhol,pg,hg,rhog,ps,Tg]
%en is an enable flag to avoid doing the calculations when running open-loop or with other
%controllers. en must match this controller's value for the calculations to be performed.
%**********************************
%Feedback linearization controller flag = 2
%**********************************
```

```
%Therefore       x=[ cve rho,u,we,rho_d,u_d,we_d,rho_d_d,u_d_d,we_d_d,P, T, pl, hl, rhol,
%                    1  2   3  4   5     6   7    8       9      10 11  12 13  14  15
% pg,hg,rhog,ps,Tg].
% 16 17  18  19 20

%The virtual control w is arranged as

%w=[Cvl;Cvg;v], where v is integrated to give cve.



global V C1p C2p C3p C3pp C4p;

if x(21) == 2

cve=x(1);

%Calculate E

aux1=C1p*sign(x(13)-x(11))*sqrt(abs(x(13)-x(11))*x(15));   %this is f1
aux2=sign(x(11)-x(19))*sqrt(abs(x(11)-x(19))*x(2));
aux3=x(2)*getpartialrho(x(11),x(12))+x(11)-x(19);

if x(16)<2*x(11),
   aux4=C4p*sign(x(16)-x(11))*sqrt(abs(x(16)^2-x(11)^2));
else
   aux4=C2p;
end;


E=[aux1 aux4 0;aux1*(x(14)-x(3))/x(2) aux4*(x(17)-x(3))/x(2) 0; -aux3*V*cve*C3p*aux1/(2*aux2) -aux3*V*cve*aux4*C3p/(2*aux2) -V*C3p*aux2];


%Calculate D

D=[C3p*cve*aux2;C3pp*cve*aux2*x(11)/x(2)^2; -V*cve^2*C3p^2*aux3/2];

%Control gains
gam=diag([10 10 5]);


%Calculate the virtual control input

w=inv(E)*(x(8:10)-gam*(x(2:4)-x(5:7))-D);

else
    w=[0 0 0];
end
```

C.3 Sliding Mode Controller

```
%smctrl.m
%This function calculates the sliding mode controller
%Hanz Richter, NASA 2002

function sliding_control = smctrl(x)

global V c Ps rho1 rho2 P1 P2 R h1 h2 Cv k tau1 tau2 tau3 beta1 beta2 beta3

f1=x(1);
f2=x(2);
fe=x(3);
rho=x(4);
P=x(5);
Cv1=x(6);
Cv2=x(7);
Cve=x(8);
rho_d=x(9);   %rho desired
rho_dd=x(10);  %rho desired derivative
rho_ddd=x(11); %rho desired second derivative
P_d=x(12);     %P desired
P_dd=x(13);    %P desired derivative
P_ddd=x(14);   %P desired second derivative
w_d=x(15);     %flow desired
w_dd=x(16);    %flow desired derivative


krho=100;       %sliding manifold coefficients
kP=100;
kw=100;

eta1=120;       %sliding gains
eta2=2400e3;
```

```
eta3=120;

phi1=10;
phi2=1e4;
phi3=10;

f=[f1 f2 -fe]';

Cvect=[Cv1;Cv2;Cve];

Df1Dp=-0.5*c*rho1/sqrt(abs(P1-P)*rho1);
Df2Dp=-0.5*c*rho2/sqrt(abs(P2-P)*rho2);
DfeDp=0.5*c*sqrt(rho)/sqrt(abs(P-Ps));
DfDrho=[0;0;-0.5*c*sqrt(abs(P-Ps)/rho)*sign(P-Ps)];
DfDp=[Df1Dp;Df2Dp;-DfeDp];

Ap=diag([R*h1/Cv R*h2/Cv k*P/rho]);
Ac=diag([-1/tau1 -1/tau2 -1/tau3]);
Bc=diag([beta1 beta2 beta3]);

%calculation of sliding functions
s1=rho_dd-f'*Cvect/V+krho*(rho_d-rho);
s2=P_dd-f'*Ap*Cvect/V+kP*(P_d-P);
s3=kw*(w_d-Cve*fe);

%Flow Derivatives
DfDt=((Cvect'*Ap*f)*DfDp+(Cvect'*f)*DfDrho)/V;

%Matrix derivative

DApDt=zeros(3,3);
DApDt(3,3)=k*Cvect'*(Ap-P*eye(3)/rho)*f/rho/V;

%Sliding Controller Calculations
Gamma1=rho_ddd+krho*rho_dd+eta1*sat(s1/phi1)-Cvect'*(DfDt+(Ac+krho*eye(3,3))*f)/V;
Gamma2=P_ddd+kP*P_dd+eta2*sat(s2/phi2)-Cvect'*(Ap*DfDt+(Ap*(Ac+kP*eye(3,3))+DApDt)*f)/V;
Gamma3=kw*(w_dd+Cve*fe/tau3+Cve*DfDt(3))+eta3*sat(s3/phi3);

G=zeros(3,3);
G(3,3)=-kw*beta3;

syst_matrix=[f'*Bc/V;f'*Ap*Bc/V;f'*G];

epsilons=inv(syst_matrix)*[Gamma1;Gamma2;Gamma3];

sliding_control = [epsilons;s1;s2;s3];
```